AD-779 081

DESIGN OF A CONTROL SYSTEM TO
STABILIZE THE AFT FUSELAGE OF A
B-52 BOMBER IN THE PRESENCE OF A
RANDOM WIND GUST

Charles A. Harrington, III

Air Force Institute of Technology
Wright-Patterson Air Force Base, Ohio

March 1974

DESIGN OF A CONTROL SYSTEM TO

STABILIZE THE AFT FUSELAGE OF A B-52 BOMBER IN

THE PRESENCE OF A RANDOM WIND GUST

THESIS

Presented to the Faculty of the School of Engineering

of the Air Force Institute of Technology

Air University

in Partial Fulfillment of the

Requirements for the Degree of

Master of Science

by

Charles A. Harrington III, B.S.E.E.

Second Lieutenant   USAF

Graduate Guidance and Control

March 1974

Preface

The topic for this thesis was suggested by Major Bruce T. Kujawski of the Air Force Flight Dynamics Laboratory (AFFDL). A design scheme to minimize variations in pitch angle at the aft-fuselage of a B-52 bomber, due to a random vertical wind gust, was developed by the author.

I wish to express my gratitude to Captain Thomas Moriarty, my thesis advisor, for his advice and encouragement throughout the course of this study. My appreciation is also expressed to Major Bruce T. Kujawski, my thesis sponsor, and Mr. C. R. Stockdale and Mr. R. D. Poyneer of AFFDL for their helpful suggestions and comments. I would like to acknowledge Peterson's MIMIC Program, written by Mr. H. E. Peterson and Mr. F. J. Sansom, which was instrumental in the completion of this study. Finally, I wish to express my deep appreciation to my wife, Nancy, for her patience, encouragement, and assistance throughout the duration of this study.

GE/EE/74M-5

Contents

List of Figures

List of Tables

List of Symbols

B.S.   - Body Station, in.

F.C.   - Flight Condition

g - Acceleration due to gravity, in/sec^2

$K_{N_z'}$ - Gain of $N_z'(s)/\gamma(s)$ transfer function

$K_{N_z''}$ - Gain of $N_z''(s)/\delta_e(s)$ transfer function

$K_{\dot\theta'}$ - Gain of $\dot\theta'(s)/\gamma(s)$ transfer function

$K_{\dot\theta''}$ - Gain of $\dot\theta''(s)/\delta_e(s)$ transfer function

$K_{\dot\theta}$ - Gain of $\dot\theta_{xxx}(s)/\delta_e(s)$ transfer function, where xxx is the body station

L   - Integral scale of turbulence factor, in. (12,000 in. for the B-52)

$M_{(\ )}$ - $\dfrac{1}{I_{yy}}\dfrac{M}{(\ )}$; $(\ ) = \alpha,\ \dot\theta,\ \delta_e,\ n_i,\ \dot n_i,$ and w_g

where M is the pitching moment, positive nose down, in-lb, and I_{yy} is the pitching moment of inertia of the airplane, in-lb sec^2

n_i - Generalized coordinate of ith mode, in.

$n_{i(\ )}$ - $\dfrac{1}{M_i}\dfrac{F}{(\ )}$; $(\ ) = \alpha,\ \dot\theta,\ \delta_e,\ n_j,\ \dot n_j,$ and w_g

where F is the generalized force of the ith structural mode, lb, and M_i is the generalized mass of the ith structural mode, lb-sec^2/in.

N_z' - Normal Acceleration due only to wind gust, "g's"

N_z'' - Normal Acceleration due only to elevator deflection, "g's"

N_z - Total Normal Acceleration, "g's"

s   - Laplace variable

V   - Aircraft free-stream velocity, in/sec

VBM   - Vertical bending moment

V_z - Normal velocity at a given body station, in/sec

WBL   - Water Buttock Line, in.

w - Normal velocity coordinate, αV, in/sec

w_g - Wing gust, ft/sec

X - Longitudinal location of the sensor relative to the center of gravity, positive going, aft, in.

Z - Normal translation, in.

Z' - Normal translation due only to wind gust, in.

$Z_{(\ )}$ - $\dfrac{1}{mV} \dfrac{Z}{(\ )}$; $(\ ) = \alpha, \delta_e, n_i, \dot{n}_i,$ and w_g where Z is the force in the positive z direction, lb, and m is the airplane mass, lb-sec^2/in.

α - Angle-of-attack, rad

γ - White noise

δ_e - Elevator deflection angle, positive trailing edge down, rad

ζ'_i - Damping ratio of the ith mode including aerodynamic damping proportional to $\dot{n}_i$

θ - Total pitch angle, positive nose down, rad

θ_{rb} - Rigid-body pitch angle, positive nose down, rad

θ' - Pitch angle due to only wind gust, positive nose down, rad

θ'' - Pitch angle due to only elevator deflection, positive nose down, rad

θ_{172} - Pitch angle at B.S. 172, positive nose down, rad

θ_{805} - Pitch angle at B.S. 805, positive nose down, rad

$\dot{\theta}_{com}$ - Pilot pitch-rate command, positive nose down, rad/sec

λ_u - Rms gust velocity, ft/sec

Φ_i - Normalized natural mode shape of ith structural bending mode, in.

Φ'_i - $d\Phi_i/dx$, normalized natural mode slope of ith structural bending mode, in/in.

φ - Total matrix - $As^2 + Bs + C$

ω_i - Undamped natural frequency of ith mode, rad/sec

ω'_i - Undamped natural frequency of ith mode including aerodynamic contribution proportional to n_i, rad/sec

Special Notation

($\cdot$)   - Indicates derivative with respect to time

x

REPORT DOCUMENTATION PAGE		READ INSTRUCTIONS BEFORE COMPLETING FORM
1. REPORT NUMBER GE/EE/74M-5	2. GOVT ACCESSION NO.	3. RECIPIENT'S CATALOG NUMBER AD-779 081
4. TITLE (and Subtitle) DESIGN OF A CONTROL SYSTEM TO STABILIZE THE AFT FUSELAGE OF A B-52 BOMBER IN THE PRESENCE OF A RANDOM WIND GUST		5. TYPE OF REPORT & PERIOD COVERED M. S. Thesis
		6. PERFORMING ORG. REPORT NUMBER
7. AUTHOR(s) Charles A. Harrington III Second Lieutenant USAF		8. CONTRACT OR GRANT NUMBER(s)
9. PERFORMING ORGANIZATION NAME AND ADDRESS AIR FORCE INSTITUTE OF TECHNOLOGY (AFIT-EN) Wright-Patterson AFB, Ohio 45433		10. PROGRAM ELEMENT, PROJECT, TASK AREA & WORK UNIT NUMBERS
11. CONTROLLING OFFICE NAME AND ADDRESS Air Force Flight Dynamics Laboratory Wright-Patterson AFB, Ohio 45433		12. REPORT DATE March 1974
		13. NUMBER OF PAGES 101
14. MONITORING AGENCY NAME & ADDRESS(if different from Controlling Office)		15. SECURITY CLASS. (of this report) Unclassified
		15a. DECLASSIFICATION DOWNGRADING SCHEDULE

16. DISTRIBUTION STATEMENT (of this Report)

Approved for public release; distribution unlimited

17. DISTRIBUTION STATEMENT (of the abstract entered in Block 20, if different from Report)

18. SUPPLEMENTARY NOTES

Approved for public release; IAW AFR 190-17   Jerry C. Hix, Captain, USAF
Director of Information

19. KEY WORDS (Continue on reverse side if necessary and identify by block number)

Control System   Flexible
Feedback   Bending
Pitch Control   Superposition principle
B-52
Structural Modes

20. ABSTRACT (Continue on reverse side if necessary and identify by block number)

A control system was designed to stabilize the flexible aft-body of a B-52 bomber under the influence of a 1.0 ft/sec rms wind gust. The aircraft transfer functions, which include the effects of the first seven bending modes, were obtained using digital computer programs provided by the Air Force Flight Dynamics Laboratory and data and equations provided by the Boeing Aircraft Corporation. The open-loop pitch-rate and normal acceleration responses to the wind gust were obtained. The design procedure uses the principle of superposition to minimize the effects of a wind gust disturbance on the aircraft. The pitch-rate at the aft-

DD FORM 1473   EDITION OF 1 NOV 65 IS OBSOLETE
1 JAN 73

Block 20 cont.

fuselage is sensed and fed back to cause the elevator to deflect in such a way as to counter the effect of the wind gust. An 83.3% reduction in the rms variation in pitch angle was achieved, when compared to the response of the uncompensated aircraft. The rms normal translation, however, increased from 0.927 in. to 2.431 in., but was considered to be an insignificant contributor to the pointing error, when compared to the improvement in rms pitch variation. The control sytem is also shown to respond adequately to a pilot pitch-rate command, although the system would normally operate with no pilot input.

DESIGN OF A CONTROL SYSTEM TO
STABILIZE THE AFT FUSELAGE OF A B-52 BOMBER IN
THE PRESENCE OF A RANDOM WIND GUST

I. Introduction

Designers of large aircraft are confronted with a trade-off between weight and structural rigidity. For the aircraft to have a reasonable payload capacity, it must be built of light, strong, flexible materials. However, the structural elasticity causes problems due to interaction between the elastic and aerodynamic forces.

Any large aircraft exhibits these elastic characteristics, in addition to the normal short-period and phugoid modes of the simple rigid-body. For example, the fuselage of a large aircraft bends under the application of aerodynamic forces; and this bending can be expressed in terms of natural frequencies and modes of vibration for the entire free system.

Sensors located throughout the aircraft sense not only the rigid-body motion, but also the elastic motion superimposed on the basic rigid-body motion. It is true that generally the rigid-body motion is most significant in explaining the motion of an aircraft. However, in a control system where a particular parameter, such as pitch, is to be controlled accurately, the elastic effect of the fuselage must be considered and modeled in the control system design.

With this brief introduction to the general problem of controlling a large flexible aircraft, the particular problem that this thesis encompasses will be stated.

Statement of the Problem

The problem is to stabilize a large flexible vehicle to the degree necessary to point optical instruments that are mounted on the vehicle. The vehicle is a B-52 bomber since very complete equations exist for that aircraft. The optical instruments are located at body station (B.S.) 1799 in the aft portion of the fuselage. The end of the fuselage is at B.S. 1953. This location has the advantage of being a practical place for additional equipment to be installed, as well as having a wide range of unobscured lines of sight.

The Vietnam war has shown the vulnerability of B-52 bombers to surface-to-air missiles. The optical instrument could be a powerful laser aimed at the oncoming missile. The laser would have to be pointed accurately enough to destroy the control circuitry of the missile and cause it to miss its target.

Scope

To narrow the problem, only the longitudinal dynamics will be investigated. The major problems will be to develop a criteria for the degree of stabilization required and determine the residual motion that must be removed by the pointing control system. The only control surface to be used will be the elevator. The rigid-body short-period mode and the first seven symmetric structural bending modes will be included.

The input disturbance to the aircraft will be a vertical wind gust. The response to this disturbance by the aft portion of the aircraft at B.S. 1799 is to be minimized.

Assumptions

Complete data on the B-52 bomber is available through the Air Force

Flight Dynamics Laboratory (AFFDL), Wright-Patterson Air Force Base, Ohio. However, simplifying assumptions are made to facilitate easier use on the digital computer. Less significant terms in the data and equations from AFFDL will be neglected.

The phugoid mode will be neglected since its effect would be small on the overall response of the aircraft. The Boeing Aircraft Company has identified 27 symmetrical bending modes, numbered in order of ascending natural frequency (Ref 11:21-22). Since the higher frequency bending modes are less significant in describing the total aircraft dynamics, only the first seven bending modes will be included in the equations of motion.

Quasi-steady aerodynamics are assumed. For this reason, Wagner aerodynamic lags are neglected in the equations. Reaction forces due to control surface angular accelerations about the surface hinges are assumed small and neglected. The gust input is assumed to act vertically and the dynamic aircraft equations are linear and superposition holds.

These assumptions are similar to those made for the preliminary work done by AFFDL on the ride-control system for the B-52 (Ref 1). They will tend to degrade a digital computer simulation of the final design at higher frequencies, but only the lower frequency bending modes are included so the degradation will not be too severe. For design purposes a simplified model proves to be a great advantage.

Sub-problems

In order to solve this problem using classical methods, the data and equations available from AFFDL must be manipulated using the digital computer, to obtain the open-loop transfer functions that relate both

wind gust input and elevator input to corresponding normal acceleration and pitch rate at B.S. 1799. An understanding of the use of these programs must be obtained. Once the necessary transfer functions are obtained, the design of the feedback circuitry necessary to control pitch and normal translation must be accomplished. This will constitute the bulk of the study.

A method of simulating the resulting block diagrams to check the design work will be necessary. Due to the complexity of the system, caused by including seven structural bending modes, the analog computer may prove unwieldy. MIMIC is a computer program for simulating the function of an analog computer on the digital computer and will be used in the simulations (Ref 8).

Standards

Part of the problem is to establish the criteria or design specifications to be met by the system. The transfer functions that give pitch rate and normal acceleration for a given 1.0 ft/sec rms wind gust input can be used to obtain the open-loop response of the aircraft. This open-loop response establishes the nominal response of the aircraft and provides a reference value by which to judge the performance of the feedback circuitry. A tentative goal is to reduce the response by an order of magnitude.

The responses of interest are the change in pitch angle and the normal translation. The most important response to reduce is the change in pitch angle because an angular rotation of the aircraft will result in a larger deviation at the target than a mere normal translation.

II. Derivation of Aircraft System Transfer Functions

In order to control the change in both pitch and normal translation, it is necessary to determine the effect of the gust input and the elevator control on these two variables. That is, the transfer functions, $N_z'(s)/w_g(s)$, $N_z''(s)/\delta_e(s)$, $\dot{\theta}'(s)/w_g(s)$, $\dot{\theta}''(s)/\delta_e(s)$, and $w_g(s)/\gamma(s)$ must be found.

To obtain these desired transfer functions the dynamic equations of motion must be analyzed. Methods used to manipulate these equations to obtain the transfer functions will be discussed in this chapter.

Equations of Motion

The set of differential equations which describe the longitudinal short-period dynamics of the aircraft are:

Normal Velocity

$$\dot{\alpha} = -\dot{\theta} + Z_\alpha \alpha + Z_{\delta_e} \delta_e + Z_{w_g} w_g + \sum_{i=3}^{9} Z_{\dot{n}_i} \dot{n}_i + \sum_{i=3}^{9} Z_{n_i} n_i \tag{1}$$

Pitch Rate

$$\ddot{\theta} = M_{\dot{\theta}} \dot{\theta} + M_\alpha \alpha + M_{\delta_e} \delta_e + M_{w_g} w_g + \sum_{i=3}^{9} M_{\dot{n}_i} \dot{n}_i + \sum_{i=3}^{9} M_{n_i} n_i \tag{2}$$

Structural Bending Modes

$$\ddot{n}_i = -2\zeta_i' \omega_i' \dot{n}_i - (\omega_i')^2 n_i + n_{i_\alpha} \alpha + n_{i_{\dot{\theta}}} \dot{\theta} + n_{i_{\delta_e}} \delta_e +$$

$$n_{i_{w_g}} w_g + \sum_{\substack{j=3 \\ j \neq i}}^{9} n_{i_{\dot{n}_j}} \dot{n}_j + \sum_{\substack{j=3 \\ j \neq i}}^{9} n_{i_{n_j}} n_j , \quad i = 3, 4, \ldots 9 \tag{3}$$

In each equation the summation refers to the contribution of the seven

bending modes. The subscripts, i equal to 1 and 2, are reserved for the two rigid-body terms. These equations are a result of transformations made from the variables s and θ, in the non-rotating inertial axes used by Boeing, to the body-axis variables σ and $\dot{σ}$. The phugoid mode is thereby removed from the Boeing equations. The interested reader is directed to Reference 1 for a more complete description of this transformation.

Complete data for the B-52 bomber is available through AFFDL which has a data tape and several computer programs that facilitate using the data tape. The first program, MANIP, eliminates the phugoid by accomplishing the transformation of variables mentioned above. The second program, MATASEM, assembles the data into a polynomial matrix of second order in the frequency domain. In this form it can be utilized in conventional eigenvalue computational techniques. These two programs, when used together, give three resulting matrices, A, B, and C, which make up the matrix equations for the basic aircraft. Each of these three matrices is a square matrix of dimension 96 x 96. The form of this equation is

$$\varphi(s) \; n_1 \;\; = \;\; 0 \qquad\qquad (4)$$

where $\varphi(s) = As^2 + Bs + C$ and n_1 are the generalized coordinates (Ref 9:20-21). Table I lists the description of each of the n_1 generalized coordinates (Ref 9). It should be noted that the generalized coordinates, n_3 through n_9, inclusive, correspond to the first seven bending modes. This is done to reserve n_1 and n_2 for the two rigid-body terms.

A separate set of A, B, and C matrices must be obtained from MATASEM for each flight condition. An input of both free stream velocity

6

Table I

Description of Generalized Coordinates (Ref 10)

n_i	Description	n_i	Description	n_i	Description
1	Rigid Body, w	33	L. Out. Aileron	65	Blank
2	Rigid Body, $\dot{\theta}_{rb}$	34	Left Spoiler	66	Blank
3	1 Bending Mode	35	Blank	67	Blank
4	2 Bending Mode	36	Blank	68	Blank
5	3 Bending Mode	37	1 Wagner	69	Wind Coeff.
6	4 Bending Mode	38	2 Wagner	70	Wind Coeff.
7	5 Bending Mode	39	3 Wagner	71	Wind Coeff.
8	6 Bending Mode	40	4 Wagner	72	Blank
9	7 Bending Mode	41	5 Wagner	73	Blank
10	8 Bending Mode	42	6 Wagner	74	Blank
11	9 Bending Mode	43	7 Wagner	75	Blank
12	10 Bending Mode	44	8 Wagner	76	N_z B.S. 172
13	11 Bending Mode	45	9 Wagner	77	Blank
14	12 Bending Mode	46	10 Wagner	78	Blank
15	13 Bending Mode	47	11 Wagner	79	$\dot{\theta}$ B.S. 426
16	14 Bending Mode	48	12 Wagner	80	Blank
17	15 Bending Mode	49	13 Wagner	81	N_z B.S. 1655
18	16 Bending Mode	50	14 Wagner	82	N_z B.S. 860
19	17 Bending Mode	51	15 Wagner	83	VBM B.S. 475
20	18 Bending Mode	52	16 Wagner	84	VBM B.S. 760
21	19 Bending Mode	53	17 Wagner	85	VBM B.S. 1222
22	20 Bending Mode	54	18 Wagner	86	VBM B.S. 1412
23	21 Bending Mode	55	19 Wagner	87	VBM B.S. 222
24	22 Bending Mode	56	20 Wagner	88	VBM B.S. 820
25	23 Bending Mode	57	21 Wagner	89	VBM B.S. 974
26	24 Bending Mode	58	22 Wagner	90	VBM B.S. 56
27	25 Bending Mode	59	23 Wagner	91	N_z B.S. 800
28	26 Bending Mode	60	24 Wagner	92	N_z WBL 925
29	27 Bending Mode	61	25 Wagner	93	N_z WBL 565
30	Left Elevator	62	26 Wagner	94	$\dot{\theta}$ B.S. 566
31	Left Flaperon	63	27 Wagner	95	$\dot{\theta}$ B.S. 800
32	L. In. Aileron	64	Blank	96	$\dot{\theta}$ B.S. 1377

and atmospheric density must be given to both MANIP and MATASEM to obtain the correct A, B, and C matrices for each flight condition.

The simplifying assumptions made in Chapter I are now applied to remove those equations not needed for the simplified model of the aircraft. MATASEM can be used to remove the Wagner equations, all controls but the elevator (number 30 in Table I), and the bending modes 8 - 27. Only one wind coefficient (number 69 in Table I) was kept. This caused the wind gust to be resolved into a single gust acting at the aircraft center of gravity. After reduction from the basic 96 x 96 matrix, the dimension of the basic unaugmented matrix was 11 x 11. An example of the A, B, and C matrices is shown in Figures 1 through 3, respectively, for a velocity of 8223.62 in/sec and an altitude of 21,000 ft. This flight condition is defined as F.C. 1 throughout this thesis.

The first two rows and columns of the unaugmented matrix contain the two rigid-body equations for w and $\dot{\theta}_{rb}$, where w is the angle-of-attack multiplied by the free-steam velocity of the aircraft. Row and column 3 through 9, inclusive, contain the equations for the first seven bending modes. Row and column 10 is the equation for the one control to be used, δ_e, the elevator deflection, and the final row and column is reserved for the wind gust, w_g. The basic matrix can be augmented by adding on equations for the wind filter, normal acceleration at B.S. 1799, and pitch rate at B.S. 1799. Each of these equations will be discussed now before going on to solve the augmented matrix for the desired transfer functions.

Wind Filter

The wind gust due to atmospheric turbulence is approximated by the

A MATRIX

```
              (  1)          (  2)          (  3)          (  4)
(   1)     0.             0.             .35837E-C1     .94166E-01
(   2)     0.             0.            -.72J09E-05    -.19372E-03
(   3)     0.             0.             .10J00E+01     .90826E-02
(   4)     0.             0.             .675b1E-C2     .10.00E+01
(   5)     0.             0.            -.3J775E-02    -.28437E-02
(   6)     0.             0.             .35773E-02     .40012E-02
(   7)     0.             0.            -.37755E-03     .15253E-02
(   8)     0.             0.             .39+43E-02     .43155E-02
(   9)     0.             0.             .32831E-02     .41835E-02
(  10)     0.             0.             0.             0.
(  11)     0.             0.             0.             0.


              (  5)          (  E)          (  7)          (  E)
(   1)    -.55532E-J2      .21751E-01   -.1CE42E+0C      .87586E-02
(   2)     .18421E-C4    -.22003E-04     .40545E-03    -.85922E-05
(   3)    -.91720E-03      .69628E-02     .65203E-02     .55719E-02
(   4)    -.59025E-C3      .42547E-02     .27594E-02     .34257E-02
(   5)     .10000E+C1    -.21415E-02    -.20823E-02    -.17872E-02
(   6)    -.46472E-03      .10000E+01     .25161E-02     .26892E-02
(   7)    -.37844E-C3      .26675E-02     .10000E+01     .15131E-02
(   8)    -.49748E-C3      .35556E-02     .30801E-02     .10000E+01
(   9)    -.62645E-03      .34910E-02     .26884E-02     .26382E-02
(  10)     0.             0.             0.             0.
(  11)     0.             0.             0.             0.


              (  9)          ( 10)          ( 11)
(   1)    -.58313E-01     0.             0.
(   2)     .34764E-03     0.             0.
(   3)     .10296E-01     0.             0.
(   4)     .45019E-02     0.             0.
(   5)    -.23359E-02     0.             0.
(   6)     .25405E-02     0.             0.
(   7)    -.59672E-04     0.             0.
(   8)     .30387E-02     0.             0.
(   9)     .10000E+01     0.             0.
(  10)     0.             0.             0.
(  11)     0.             0.            -0.
```

Figure 1. Basic Unaugmented A Matrix

9

E MATRIX

	(1)	(2)	(3)	(4)
(1)	.10000E+01	-.13486E+01	.64687E+01	.22117E+02
(2)	-.25253E-04	.10000E+01	.16893E-01	-.17542E-01
(3)	-.29438E-04	.15932E-01	.22927E+01	.27919E+01
(4)	.76674E-04	-.17783E-02	.84515E+00	.16334E+01
(5)	-.56144E-05	-.24353E-02	-.45963E+00	-.67126E+00
(6)	.59585E-04	-.16825E-01	.75690E+00	.73876E+00
(7)	.62909E-04	-.44129E-01	.17790E-01	.67297E-01
(8)	.42293E-04	-.11131E-01	.63643E+00	.93809E+00
(9)	.11239E-03	-.63282E-01	.17923E+00	.47840E+00
(10)	0.	0.	0.	0.
(11)	0.	0.	0.	0.

	(5)	(6)	(7)	(8)
(1)	-.17377E+01	.92304E+01	-.89416E+01	.47713E+01
(2)	.75851E-03	-.22348E-01	-.29718E-01	-.11441E-01
(3)	-.24711E+00	.14753E+01	.15018E+00	.10229E+01
(4)	-.12271E+00	.68192E+00	-.11018E+00	.44919E+00
(5)	.18632E+00	-.40036E+00	-.75913E-02	-.25923E+00
(6)	-.55233E-01	.67935E+00	.13992E+00	.29556E+00
(7)	.50424E-02	.34823E+00	.90755E+00	.18932E+00
(8)	-.82416E-01	.69357E+00	.22920E+00	.64151E+00
(9)	-.35966E-01	.57573E+00	.59495E+00	.23843E+00
(10)	0.	0.	0.	0.
(11)	0.	0.	0.	0.

	(9)	(10)	(11)
(1)	-.23262E+00	0.	0.
(2)	-.34148E-01	0.	0.
(3)	.16195E+01	0.	0.
(4)	.69986E+00	0.	0.
(5)	-.38911E+00	0.	0.
(6)	.64687E+00	0.	0.
(7)	.84318E+00	0.	0.
(8)	.61127E+00	0.	0.
(9)	.14002E+01	0.	0.
(10)	0.	0.	0.
(11)	0.	0.	-0.

Figure 2. Basic Unaugmented B Matrix

10

C MATRIX

	(1)	(2)	(3)	(4)
(1)	.11382E+01	.81163E+04	.17463E+03	.16522E+04
(2)	-.73328E-03	.15766E+01	.23803E-01	-.21903E+01
(3)	.30072E-01	.10345E+02	.41237E+02	.10889E+03
(4)	.14203E-01	.24734E+01	.43306E+01	.16660E+03
(5)	-.40811E-02	-.11565E+01	-.17893E+01	-.20630E+02
(6)	.59613E-02	-.97108E+00	.11735E+01	.23115E+02
(7)	.23108E-02	-.56717E+01	-.75253E+00	.14639E+02
(8)	.97036E-02	.17149E+01	.26025E+01	.35911E+02
(9)	.83562E-02	-.53353E+01	.89133E+00	.26816E+02
(10)	0.	0.	0.	0.
(11)	0.	0.	0.	0.

	(5)	(6)	(7)	(8)
(1)	-.12771E+03	.77241E+03	-.78242E+03	.19482E+03
(2)	.37094E-01	-.19496E+01	-.10475E+01	-.31083E+00
(3)	-.70552E+01	.65781E+02	-.55563E+02	.11347E+02
(4)	-.29542E+01	.29020E+02	-.25500E+02	.21174E+01
(5)	.15792E+03	-.13971E+02	.11174E+02	-.22587E+01
(6)	-.14327E+01	.19444E+03	-.10358E+02	.17684E+01
(7)	-.93916E+00	.16867E+02	.22763E+03	-.57385E+00
(8)	-.26760E+01	.27403E+02	-.18419E+02	.24656E+03
(9)	-.18655E+01	.21406E+02	-.37696E+01	.18943E+01
(10)	0.	0.	0.	0.
(11)	0.	0.	0.	0.

	(9)	(10)	(11)
(1)	.92766E+02	.42470E+03	.11382E+01
(2)	-.34571E+01	-.33113E+01	-.73328E-03
(3)	.28065E+02	-.19828E+02	.30072E-01
(4)	.15197E+02	-.67636E+01	.14203E-01
(5)	-.97737E+01	.45991E+01	-.40813E-02
(6)	.17905E+02	.16891E+01	.59612E-02
(7)	.29501E+02	.16560E+02	.23108E-02
(8)	.23127E+02	-.63659E+00	.97038E-02
(9)	.37311E+03	.20882E+02	.83561E-02
(10)	0.	-.10000E+01	0.
(11)	0.	0.	-0.

Figure 3. Basic Unaugmented C Matrix

11

use of the Dryden wind filter. This wind filter was obtained from wind tunnel analysis and is shown in Laplace notation below:

$$W(s) = \lambda_u \sqrt{\frac{3V}{2\pi L}} \quad \frac{s + \frac{V}{\sqrt{3}L}}{(s + \frac{V}{L})^2} \tag{5}$$

where λ_u is the rms gust velocity which was chosen to be unity (1 ft/sec or, equivalently, 12 in/sec). The symbol, L, is the integral scale of turbulence factor (12,000 in. for the B-52) and V is the aircraft free-stream velocity in units of in/sec (Ref 10:2-8). For V = 6876.1 in/sec and λ_u = 12 in/sec

$$W(s) = \frac{6.277s + 2.058}{s^2 + 1.146s + 0.328} \tag{6}$$

The wind filter, $W(s)$, is actually the transfer function, $w_g(s)/\gamma(s)$, where w_g is the wind gust and γ is white noise.

Normal Acceleration Equation

The normal acceleration equation is given below (Ref 9:17).

$$N_z = \frac{1}{g}(V\dot{\theta}_{rb} + sw + s\dot{\theta}_{rb}X + s^2 \sum_{i=3}^{9} \Phi_i n_i) \tag{7}$$

The flexible mode shapes for B.S. 1799 are obtained from data supplied by Boeing and tabulated in a report by Beta Industries, Inc. of Dayton, Ohio (Ref 1). The elastic mode shapes, Φ_i, as well as the corresponding mode slopes, Φ_i', are shown in Table II. To give a better understanding of the concept of mode shapes and mode slopes, Figure 4 shows the contribution to fuselage deflection made by each of the seven vertical symmetric bending modes over the length of the fuselage. It should be remembered that bending modes 1 - 7 correspond to i-subscripts 3 - 9, re-

Table II

Elastic Mode Shapes and Mode Slopes at B.S. 1799

Subscript (i)	Mode Shapes Φ_i (in.)	Mode Slopes $-\Phi_i'$ (in/in)
3	-34.97	0.0307
4	-20.97	0.0503
5	3.16	-0.00803
6	4.25	-0.00628
7	51.19	-0.160
8	-2.89	0.0116
9	44.19	-0.203

(From Ref 1)

spectively. This is done to reserve the first two subscripts for the rigid-body terms. By comparing Table II to Figure 4 it can be seen that the mode shapes are the components of fuselage deflection due to the particular bending modes. The mode slopes are the slopes of the curves at the body station in question (Ref 11:24).

Pitch-Rate Equation

The equation for pitch rate at B.S. 1799 is as follows:

$$\dot{\theta} = \dot{\theta}_{rb} + s \sum_{i=3}^{9} \Phi_i' n_i \qquad (8)$$

where $\dot{\theta}_{rb}$ is the rigid-body contribution to pitch rate (the second row and column in the basic matrix) and Φ_i' represents the mode slopes at
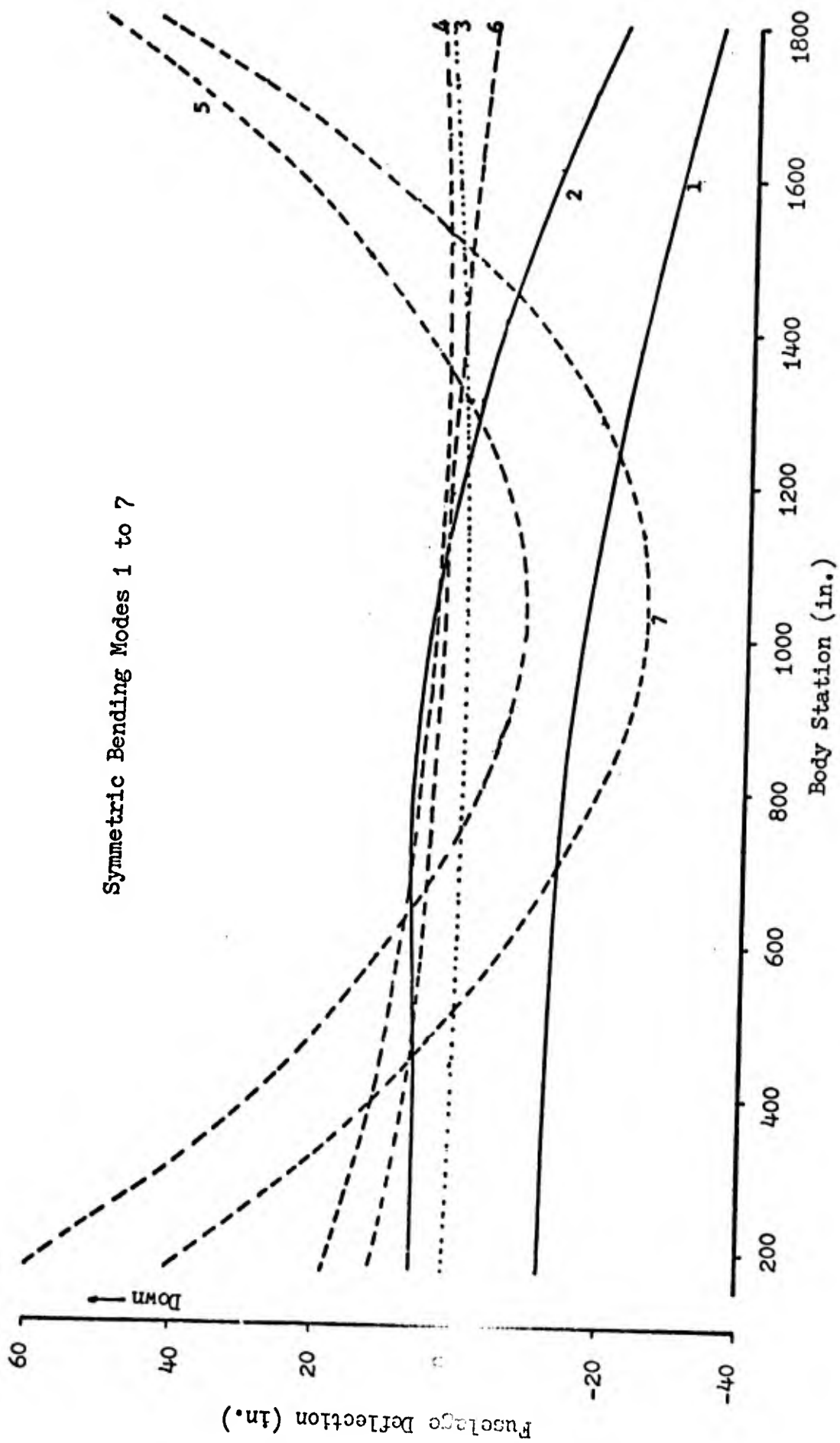
13

Figure 4. Vertical Symmetric Bending Mode Deflections (Ref 11:24)

B.S. 1799 for the ith mode (Ref 1). These mode slopes are listed in Table II on page 13. Thus $\dot{\theta}$ is the complete pitch rate, including the effects of the rigid body as well as the flexible nature of the aircraft.

Matrix Solution for the Desired Transfer Functions

The number of equations necessary to represent the basic aircraft, including the first seven bending modes, makes a matrix method of solution appear very advantageous. The remainder of this chapter describes how a computer program was used to obtain the transfer functions.

VALUE Program. The Control Configured Vehicle (CCV) Flight Control Division of AFFDL has a program called VALUE which is designed to determine transfer function poles and zeros. This is done by solving the generalized eigenvalue problem from Laplace domain system equations (Ref 12).

Application of the VALUE Program to Obtain the Desired Transfer Functions. The basic 11 x 11 matrix, obtained by using MANIP and MATASEM, must be augmented by adding a row and column each for the wind filter, normal acceleration equation, and pitch-rate equation. The result is a 14 x 14 matrix that can be used directly in VALUE to obtain the four desired transfer functions: $N_z'(s)/\gamma(s)$, $N_z''(s)/\delta_e(s)$, $\dot{\theta}'(s)/\gamma(s)$, and $\dot{\theta}''(s)/\delta_e(s)$. This matrix is shown, symbolically, in Figure 5. Only a few elements of the matrix are filled in for clarity and for the purpose of explaining how the VALUE program manipulates this matrix. It will be noted that only rows 10 and 14, which correspond to δ_e and γ, have a number of magnitude one as their diagonal elements. The poles are found by solving for the eigenvalues of the unmodified matrix, as shown in Figure 5. These poles are then common for all the other transfer functions.

$$
\begin{array}{c}
\quad\ w\ \ \dot\theta_{rb}\ \ n_3\ \ n_4\ \ n_5\ \ n_6\ \ n_7\ \ n_8\ \ n_9\ \ \delta_e\ \ w_g\ \ N_z\ \ \dot\theta\ \ \gamma \\[4pt]
\begin{array}{c}
w \\ \dot\theta_{rb} \\ n_3 \\ n_4 \\ n_5 \\ n_6 \\ n_7 \\ n_8 \\ n_9 \\ \delta_e \\ w_g \\ N_z \\ \dot\theta \\ \gamma
\end{array}
\left[
\begin{array}{c}
\text{Basic Unaugmented}\\
\text{A, B, and C Matrices}\\[4em]
-1\\[3em]
+1
\end{array}
\right]
\left[
\begin{array}{c}
n_1 \\ n_2 \\ n_3 \\ n_4 \\ n_5 \\ n_6 \\ n_7 \\ n_8 \\ n_9 \\ n_{10} \\ n_{11} \\ n_{12} \\ n_{13} \\ n_{14}
\end{array}
\right] = 0
\end{array}
$$

Figure 5. Matrix Equation Form for
use in the VALUE Program

To obtain the transfer function, $N_z''(s)/\delta_e(s)$, for example, the -1 in row 10 and column 10 must be made zero and a -1 must be placed in row 10 and column 12. After this modification the eigenvalues are again found for the modified matrix and result in the zeros of the transfer function $N_z''(s)/\delta_e(s)$. The lead coefficient or gain of the transfer function is also given by the program. The other transfer functions are found in a similar manner.

It must be remembered that the transfer functions with respect to the white noise input, γ, contain the wind filter, $W(s)$. This wind

filter can be factored out so that the main transfer function is broken up into two parts, as shown in Eq (9) for $N_z^{\bullet}(s)/\gamma(s)$ below:

$$\frac{N_z^{\bullet}(s)}{\gamma(s)} = \frac{w_g(s)}{\gamma(s)} \frac{N_z^{\bullet}(s)}{w_g(s)} \tag{9}$$

Tables III through VII give the tabulated gains and roots of the four desired transfer functions. The transfer functions with respect to white noise, γ, have had the wind filter, $W(s)$, factored out. In this case, the denominator is common for all four transfer functions. The wind filter for F.C. 2 was given on page 12 as Eq (6). Flight condition 2 is defined as being at an altitude of 2000 ft and a velocity of 6876.1 in/sec. The wind filter for F.C. 1 is shown below in Eq (10):

$$W(s) = \frac{6.864s + 2.716}{s^2 + 1.371s + 0.470} \tag{10}$$

Bode plots for the five transfer functions, including the wind filter, for F.C. 1 are shown in Figures 6 through 10, respectively.

Table III

Zeros of $\dot{\theta}''(s)/\delta_e(s)$ Numerator

		F.C. 1	F.C. 2
Gain	$K_{\dot{\theta}''}$	11.147	14.166
1st Term	a	-0.704	-1.015
2nd Term	b	$-0.621 \pm j6.092$	$-0.825 \pm j6.262$
3rd Term	c	$-0.516 \pm j9.612$	$-0.765 \pm j9.631$
4th Term	d	$-0.176 \pm j12.358$	$-0.146 \pm j12.357$
5th Term	e	$-0.270 \pm j12.841$	$-0.276 \pm j12.884$
6th Term	f	$-0.366 \pm j15.435$	$-0.262 \pm j15.199$
7th Term	g	$-0.987 \pm j14.368$	$-2.082 \pm j14.938$
8th Term	h	$-0.655 \pm j16.859$	$-0.788 \pm j16.532$

$$\frac{\dot{\theta}''(s)}{\delta_e(s)} = \frac{K_{\dot{\theta}''}(s-a)(s-b)(s-c)(s-d)(s-e)(s-f)(s-g)(s-h)}{\text{Denom}^*}$$

*: See Table VII

Table IV

Zeros of $\dot{\theta}'(s)/w_g(s)$ Numerator

		F.C. 1	F.C. 2
Gain	$K_{\dot{\theta}'}$	-0.00105	-0.00135
1st Term	a	0.000	0.000
2nd Term	b	-11.654 + j0.921	-8.717
3rd Term	c	-11.654 - j0.921	-17.145
4th Term	d	9.592 ± j5.300	9.831 ± j4.974
5th Term	e	-0.248 ± j8.413	-0.368 ± j8.318
6th Term	f	-0.058 ± j12.472	-0.053 ± j12.434
7th Term	g	-0.082 ± j13.286	-0.088 ± j13.231
8th Term	h	0.220 ± j15.430	0.230 ± j15.365
9th Term	i	-0.617 ± j15.740	-0.728 ± j15.775

$$\frac{\dot{\theta}'(s)}{w_g(s)} = \frac{K_{\dot{\theta}'}(s-a)(s-b)(s-c)(s-d)(s-e)(s-f)(s-g)(s-h)(s-i)}{\text{Denom}^*}$$

*: See Table VII

Table V

Zeros of $N_z''(s)/\delta_e(s)$ Numerator

		F.C. 1	F.C. 2
Gain	$K_{N_z''}$	-15.90	-20.257
1st Term	a	1.965	2.737
2nd Term	b	-2.681	-2.764
3rd Term	c	$-0.637 \pm j6.095$	$-0.851 \pm j6.232$
4th Term	d	$-0.089 \pm j12.472$	$-0.103 \pm j12.421$
5th Term	e	$-0.464 \pm j11.972$	$-0.602 \pm j12.226$
6th Term	f	$-0.134 \pm j13.799$	$-0.348 \pm j13.781$
7th Term	g	$-1.219 \pm j14.144$	$-1.987 \pm j14.625$
8th Term	h	$-0.371 \pm j15.558$	$-0.407 \pm j15.347$
9th Term	i	$-0.797 \pm j17.727$	$-1.115 \pm j17.414$

$$\frac{N_z''(s)}{\delta_e(s)} = \frac{K_{N_z''}(s-a)(s-b)(s-c)(s-d)(s-e)(s-f)(s-g)(s-g)(s-i)}{Denom^*}$$

*: See Table VII

Table VI

Zeros of $N_z'(s)/w_g(s)$ Numerator

		F.C. 1	F.C. 2
Gain	$K_{N_z'}$	0.0026	0.0035
1st Term	a	0.000	0.000
2nd Term	b	-1.082	-1.239
3rd Term	c	$-0.691 \pm j7.633$	$-0.932 \pm j7.589$
4th Term	d	$-0.062 \pm j12.448$	$-0.058 \pm j12.409$
5th Term	e	$-0.074 \pm j13.152$	$-0.099 \pm j13.078$
6th Term	f	$0.469 \pm j15.440$	$0.480 \pm j15.288$
7th Term	g	$-0.553 \pm j15.844$	$-0.634 \pm j15.874$
8th Term	h	$3.517 \pm j16.025$	$3.263 \pm j16.612$
9th Term	i	$-7.557 \pm j12.882$	$-8.865 \pm j12.264$

$$\frac{N_z'(s)}{w_g(s)} = \frac{K_{N_z'}(s-a)(s-b)(s-c)(s-d)(s-e)(s-f)(s-g)(s-h)(s-i)}{\text{Denom}^*}$$

* : See Table VII

Table VII

Poles of Transfer Function Denominators

		F.C. 1	F.C. 2
Rigid-Body	a	$-1.362 \pm j1.876$	$-2.052 \pm j1.864$
1st Bending Mode	b	$-0.670 \pm j6.091$	$-0.880 \pm j6.183$
2nd Bending Mode	c	$-0.372 \pm j12.282$	$-0.356 \pm j12.565$
3rd Bending Mode	d	$-0.159 \pm j12.561$	$-0.185 \pm j12.421$
4th Bending Mode	e	$-1.368 \pm j14.555$	$-2.348 \pm j14.701$
5th Bending Mode	f	$-0.085 \pm j14.734$	$-0.047 \pm j14.785$
6th Bending Mode	g	$-0.347 \pm j15.709$	$-0.430 \pm j15.664$
7th Bending Mode	h	$-0.927 \pm j19.233$	$-1.300 \pm j19.221$

Denom = $(s-a)(s-b)(s-c)(s-d)(s-e)(s-f)(s-g)(s-h)$
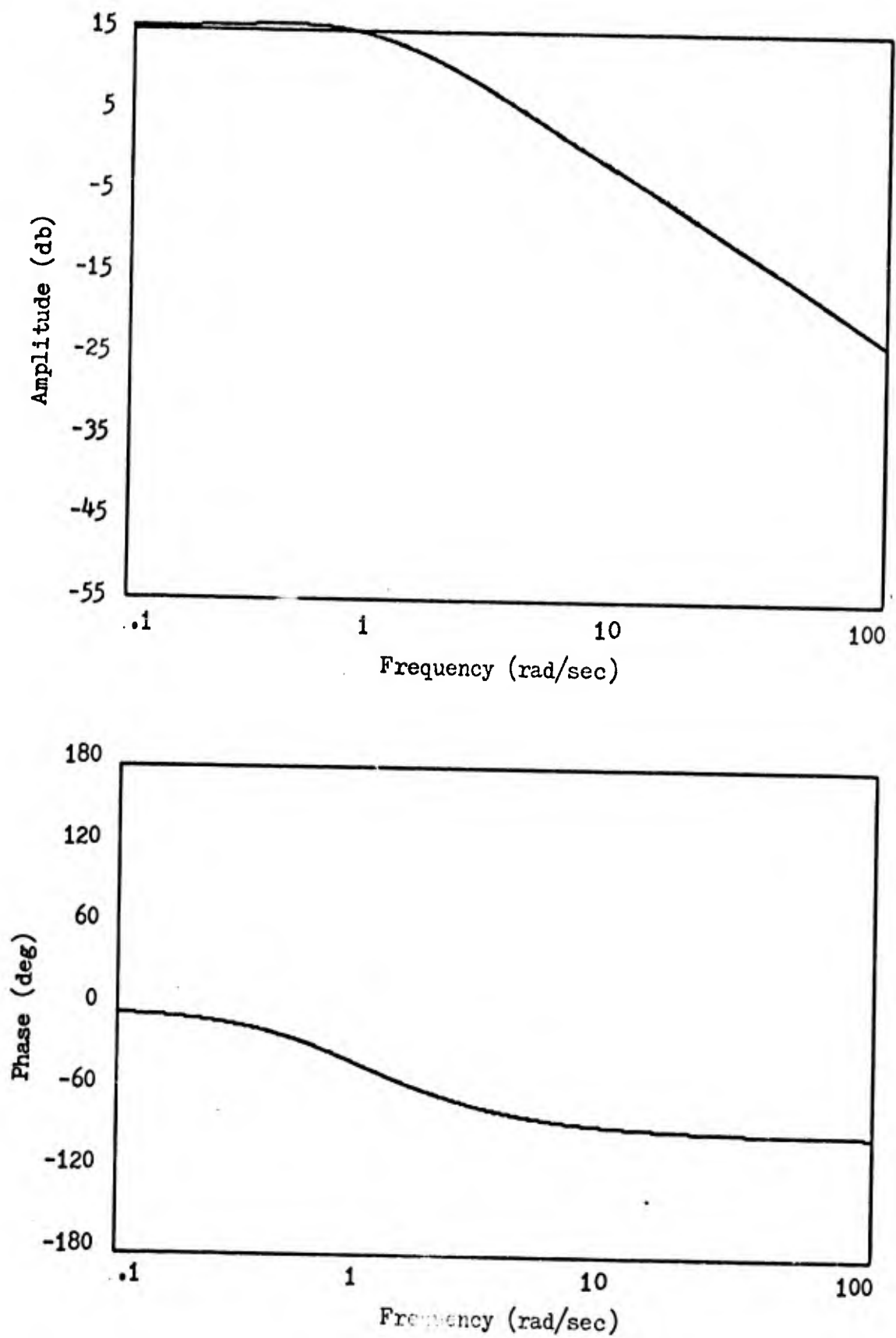
Figure 6. Bode Plot of $w_g(s)/\gamma(s)$ Transfer Function
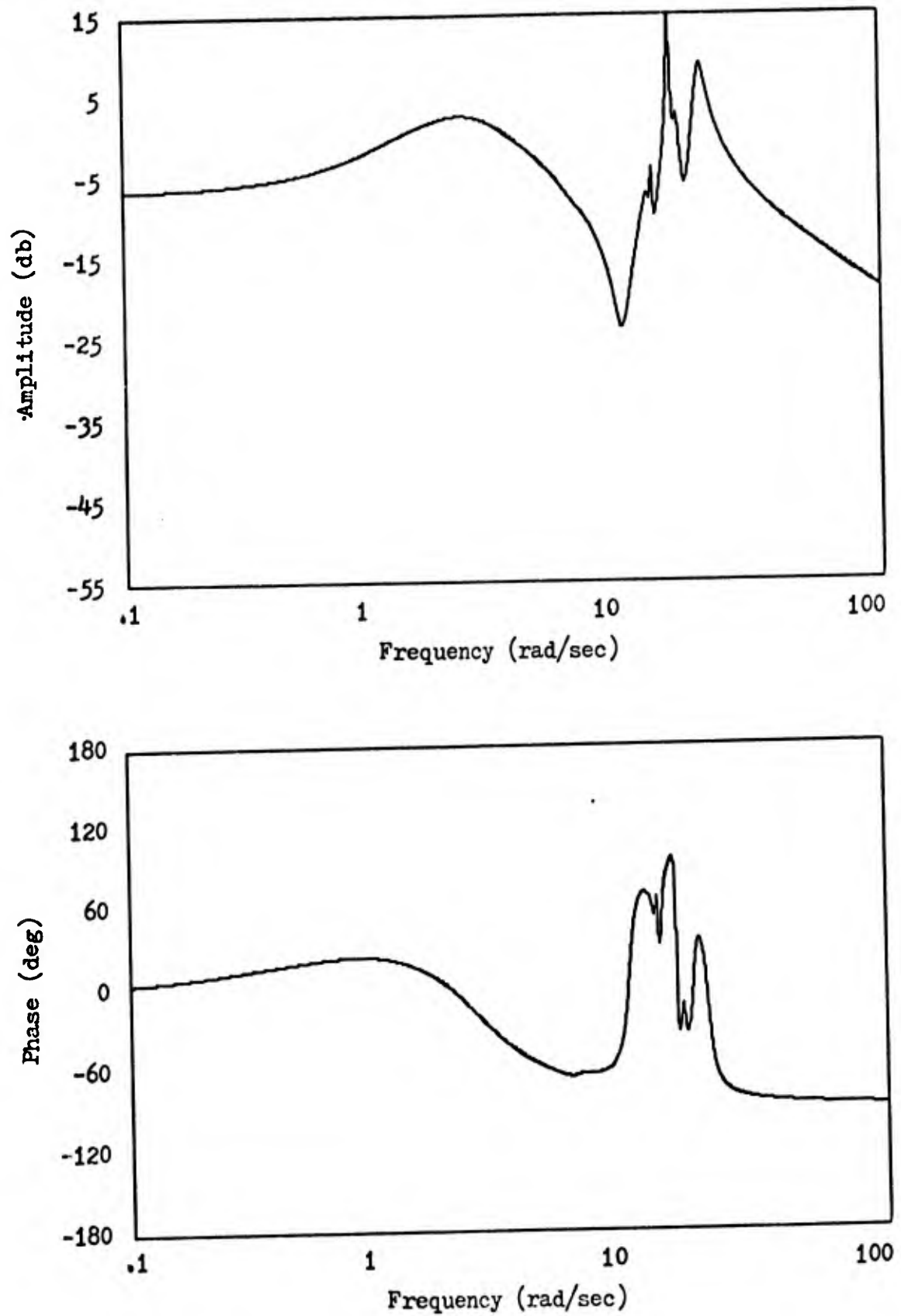
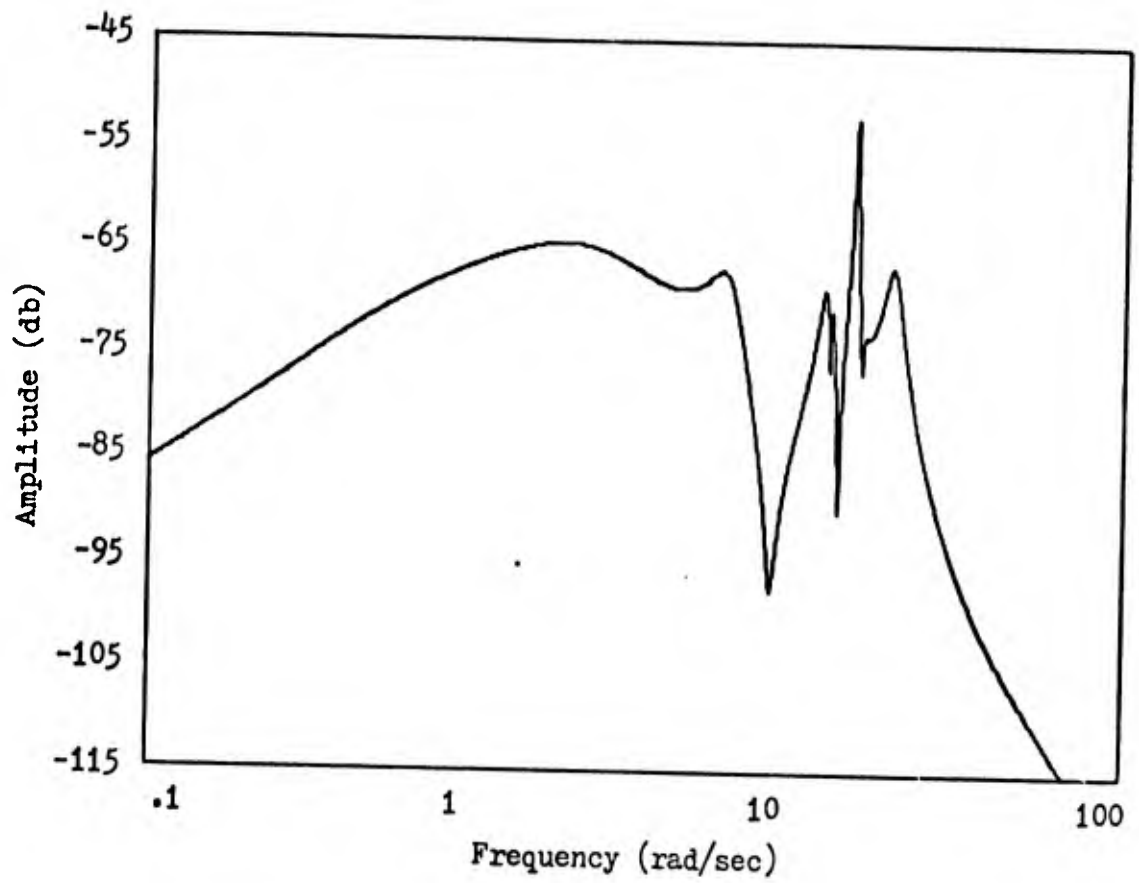Figure 7. Bode Plot of $\dot{\theta}''(s)/\delta_e(s)$ Transfer Function
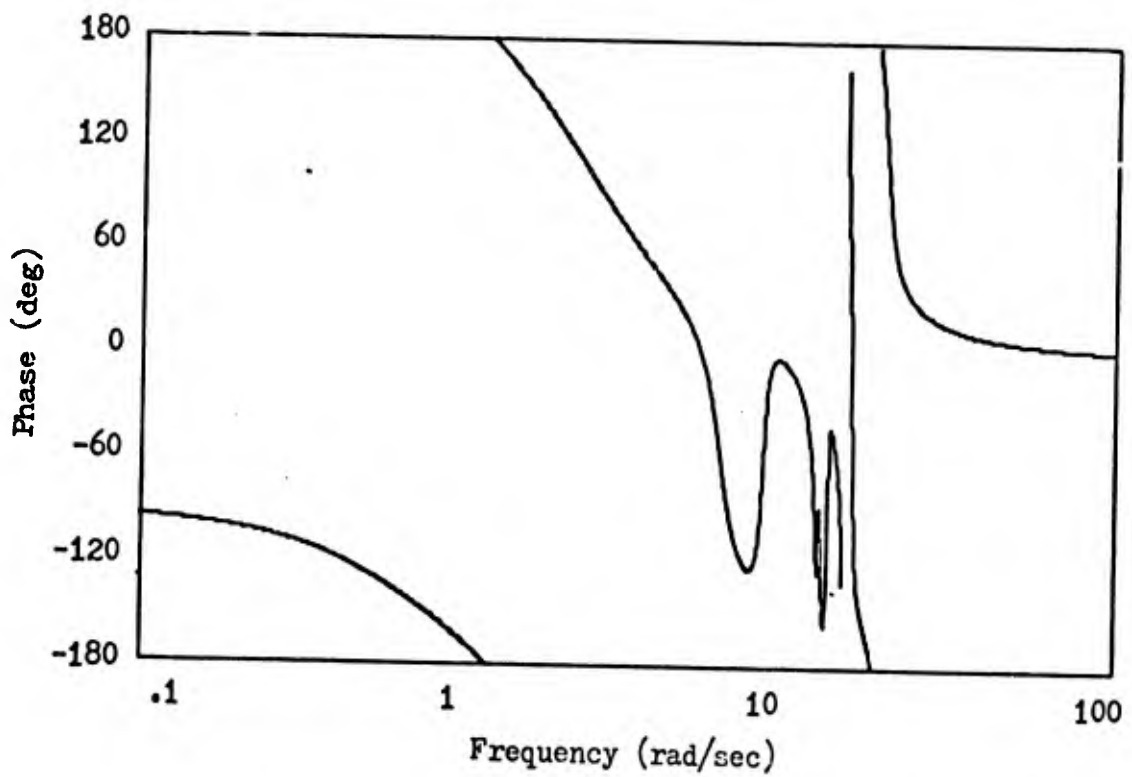
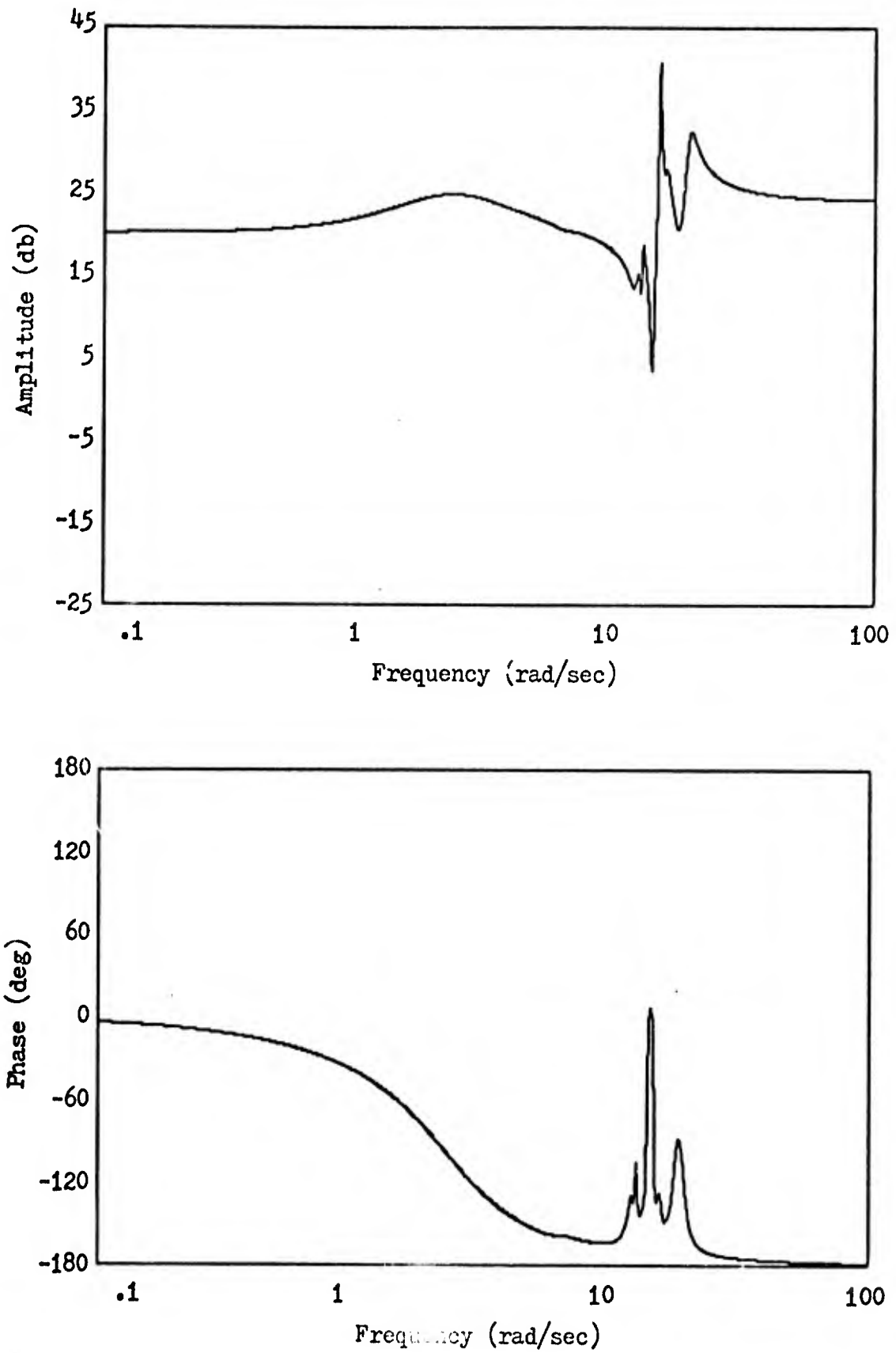Figure 8. Bode Plot of $\dot{\theta}'(s)/\gamma(s)$ Transfer Function

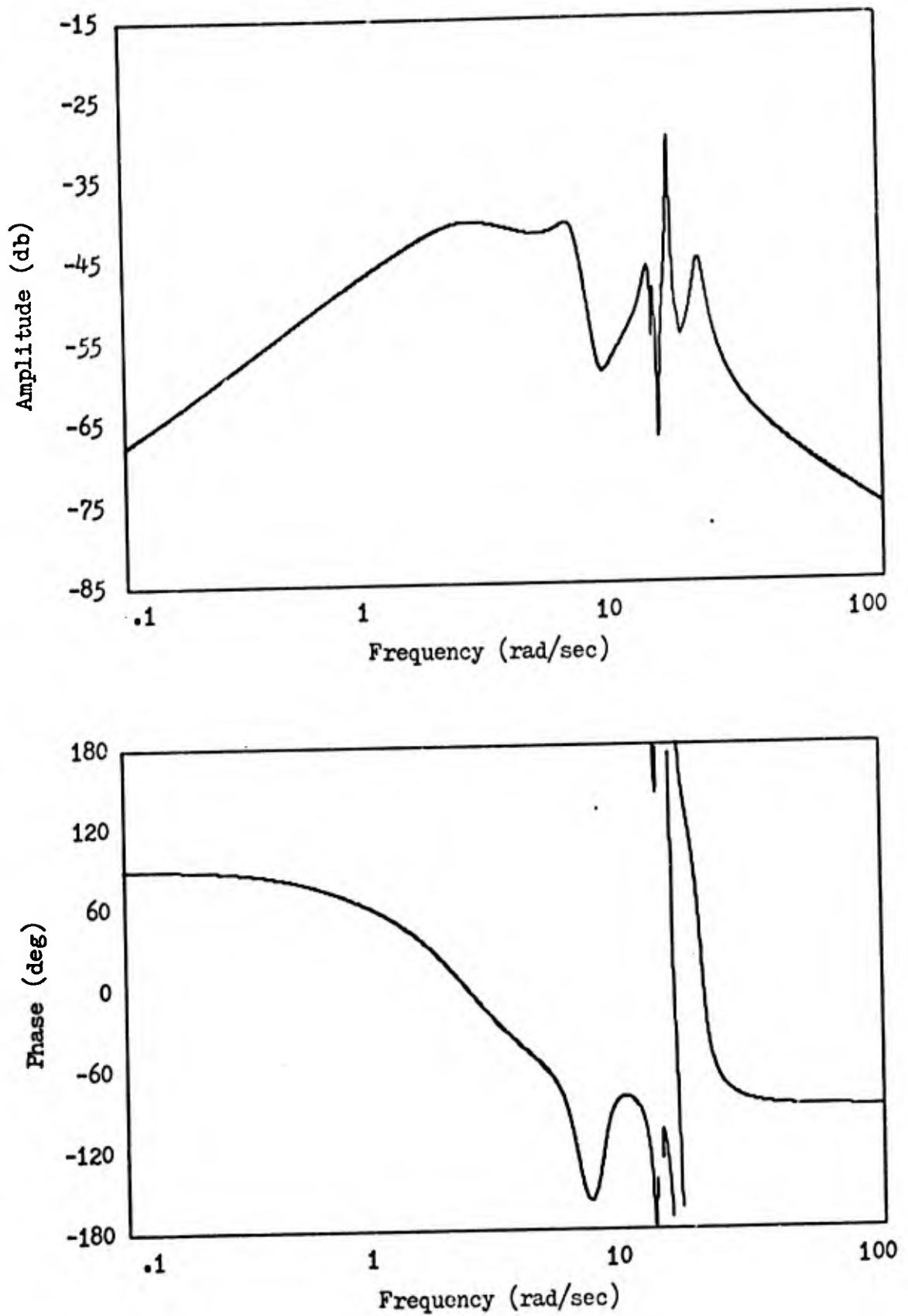Figure 9. Bode Plot of $\ddot{A}_z(s)/\delta_e(s)$ Transfer Function

Figure 10. Bode Plot of $N_z^{\bullet}(s)/\gamma(s)$ Transfer Function

III. Basic Aircraft Response

The dynamic response of the uncompensated aircraft to both an elevator deflection and a random wind gust of 1.0 ft/sec rms will be investigated and responses for Flight Conditions 1 and 2 will both be evaluated and compared. Appendix A shows how the individual transfer functions that were obtained in Chapter II are written for use in MIMIC.

Aircraft Dynamic Response to a Step Elevator Deflection

Both normal acceleration and pitch rate for B.S. 1799 are investigated for the two flight conditions.

Normal Acceleration. For F.C. 2 the elevator deflection necessary to obtain a normal acceleration, N_z'', of -1.0 g was calculated using the Final Value Theorem. The required δ_e is -0.07754 rad. The elevator deflection was input to the $N_z''(s)/\delta_e(s)$ transfer function for both flight conditions. The output is the open-loop step response of the aircraft. Figure 11 shows the time response of the aircraft for δ_e equal to -0.07754 rad for both flight conditions.

For F.C. 2 the steady-state N_z'' rises to -1.0 g, as predicted. The output is composed of the rigid-body effect plus superimposed oscillations, due to the bending modes, which are very lightly damped. A more detailed explanation of these oscillations will be given in the discussion of the pitch-rate response to the elevator step.

The normal acceleration at B.S. 1799 for F.C. 1 is also shown in Figure 11 for comparison to F.C. 2. For the same δ_e input of -0.07754 rad the normal acceleration goes to -0.782 g. The oscillations will be discussed in the next section.
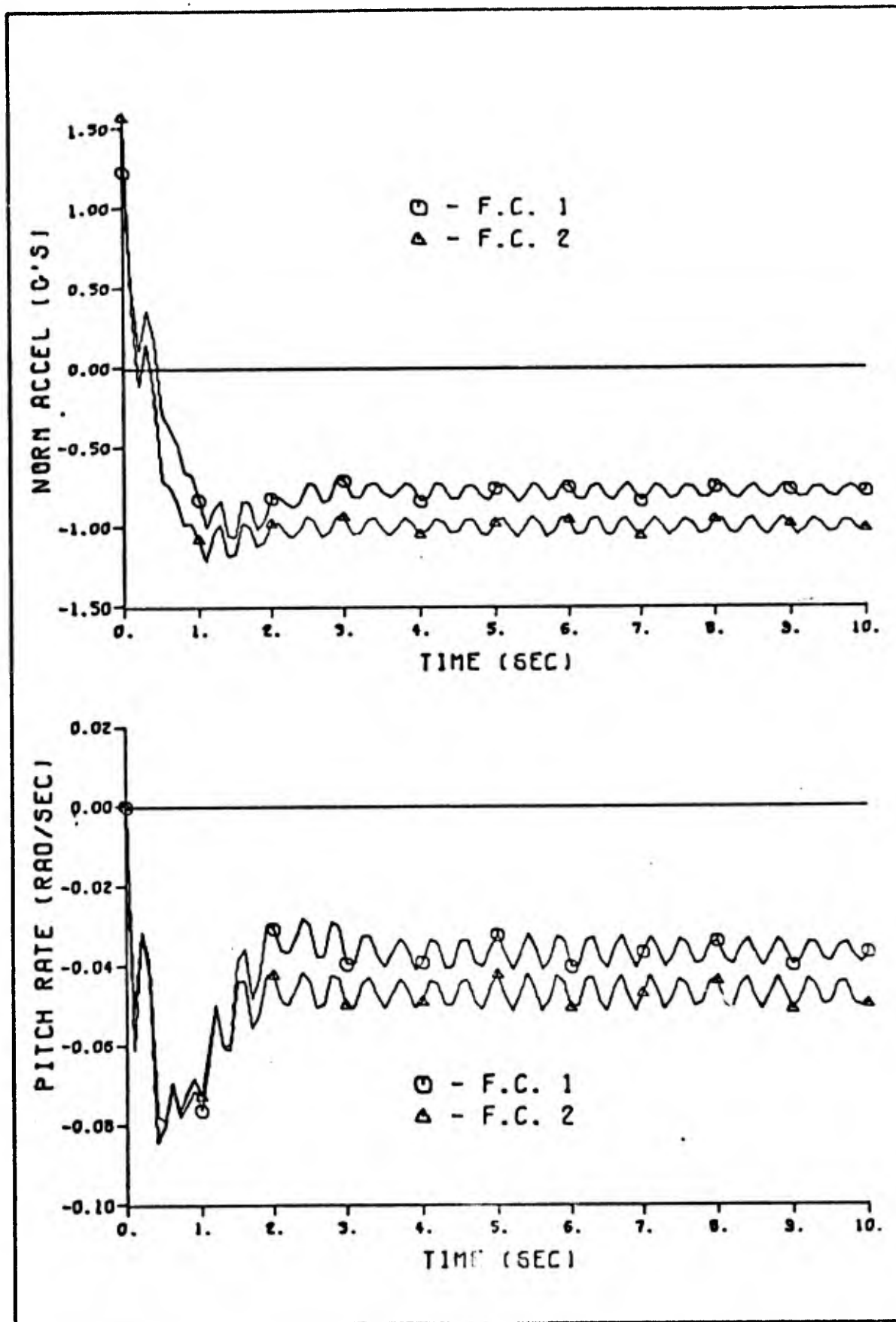
Figure 11. Normal Acceleration and Pitch Rate due to an Elevator Deflection of -0.07754 rad for both F.C. 1 and F.C. 2.

Pitch-Rate Response. For the same elevator step of -0.07754 rad the corresponding open-loop pitch-rate response for both flight conditions was obtained using MIMIC and also is shown in Figure 11. As with normal acceleration, the response combines the rigid-body effect with the oscillatory bending mode effect superimposed. For both flight conditions the response is quite rapid and oscillatory with about a 70% overshoot. The time to peak is 0.4 sec and settling time is 2.0 sec. For F.C. 2 the response oscillates about -0.047 rad/sec with a frequency of 14.9 rad/sec. For F.C. 1 the response oscillates about -0.037 rad/sec with a frequency essentially the same as for F.C. 2.

The oscillation in the response of both normal acceleration and pitch rate is due primarily to the 5th bending mode. This bending mode has the most dominant pole of all the seven bending modes. For F.C. 2 it is located at $s = -0.047 \pm j14.785$ and for F.C. 2 it is located slightly further away at $s = -0.085 \pm j14.734$, as shown in Table VII. The location of this dominant pole explains the oscillations present and correlates well with the frequency of oscillation observed in the time response.

These elevator step responses serve to characterize the aircraft and supply an idea of how quickly it can respond to a control input to the elevator. The elevator will be the only control surface used in this study and therefore the dynamic response of the aircraft to this control surface is very important.

Aircraft Dynamic Response to a Wind Gust

The basic uncompensated aircraft response to a random wind gust, w_g, must be obtained in order to have a basis of comparison for the com-
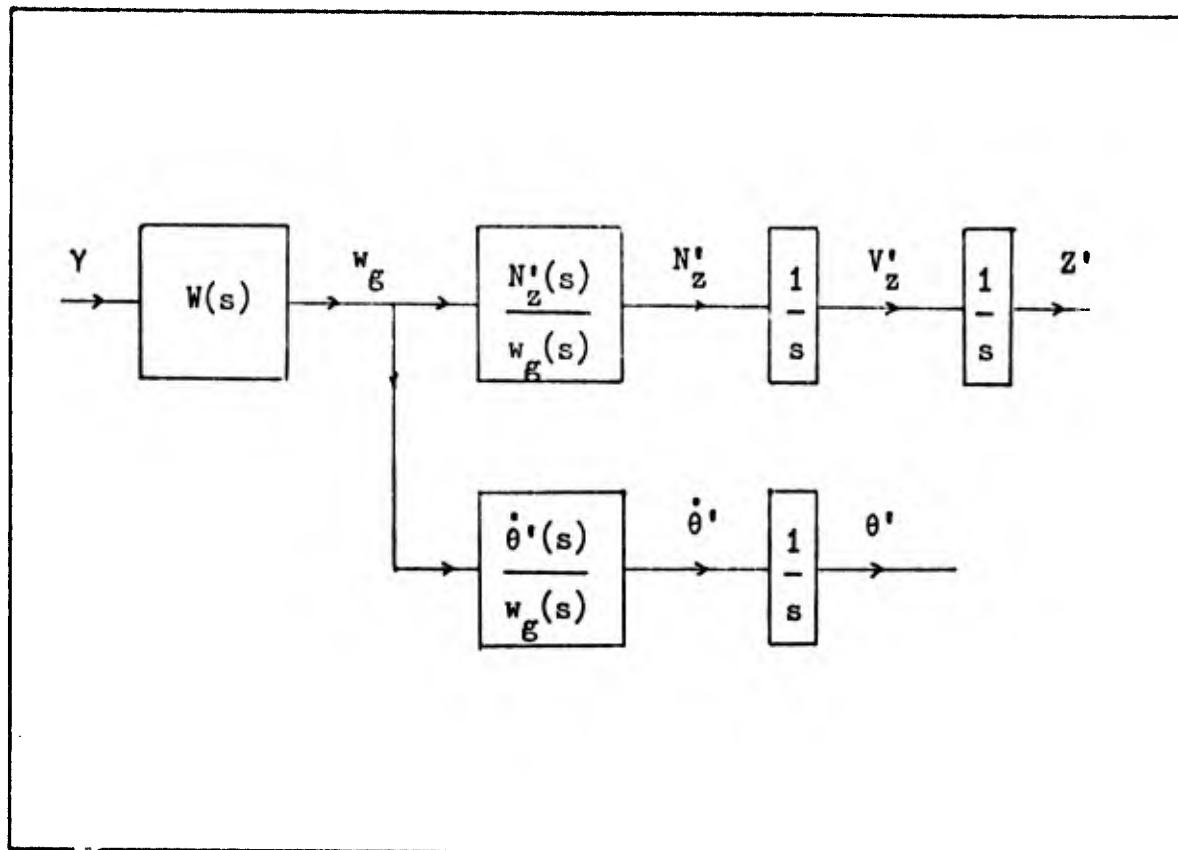
Fig re 12. Block Diagram of the MIMIC Program to Sim-
ulate the Aircraft Response to a Wind Gust

pensated aircraft response. The open-loop response is obtained, using

MIMIC, by setting up a program based on the block diagram shown above in

Figure 12.

The three transfer functions, $W(s)$, $\dot{\theta}'(s)/w_g(s)$, and $N_z'(s)/w_g(s)$

are required, in addition to three integrators. The white noise, γ, is

supplied by a random number generator which is an internal generator

within the MIMIC program. Random numbers are generated by MIMIC with a

Gaussian distribution, a mean of zero, and a standard deviation of 1.0.

A new random number is supplied at each step of the integration routine

within MIMIC.

For a printing step size of 0.2 sec, and a minimum integration step

size of 0.02 sec, plots of 20.0 sec duration were obtained for the dif-

ferent variables shown in Figure 12. Figure 13 shows the basic wind gust used for this study which is the same for all MIMIC runs. Figures 14 through 18 show the resulting output, $\dot{\theta}'$, θ', N_z', V_z', and Z' respectively. In each figure the two flight conditions are compared. The rms values of each of the variables are listed in Table VIII below. The method of computing the rms values is described in Appendix B.

Table VIII

Root Mean Square Values of

$\dot{\theta}'$, θ', N_z', V_z', and Z' for F.C. 1 and 2

F.C.	$\dot{\theta}'$ (10^{-6}rad/sec)	θ' (10^{-6}rad)	N_z' (g's)	V_z' (in/sec)	Z' (in.)
1	284.2	85.5	0.0040	0.370	0.927
2	283.6	75.2	0.0045	0.381	1.100

The data in Table VIII shows that there is very little difference in the response of the aircraft for the two flight conditions listed. Due to this very small variation with flight condition, the design work that follows will consider only F.C. 1.

The data displayed in Table VIII is not completely representative of the true aircraft because only a 20.0 sec period of time was used to obtain the results. In order to achieve greater accuracy the time response would have to be allowed to run on for several minutes which would have been prohibitive in terms of digital computer time used. It will be shown that a long time response will not be necessary, since MIMIC has the capability of comparing the uncompensated aircraft response
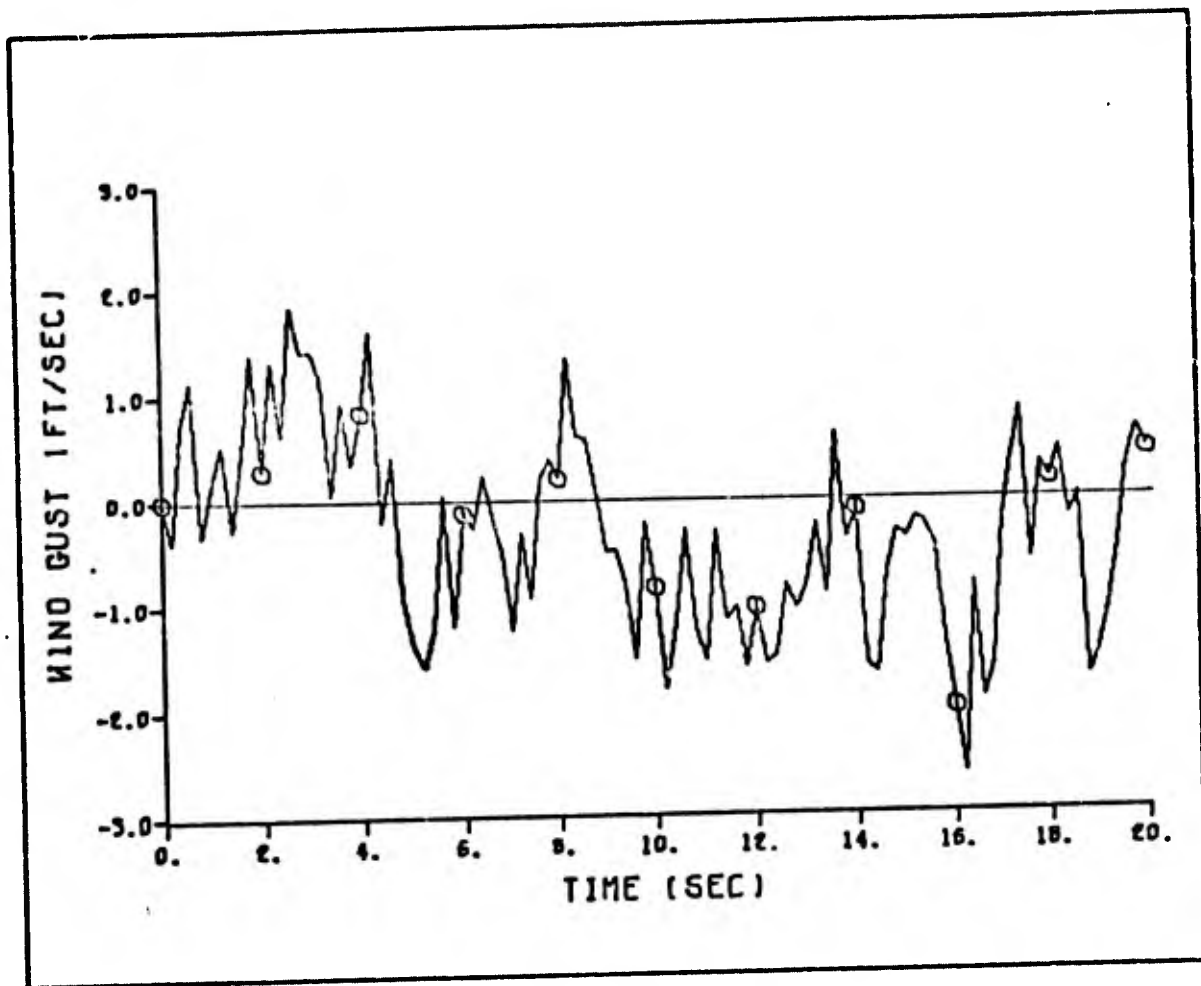
Figure 13. Normal Wind Gust of 1.0 ft/sec rms
Acting at the Aircraft Center of Gravity

simultaneously with the compensated response. The relative comparison

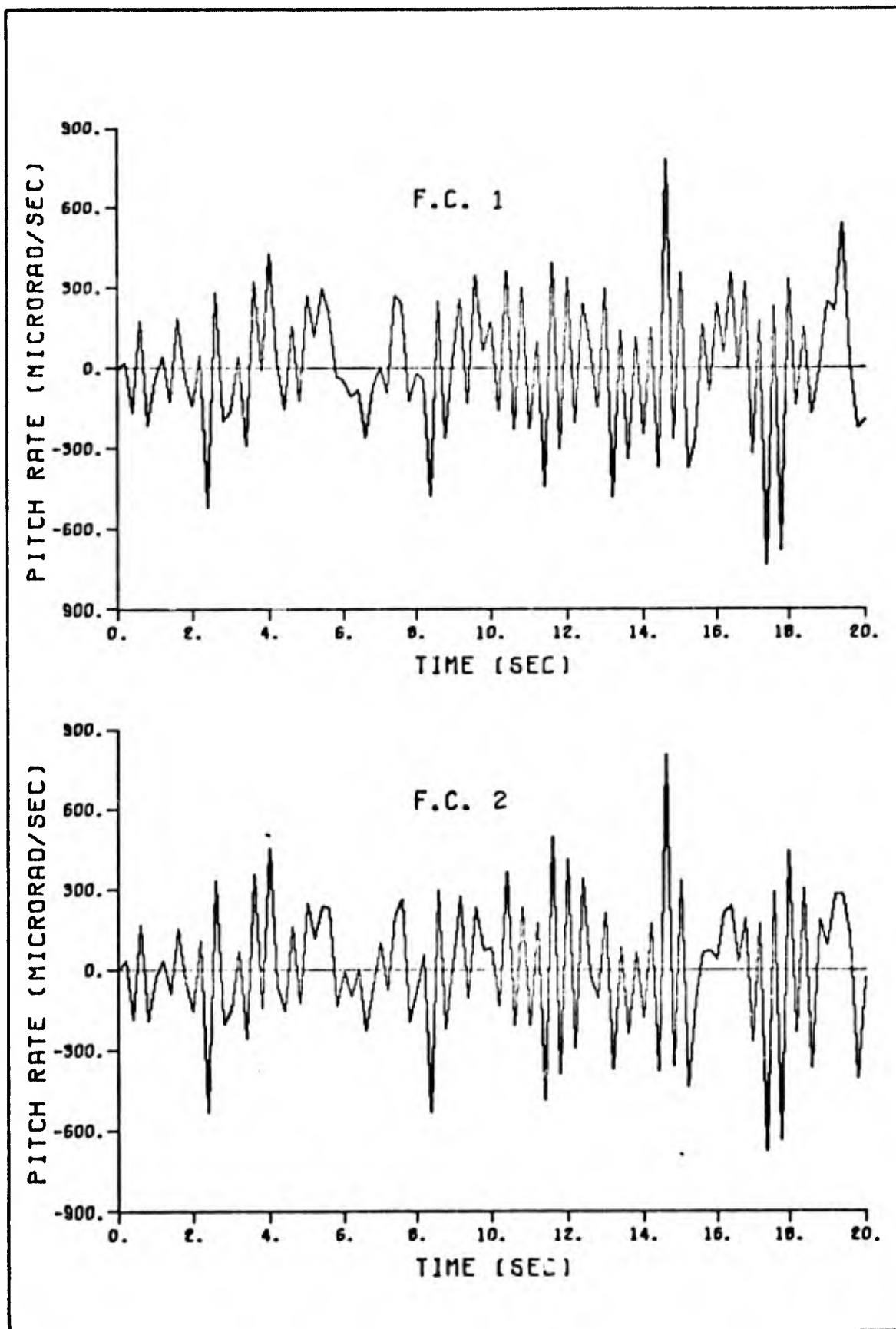of the rms values at any point in time will be of prime importance.

Figure 14. Uncompensated Pitch-Rate Response to
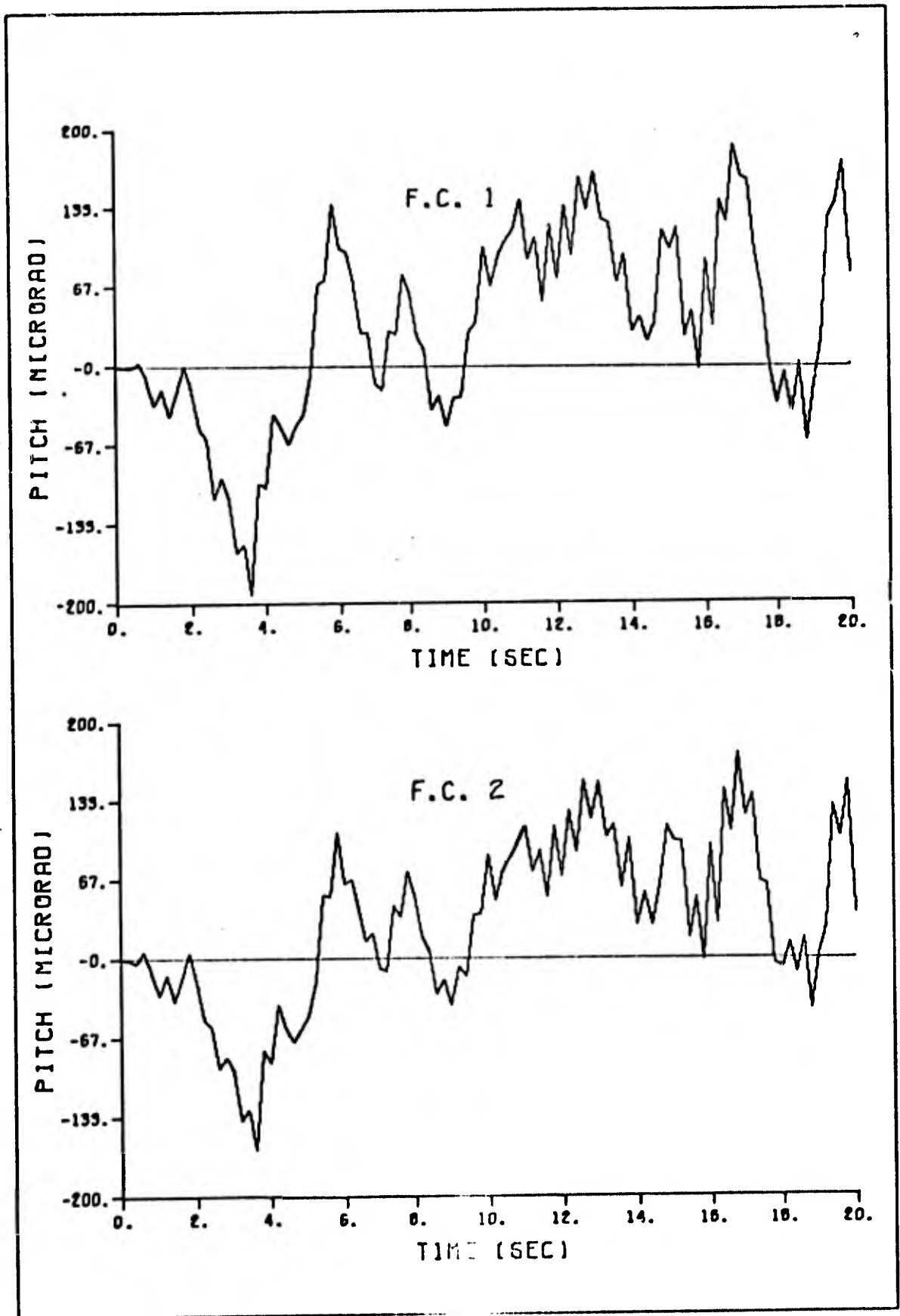a Random Wind Gust of 1.0 ft/sec rms

34

Figure 15.   Uncompensate ... on Response due to a
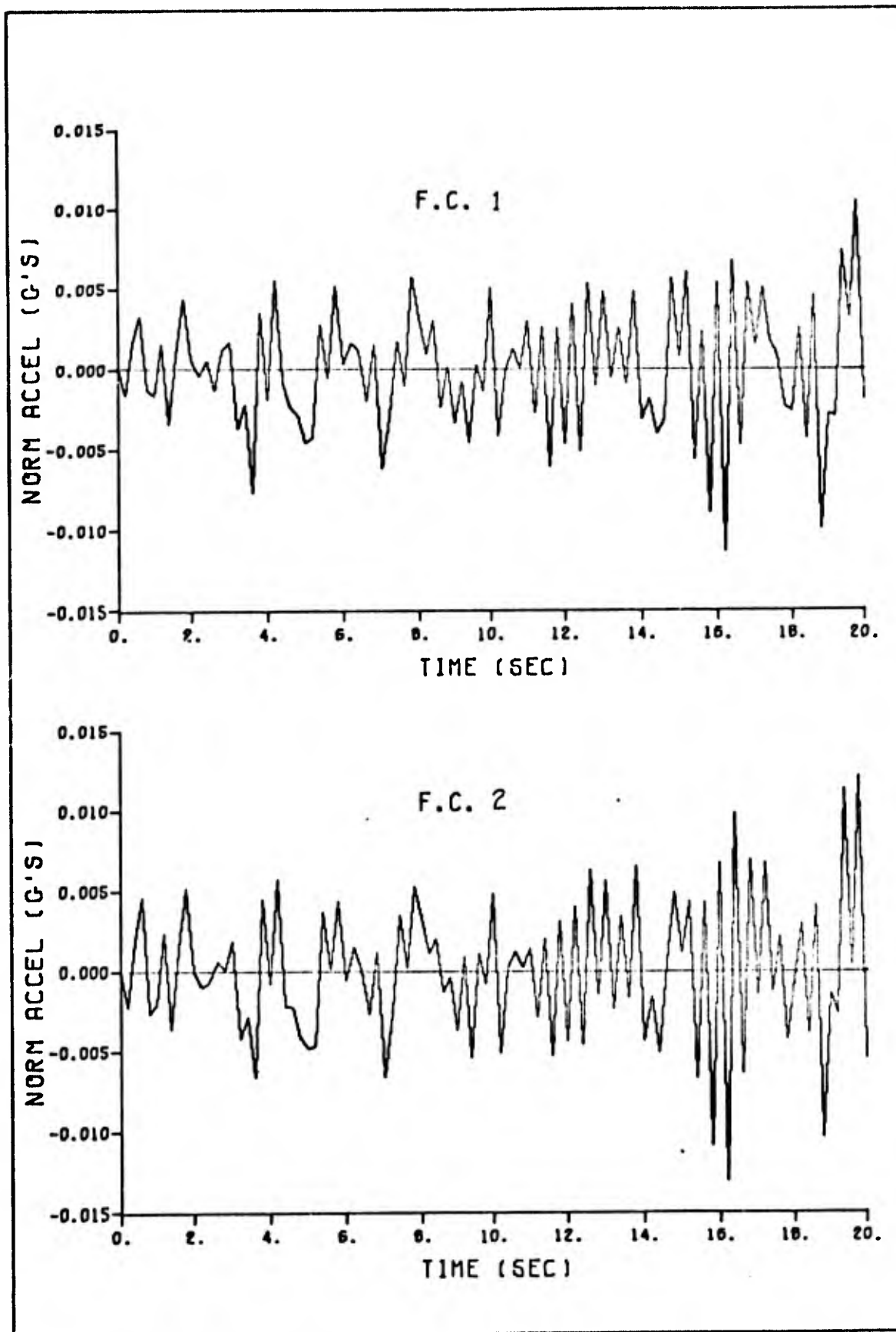
Random Wind Gust of 1.0 ft/sec rms

Figure 16.   Uncompensated Normal Acceleration due
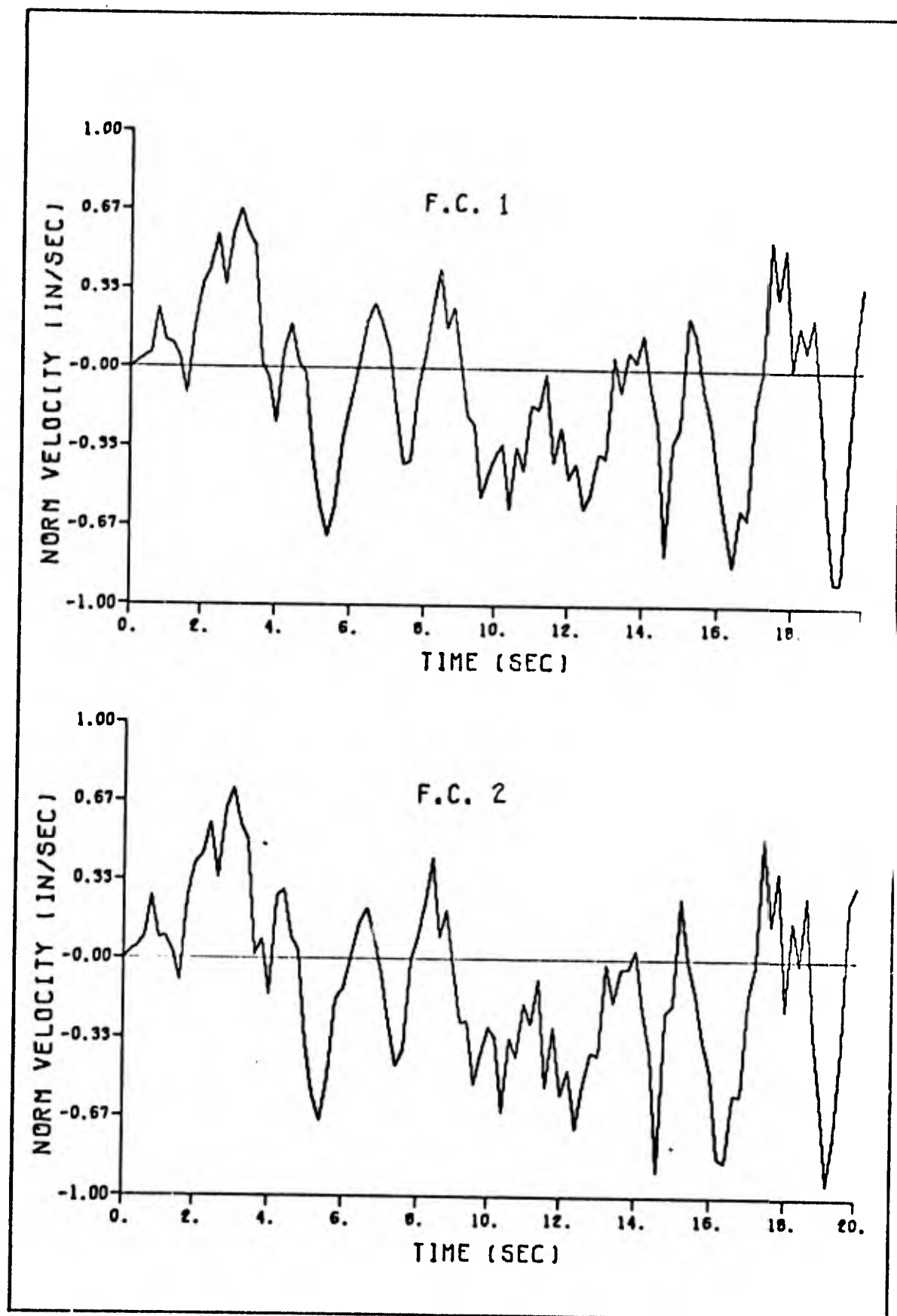
to a Random Wind Gust of 1.0 ft/sec rms

Figure 17. Uncompensated Normal Velocity due to
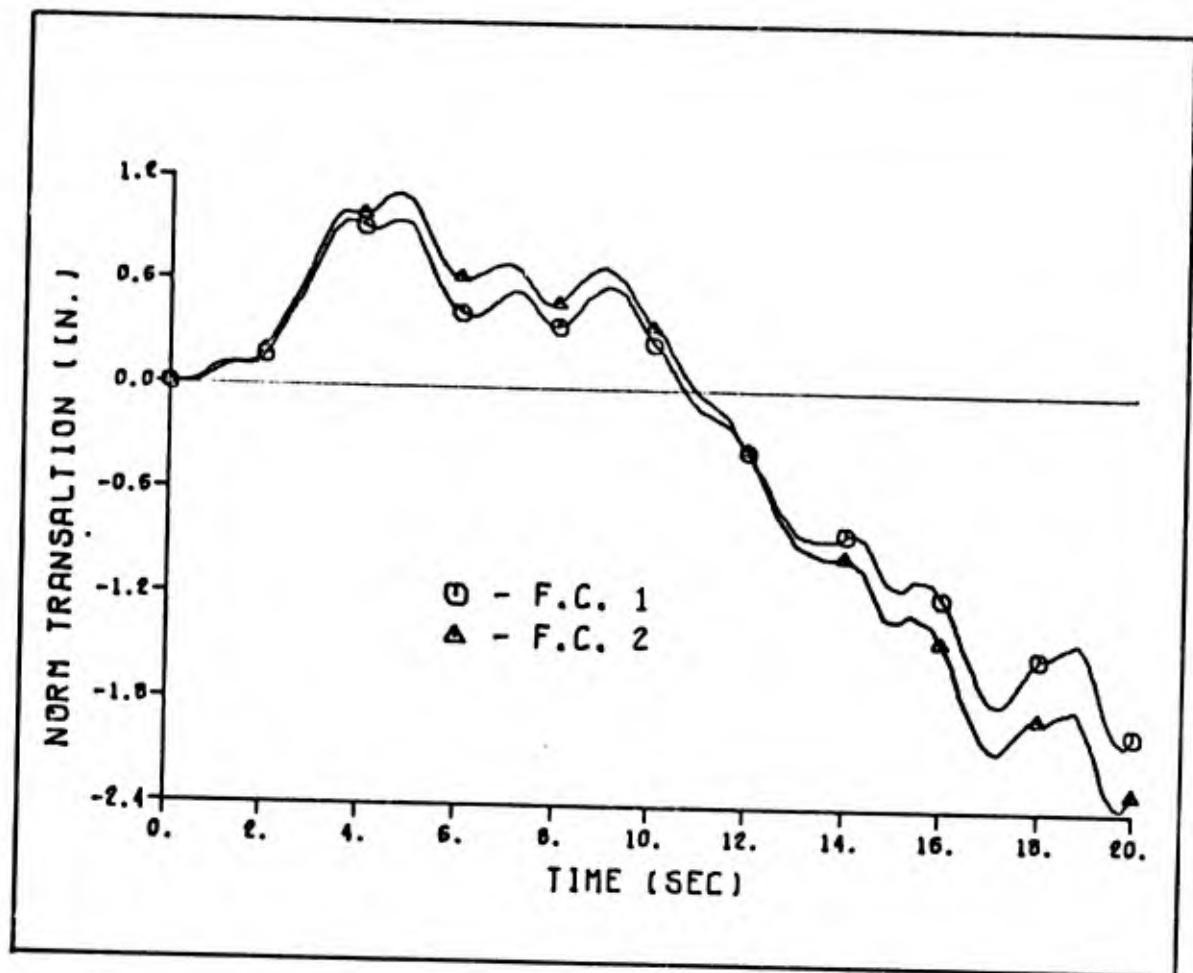
a Random Wind Gust of 1.0 ft/sec rms

Figure 18. Uncompensated Normal Translation due
to a Random Wind Gust of 1.0 ft/sec rms

IV. Design of the Control System

The description of the design of the control system is divided into three parts: (1) a discussion of the design philosophy, (2) a description of the preliminary work, and (3) a description of the final design procedure. A discussion of each part is given below.

Design Philosophy

The general control problem is that of minimizing the effects of an unwanted disturbance. D'Azzo and Houpis outline several methods to treat unwanted disturbances in their text (Ref 5:517-532). These methods include: the linear superposition theorem, feed forward compensation, conditional feedback, and the principle of invariance.

Each method lends itself to particular applications. For the application in this thesis the disturbance is the primary input to the system, with the pilot input nominally kept at zero, except in emergency. Thus, the feed forward compensation would not be effective. The principle of invariance assumes that the wind gust can be accurately measured which is not physically the case. Conditional feedback is a feasible approach, but because it uses a form of feed forward compensation, it appears to involve more complexity than using the superposition theorem. Because of this fact, the superposition approach was used in this thesis. A detailed description of the use of superposition will be made in the section on design procedure.

Preliminary Work

The objective of the control system is to minimize variations in pitch angle and normal translation at B.S. 1799 of the aircraft due to

a wind gust. This requires that sensors be placed at B.S. 1799 to sense pitch rate, $\dot{\theta}$, and normal acceleration, N_z. This information would then be fed back through a compensator system to the input of the elevator servoactuator. The elevator would be commanded to deflect in such a way as to counter the effects of the wind gust. A tentative feedback control system is block diagramed in Figure 19.
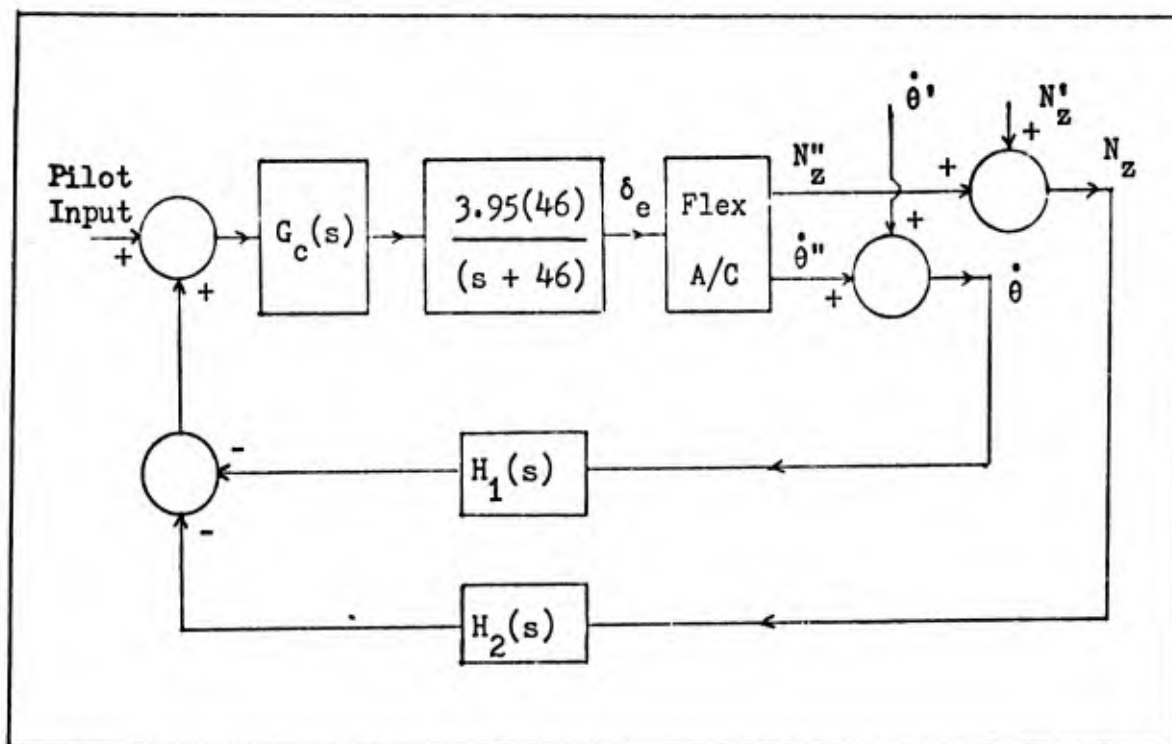
Figure 19. Tentative Form of the Control System

In Chapter II it was found that the basic aircraft, for F.C. 1, had an rms normal translation, Z'_{rms}, of 0.927 in. with an rms variation in pitch, θ'_{rms}, of 85.5 microrad for a 1.0 ft/sec rms wind gust. If the optical instrument is pointed at a target 40,000 ft away, the normal translation will have little effect, but the pitch angle will be significant. The rms deviation from the target at a range of 40,000 ft, due to pitch would be 3.0 ft. The rms deviation, due to normal trans-

lation, would be 0.927 in. regardless of range. If the deviation due to variation in pitch could be reduced by 90%, the deviation at the target, due to pitch variation would still be 3.9 times as large as the deviation due to translation. For this reason, the control of pitch rate is the more important consideration.

Another reason for considering the pitch-rate loop to be the more important loop is that a simultaneous improvement in both pitch and translation could not reasonably be made using only one control surface. The error signal going to the elevator servoactuator would be composed of two signals -- one from the pitch-rate loop and one from the normal-acceleration loop. Even if a simultaneous reduction of both pitch and translation could be achieved, the reduction in translation would be the least significant portion of the total reduction in rms deviation from the target at a range of 40,000 ft.

This description of some of the preliminary work that was done has served as an introduction. The rest of this chapter will describe the feedback system that became the final design. The foregoing discussion has narrowed the objective to one of minimizing the variation in pitch and merely monitoring the normal translation.

Final Design Procedure

The basic reduced system can be block diagramed as is shown in Figure 20. By the superposition theorem. the total pitch rate can be found for both the desired and undesired in t to the system (Ref 5:520-521). For w_g equal to zero

$$\dot{\theta}(s)\Big|_{w_g=0} = \frac{C_1(s)}{1 + C_1(s)H_1(s)} \dot{\theta}_{com}(s) \tag{11}$$
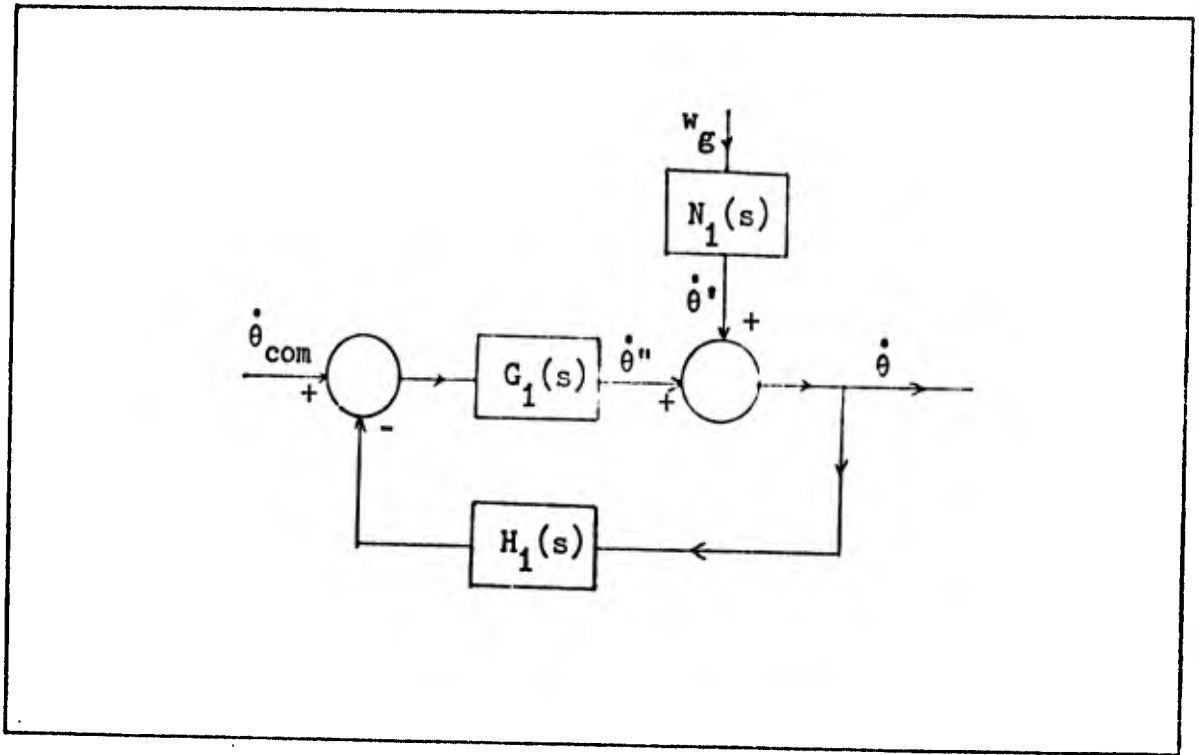
Figure 20. Reduced Design Block Diagram
(Adapted from Ref 5:520)

For $\dot{\theta}_{com}(s)$ equal to zero

$$\dot{\theta}(s)\bigg|_{\dot{\theta}_{com}=0} = \frac{N_1(s)}{1 + G_1(s)H_1(s)} \, w_g(s) \tag{12}$$

Combining Eqs (12) and (13) results in

$$\dot{\theta}(s) = \dot{\theta}(s)\bigg|_{w_g=0} + \dot{\theta}(s)\bigg|_{\dot{\theta}_{com}=0}$$

$$= \frac{G_1(s)}{1 + G_1(s)H_1(s)} \, \dot{\theta}_{com}(s) + \frac{N_1(s)}{1 + G_1(s)H_1(s)} \, w_g(s) \tag{13}$$

The effect of the wind gust on pitch rate can be minimized by examining these equations. Equations (11) and (12) have a common factor $1/[1 + G_1(s)H_1(s)]$. Using frequency response calculations it can be

seen that in order to minimize the effect of the wind gust, the ratio

$$\frac{\dot{\theta}(s)\Big|_{\dot{\theta}_{com}=0}}{\dot{\theta}(s)\Big|_{w_g=0}} = \frac{N_1(s)w_g(s)}{G_1(s)\dot{\theta}_{com}(s)} \tag{14}$$

should be made as small as possible. $N_1(s)$ represents a physical charac-teristic of the system so it cannot be altered. Thus $G_1(s)$ is the only available quantity to work with and should be made as large as possible.

For the basic aircraft the block, $G_1(s)$, contains both the flexible aircraft dynamics, which cannot reasonably be altered, and the elevator servoactuator. The design procedure followed in this study will be to add a simple cascade compensator to $G_1(s)$ to accomplish the goal of re-ducing the variations in pitch angle. A block diagram of the resulting system is shown in Figure 21.
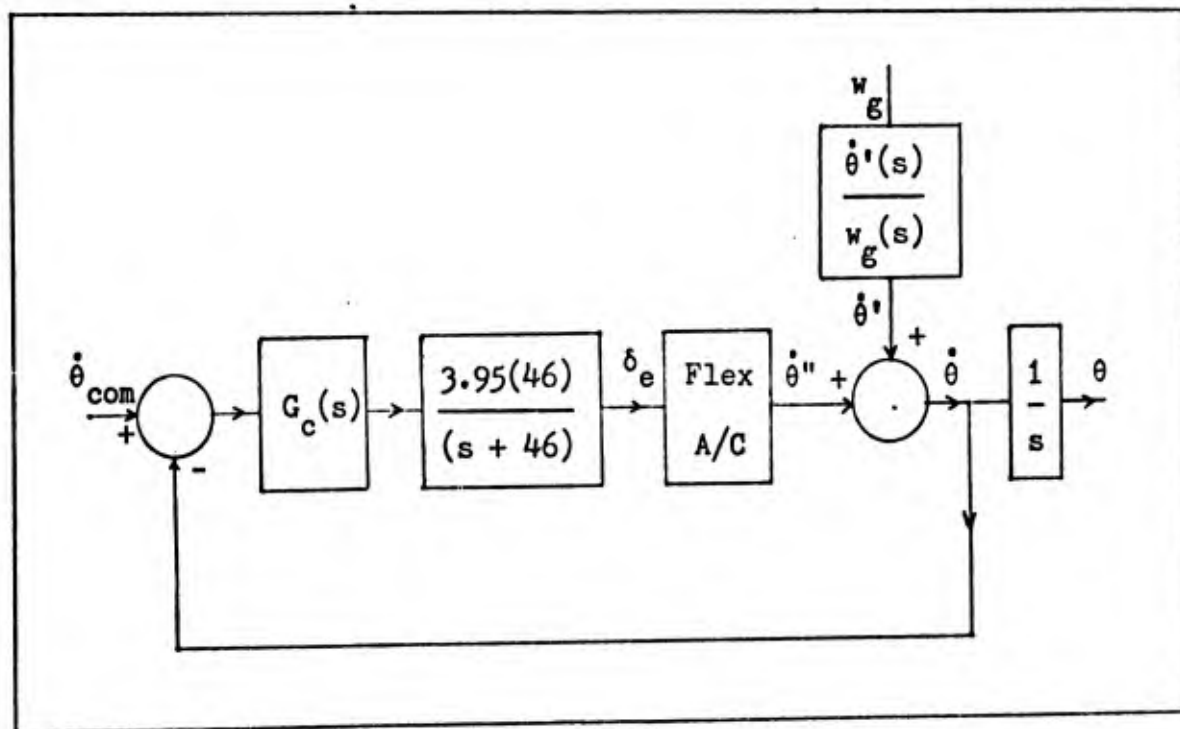

Figure 21. Pitch-Rate Loop for Design Purposes

$H_1(s)$ is assumed equal to unity so that the input, $\dot{\theta}_{com}$, can be directly compared with the output, $\dot{\theta}$. This assumes that the bandwidth of the pitch-rate sensor is wide enough to actually feedback the correct signal.

For F.C. 1 the root locus of the pitch-rate loop without any cascade compensation was plotted and is shown in Figure 22, from which it can be seen that the root locus is stable for all gain. Figure 23 contains a more detailed root locus of the region within the dotted line of Figure 22. The small triangles indicate the location of the roots for a gain of 2. By inserting increased gain only in the cascade compensation block, $G_c(s)$, the effect of the wind gust should be minimized. However, increasing the gain drives the roots from the bending mode pole at $s = -2.348 \pm j14.701$ into the zero at $s = -0.516 \pm j9.612$. For infinite gain the damping ratio would be 0.054 which would be very lightly damped.

Other dominant roots of the root locus occur between the poles and zeros of the other bending modes, which almost cancel each other. Due to this near cancellation, the effect of these roots would appear to be less significant in the time response. If, however, the aircraft was excited at one of its resonant frequencies violent oscillations would occur. The wind gust is of low frequency as seen from the Bode diagram of $w_g(s)/\gamma(s)$ in Figure 6.

For a gain of 2.0 the roots of the root locus are shown in Table IX on page 47. The roots at $s = -25.338 \pm j62.076$, which migrate from the rigid-body poles, are not significant in the over-all step response because they have such a short time constant. However, the effect of these roots is to initially speed up the rise time due to the high damped-natural frequency.

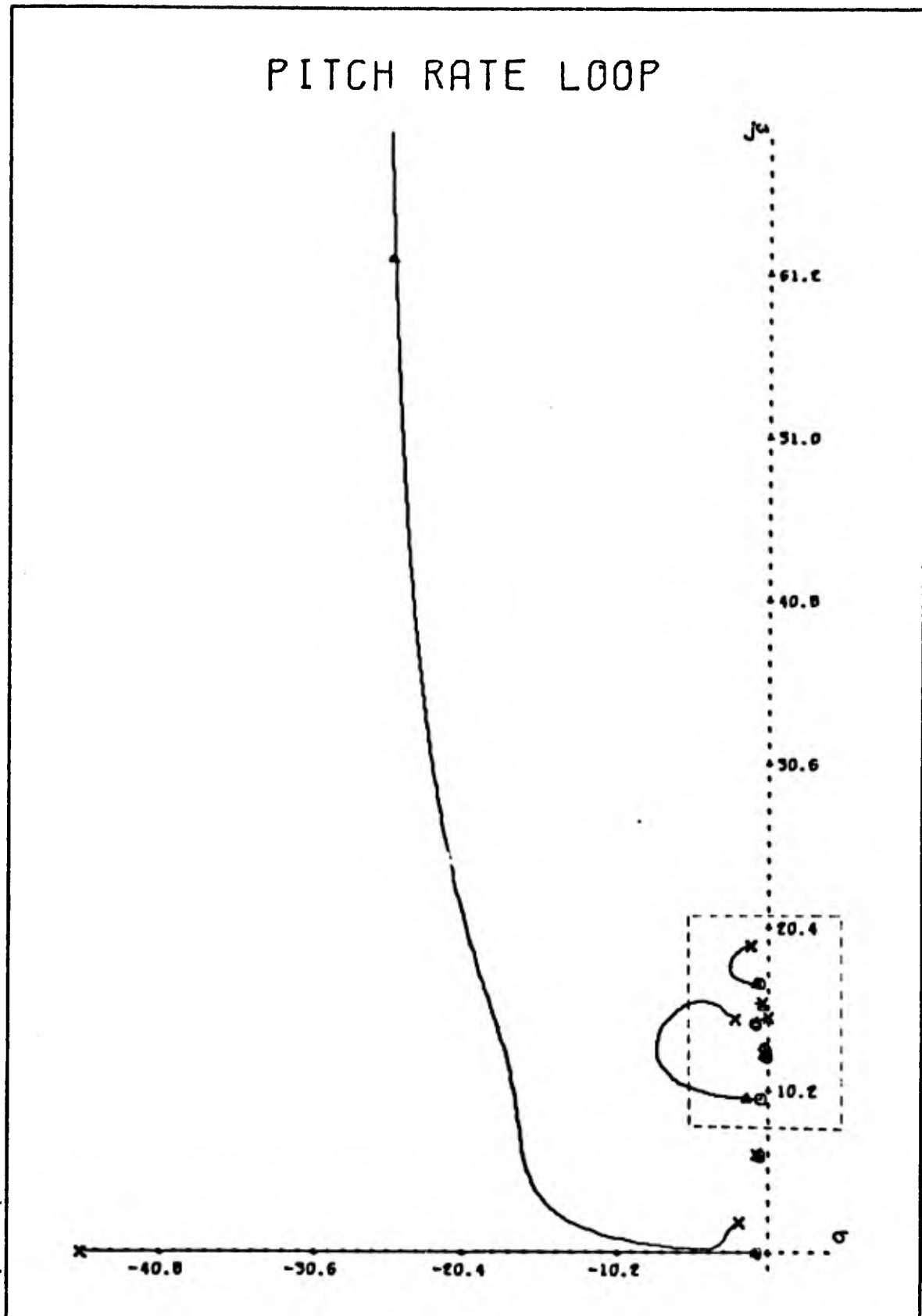A trade-off must be made between a high-gain system, which would be

Figure 22.   Root Locus of Pitch-Rate Loop.
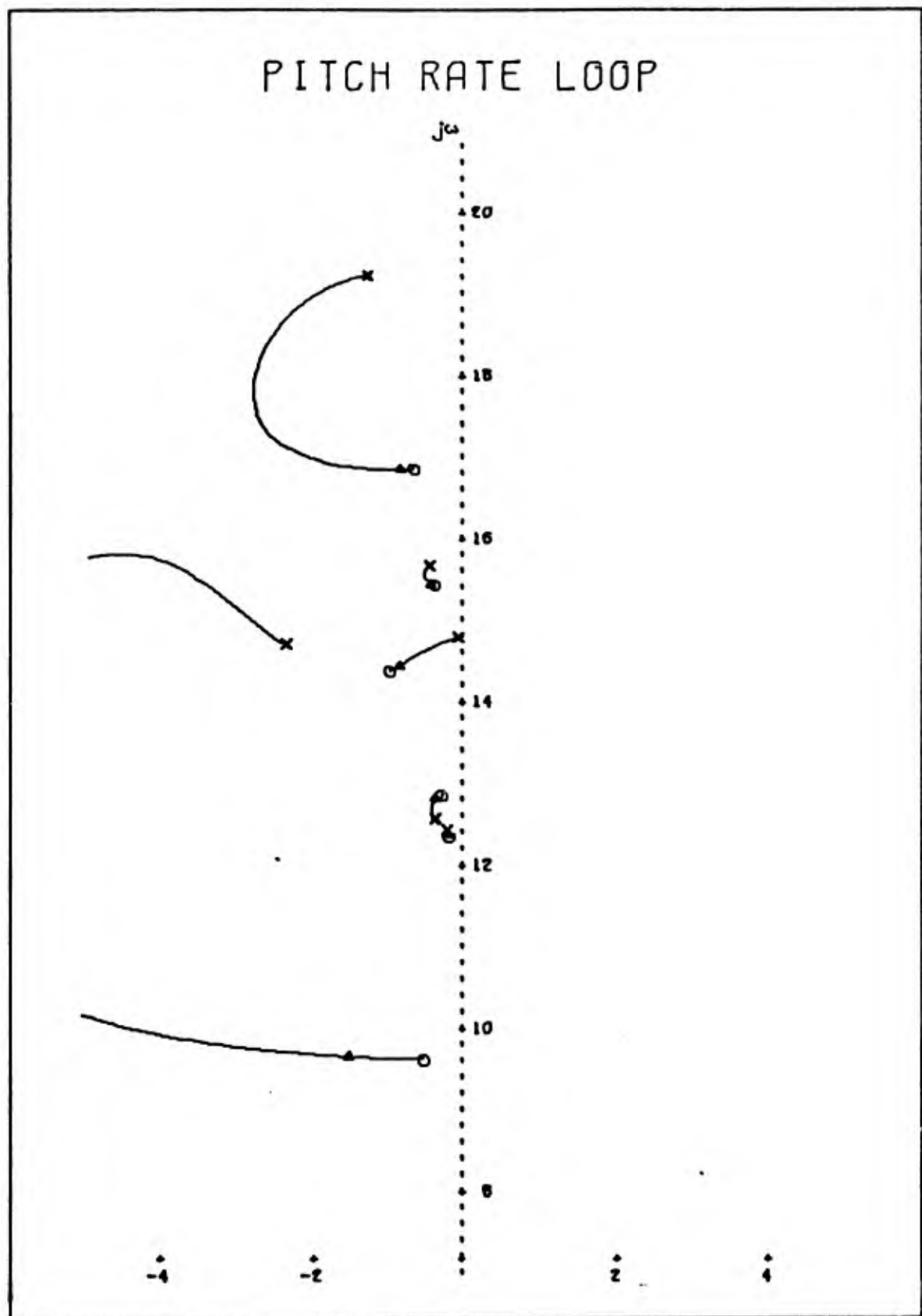Note: See Figure 23 for inset.

Figure 23. Root Locus of Pitch-Rate Loop -- Inset.

Table IX

Roots of Pitch-Rate Root Locus for a Gain of 2.0

---

s_1 = -0.884

$s_{2,3}$ = -0.679 ± j6.043

$s_{4,5}$ = -1.548 ± j9.646

$s_{6,7}$ = -0.172 ± j12.370

$s_{8,9}$ = -0.344 ± j12.816

$s_{10,11}$ = -0.844 ± j14.430

$s_{12,13}$ = -0.401 ± j15.435

$s_{14,15}$ = -0.831 ± j16.849

$s_{16,17}$ = -25.338 ± j62.076

---

lightly damped, and a low-gain system of higher effective damping ratio. The high-gain system would achieve the goal of minimizing the effect of the wind gust, but would be oscillatory to a pitch-rate command. A low-gain system would respond better to a pilot command, but would not do as good a job at minimizing the effect of the wind gust.

Since the objective of this study would best be met by a high-gain system, this is the approach that was used. However, a gain will be chosen only high enough to achieve approximately an 80% reduction in pitch variations at B.S. 1799. This ill be shown to be consistent with the sub-goal of maintaining satisfact y handling qualities. The next chapter will deal with the simulation of the aircraft dynamics and the finalization of how much gain is n   y to achieve this goal.

Effect of the System on Normal Translation. With this system the pitch variations will be the only quantity controlled. Variations in normal translation are assumed to be of secondary importance. The effect of the pitch-rate control on normal translation will be investigated using the two transfer functions, $N_z''(s)/\delta_e(s)$, and $N_z'(s)/w_g(s)$, and summing the contributions from both of them in a manner similar to that in which the pitch-rate transfer functions were used. A block diagram of the added transfer functions is shown in Figure 24.
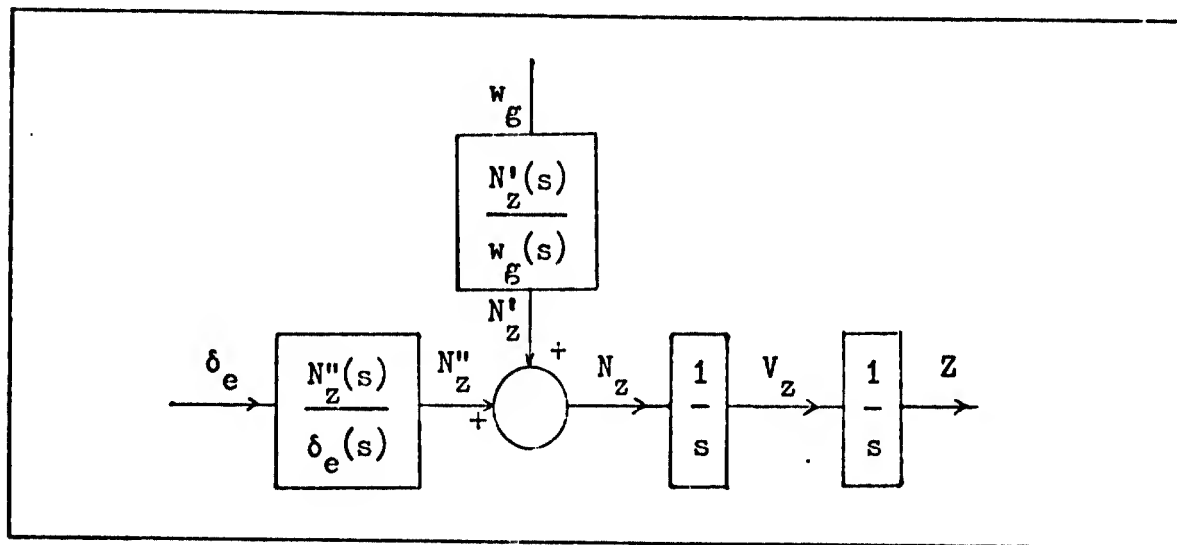
Figure 24. Normal Acceleration Block Diagram
to be added to Figure 21

Effect of the System on Other Body Stations. The analysis has focused attention on only B.S. 1799. Although this body station is of prime importance, the effect of the control system at the pilot station, B.S. 172, and near the center of gravity of the aircraft at B.S. 805, will be investigated. The transfer functions for the pitch rates due to elevator deflection at each of these body stations were found using the VALUE program. The mode slopes at each body station are tabulated in Table X. The values from Table X are substituted into the equation for

Table X

Elastic Mode Slopes at B.S. 172 and B.S. 805

Subscripts	Mode Slopes	
(i)	$-\Phi_i'$ (in/in)	
	B.S. 172	B.S. 805
3	0.002049	0.00932
4	0.000556	0.00433
5	0.003380	0.000935
6	0.03228	0.00985
7	0.1471	0.0455
8	0.02248	0.00485
9	0.1423	0.0494

(From Ref 1)

pitch rate, as given in Chapter II on page 13, and the basic VALUE pro-
gram is augmented by two new rows and columns corresponding to the two
new pitch-rate equations. By successively modifying the matrix and
solving for the eigenvalues, the desired transfer functions were obtain-
ed. Table XI lists the zeros of the numerators of each transfer function
for F.C. 1. Bode plots of each new transfer function are shown in Fig-
ures 25 and 26.

These new transfer functions can be used to obtain the pitch-rate
response at the pilot station and near the center of gravity caused by
the control system. The block diagram, to be added to Figure 21, is

Table XI

Zeros of $\dot\theta_{172}(s)/\delta_e(s)$ and $\dot\theta_{805}(s)/\delta_e(s)$

Numerators for F.C. 1

		$\dot\theta_{172}$	$\dot\theta_{805}$
Gain	$K_{\dot\theta}$	-2.044	2.667
1st Term	a	-0.814	-0.791
2nd Term	b	$-0.665 \pm j6.097$	$-0.656 \pm j6.096$
3rd Term	c	$-0.301 \pm j12.330$	$-0.345 \pm j12.281$
4th Term	d	$-0.203 \pm j12.616$	$-0.160 \pm j12.582$
5th Term	e	$-0.983 \pm j14.668$	$-1.277 \pm j14.690$
6th Term	f	$-0.717 \pm j15.314$	$-0.358 \pm j15.120$
7th Term	g	$-0.036 \pm j16.301$	$0.174 \pm j16.145$
8th Term	h	-21.635	$-1.257 + j19.789$
9th Term	i	21.850	$-1.257 - j19.789$

$$\frac{\dot\theta_{xxx}(s)}{\delta_e(s)} = \frac{K_{\dot\theta}(s-a)(s-b)(s-c)(s-d)(s-e)(s-f)(s-g)(s-h)(s-i)}{Denom^*}$$

*: See Table VII

shown in Figure 27.

The pitch and pitch rate that will result from the system of Figure 27 will not be the total pitch rate and pitch. Effects of the wind gust will not be included in order to hold down the complexity of the simulation. A comparison will be ... between pitch rates at body stations 172, 805, and 1799 due only to the elevator deflection, δ_e. Corresponding comparisons of pitch angle will also be made. If the respec-
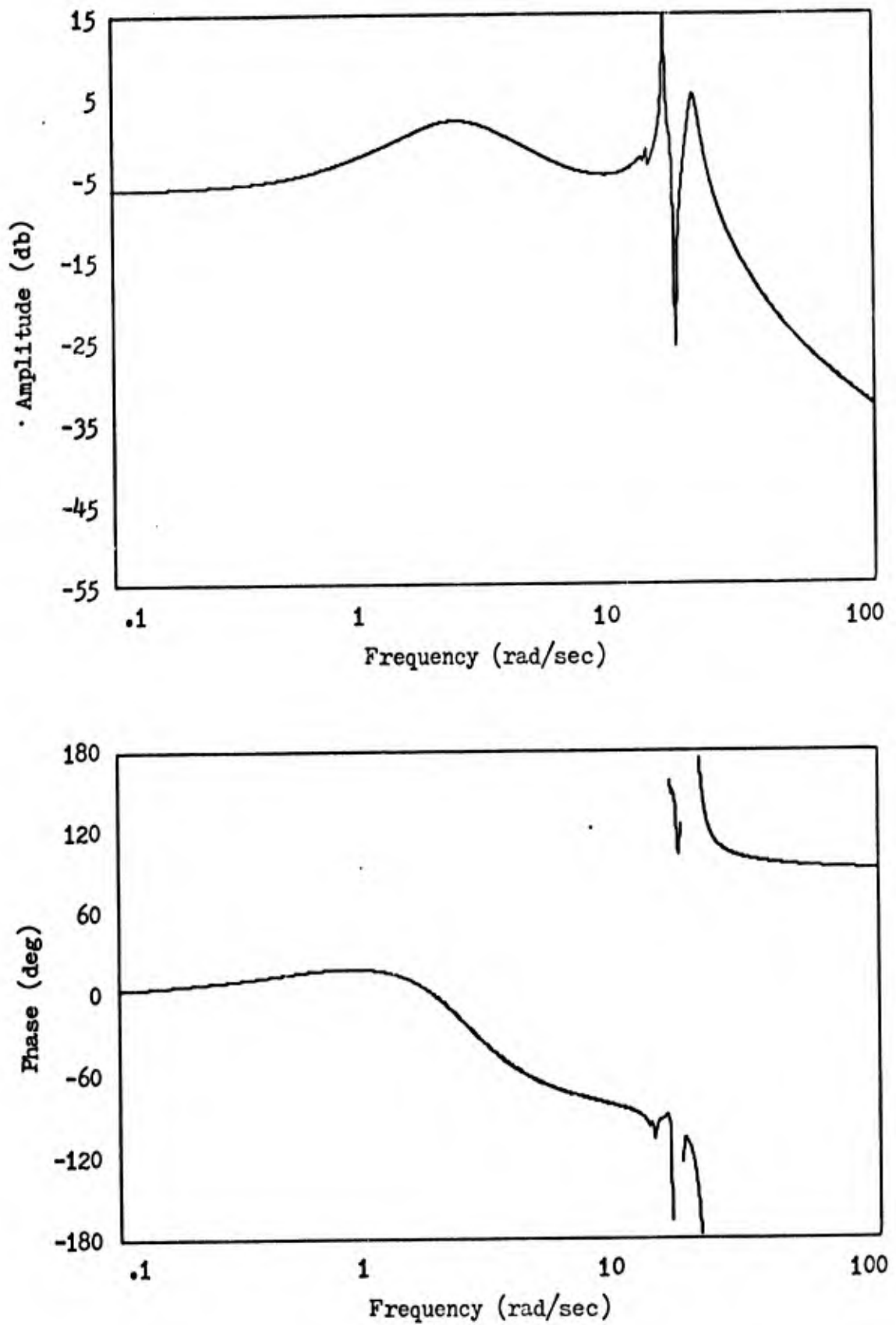
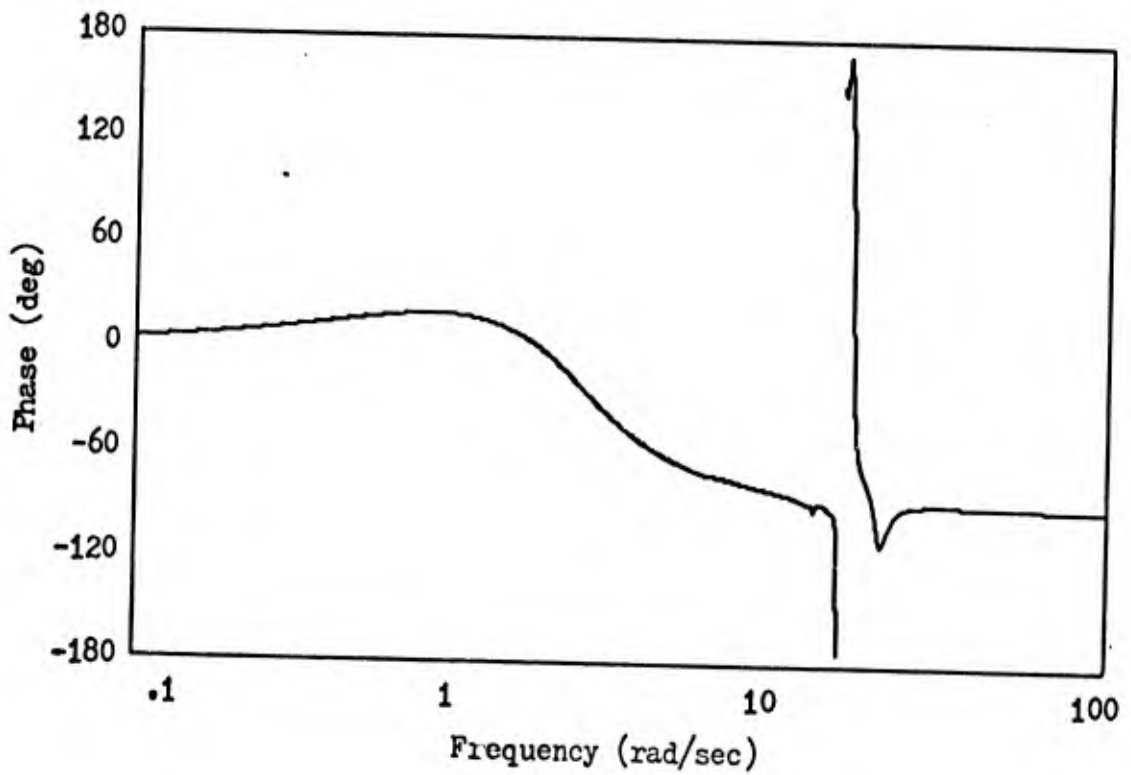Figure 25. Bode Plot of $\dot{\theta}_{172}(s)/\delta_e(s)$ Transfer Function.
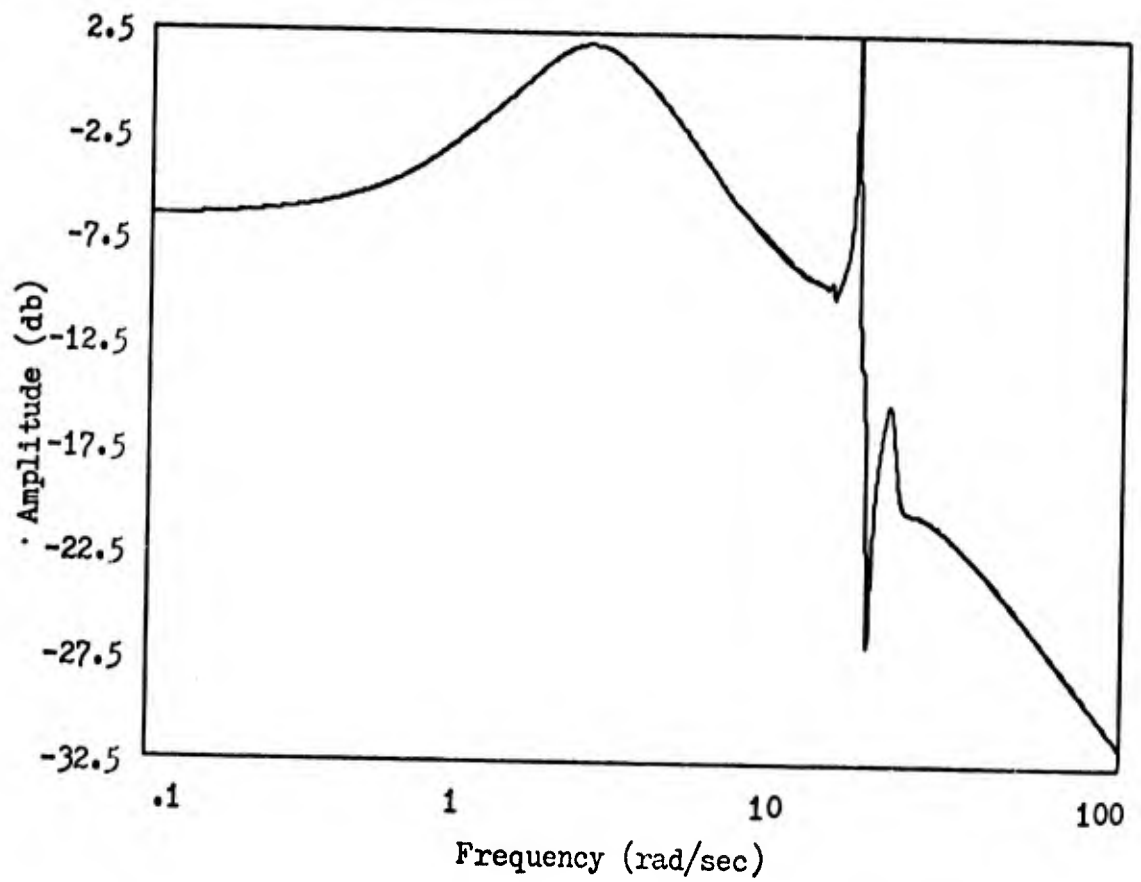
Figure 26. Bode Plot of $\dot{\theta}_{805}(s)/\delta_e(s)$ Transfer Function.

52
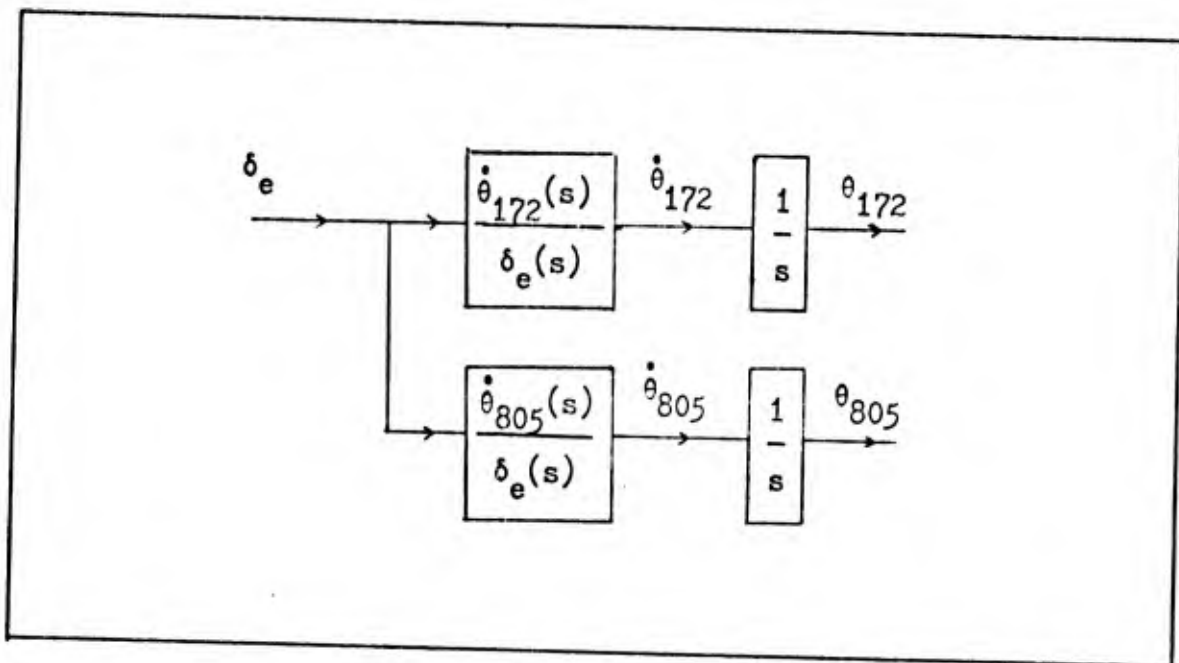
Figure 27. Block Diagram for Pitch and Pitch Rate at B.S. 172 and B.S. 805 due to Elevator Deflection, δ_e

tive rms values of these quantities are approximately equal, it will indicate that there are no major adverse effects on the total aircraft resulting from the operation of the new control system.

The basic system is shown in Figure 21. Figure 28 is a block diagram of the total simulation, including the basic system plus the normal acceleration blocks and pitch-rate blocks at B.S. 172 and B.S. 805.

Effect of Pilot Pitch-Rate Command. Since the purpose of the new system is to minimize variations in pitch angle, the system would normally only operate with a pitch-rate command, $\dot{\theta}_{com}$, of zero. All control surfaces, with the exception of the elevator, would be locked in trim condition. It would, however, be desirable for the system to be able to respond to a pitch-rate command, $\dot{\theta}_{com}$, from the pilot. A sudden maneuver may be necessary with the system turned on and if the pilot failed to switch the system off before the maneuver, the aircraft should still respond in a reasonable manner.

When the system is operating normally no stray pitch-rate command, $\dot{\theta}_{com}$, should be allowed to enter the system. The intent of the system would be defeated if this were to occur. For this reason, a dead-zone should be made to exist between the pilot command and the system. Only pilot commands above a certain set value would influence the aircraft. Thus, the system could be overridden, if necessary.

Summary of Design

The total control system will be demonstrated to work well for a gust input only, and also respond adequately to the addition of a pilot pitch-rate command. Chapter V will deal with the simulation and results.
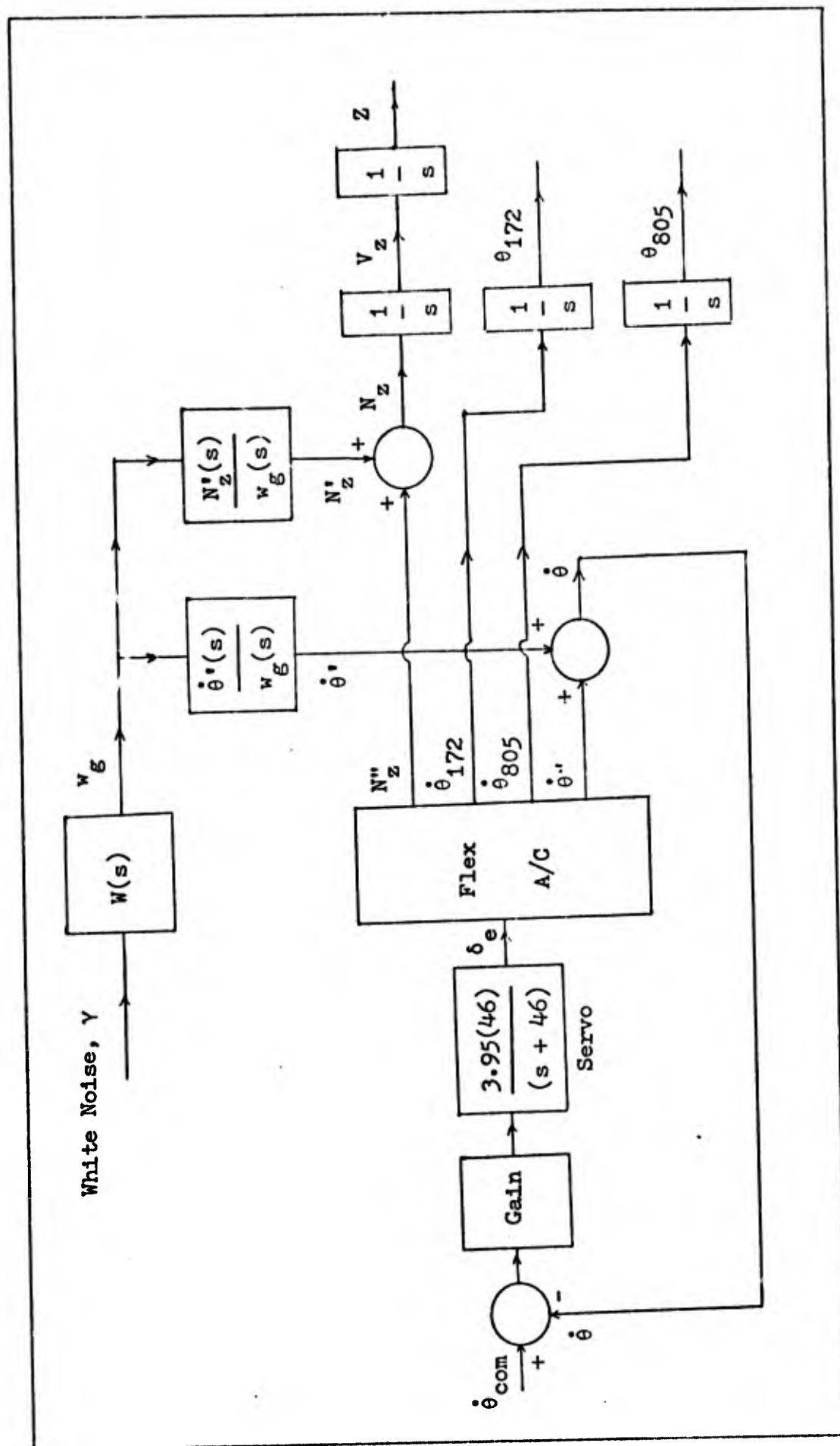
Figure 28. Total Block Diagram to be Simulated using MIMIC

V. Simulation of Results

The control system, described in Chapter IV and shown in Figure 28, was simulated using the MIMIC program. Appendix A explains how the transfer functions were written in acceptable statements for MIMIC. Appendix C contains a listing of the entire program written to simulate the block diagram shown in Figure 28. For more complete details on MIMIC the interested reader is directed to Reference 8.

Simulation

A total of 124 integrators were used to simulate the control system of Figure 28 -- 16 for each major transfer function. The rms values of all important outputs were calculated as described in Appendix B.

Elevator Limits. Since the maximum rate of deflection of the elevator is $\pm$ 1.4 rad/sec, a limiter was included in the MIMIC program to accomplish this limiting process. The maximum deflection angle, before hitting the stops, is $\pm$ .35 rad. Only at the initial portion of the pilot pitch-rate command did the deflection rate attain its maximum value. Under normal wind gust conditions the maximum deflection rate did not exceed 0.005 rad/sec in absolute value.

Wind Gust Simulation. By using the random number generator in MIMIC and the wind filter described in Chapter II, the proper form of the wind gust was available as an input to the control system. An additional gain of 5.231 was necessary to bring the rms wind gust level up to 1.0 ft/sec and was added directly after the wind filter.

Format of Data and Generation of Plots. MIMIC is very flexible.

It allows for the programmer to print out any or all of the variables defined in the program at any specified increment of time. It also allows the output of up to six printer plots with up to six variables per plot for each run. The maximum number of points plotted for each variable is 100.

The plots, which take up two printer pages, allow for easy comparison of results during the design work but are not easily included in a thesis. For this reason, the data was transferred to cards and a Calcomp plotting routine was set up to plot the data and connect the data points.

Results

The value of gain, necessary to achieve good minimization of variations in pitch angle, was found to be 2.0. This small amount of gain was sufficient to reduce the rms value of pitch variation by 83.3% compared to the uncompensated aircraft response obtained in Chapter III. Gains of up to 2000 were tried and provided for almost 100% elimination of the variations in rms pitch due to the wind gust disturbance.

This proved the theory, but such a high gain is impractical, and can prove dangerous. A component failure at that gain could drive the elevator into the stop and overload associated equipment. In addition, the added gain of 1000 only buys a further 17% improvement.

Response of Compensated System to Wind Gust. For a gain of 2.0, and with the wind gust as the only input to the aircraft, a MIMIC run was made to obtain a 20 sec time response. Data was output every 0.2 sec resulting in 100 data points for each variable. The minimum digital integration step size was 0.02 sec. The data for the variables of inter-

est were transferred to computer cards and plotted using the Cal-comp plotter.

Comparison of pitch rate, pitch, and normal translation for the compensated and uncompensated aircraft are shown in Figures 29 through 31. The rms values of these variables are listed and compared in Table XII. It should be noted that improvement in rms pitch variation resulted in a corresponding increase in rms normal translation of 2.62 times that of the uncompensated case. For a range of 40,000 ft, as argued in the preliminary work of Chapter IV, the rms normal translation is insignificant compared to the rms variation in pitch angle. These results also indicate that a simultaneous improvement of both quantities cannot be made with only the elevator as the control surface.

The rms elevator deflection necessary to accomplish this control was 0.000265 rad. Figure 32 gives a time response of the elevator deflection. The effect of the elevator deflection is to effectively reduce the variations in pitch at B.S. 1799, due to the wind gust, by 83.3%.

The effects of the elevator on the pilot station, B.S. 172, and on B.S. 805 near the center of gravity, were also investigated. Due to the flexibility of the aircraft, it was expected that the pitch and pitch rate at all three body stations would not be identical. They should, however, not vary significantly in rms magnitude. Figures 33 and 34 show the pitch rate and pitch at the three body stations. It must be pointed out that these responses are not the actual pitch rate and pitch at these body stations. They are only the contribution due to elevator deflection, excluding the wind gust effects. In order to be able to compare the total pitch rate and pitch, two additional 16th order transfer functions would have to be added to the simulation --
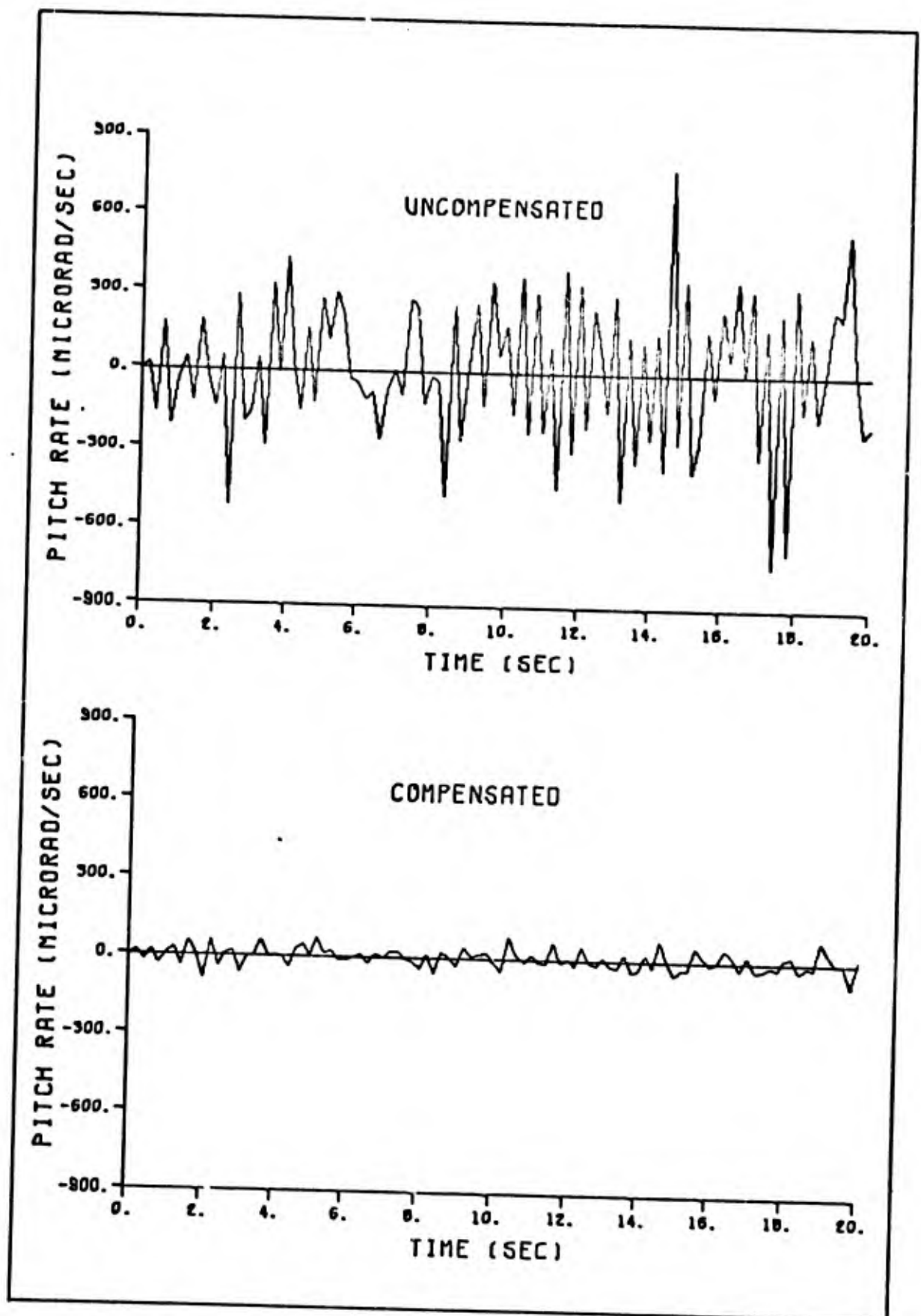
Figure 29. Comparison of Uncompensated and Compensated
Pitch-Rate Response due to the Wind Gust.

59
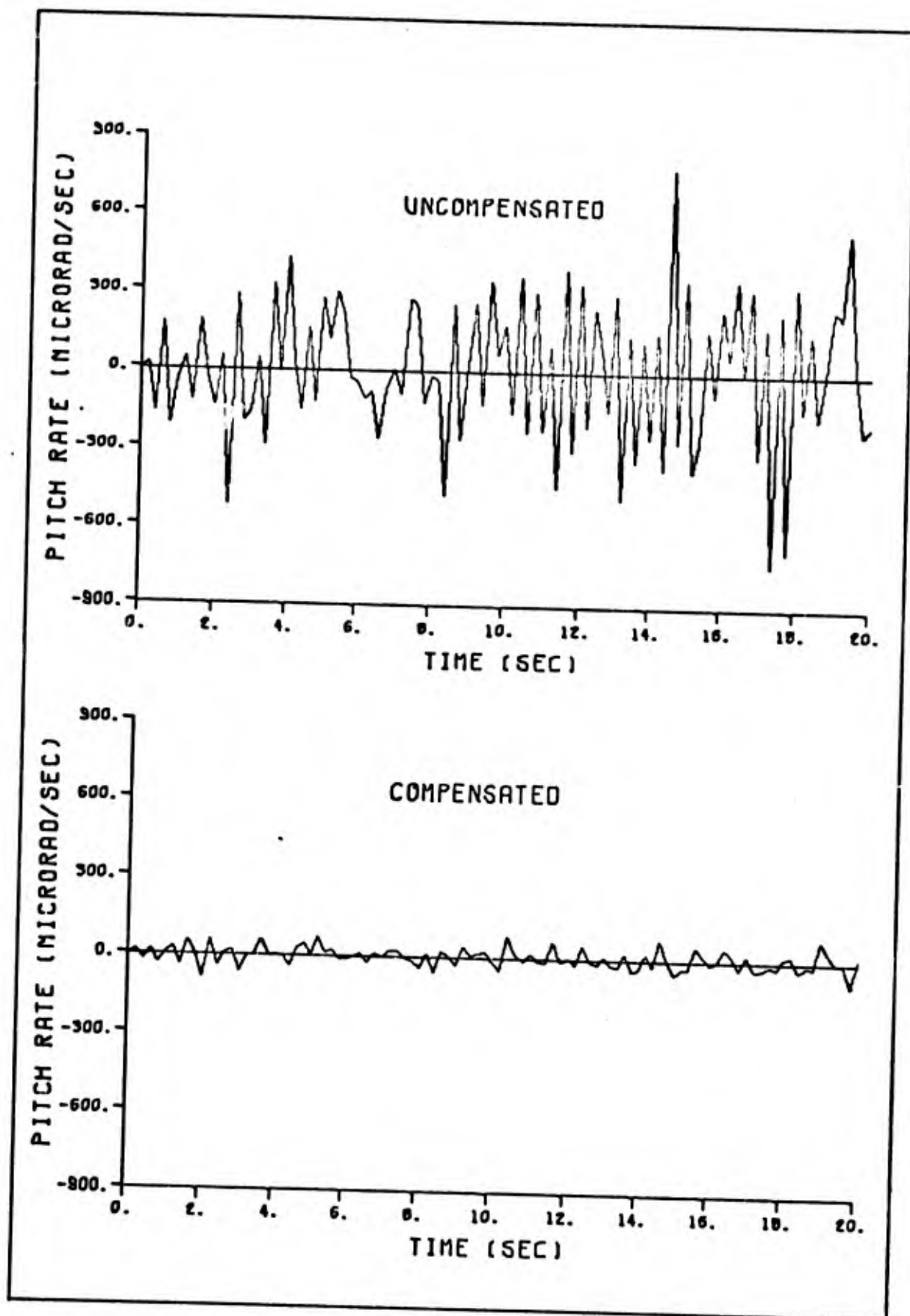
Figure 29. Comparison of Uncompensated and Compensated
Pitch-Rate Response due to the Wind Gust.
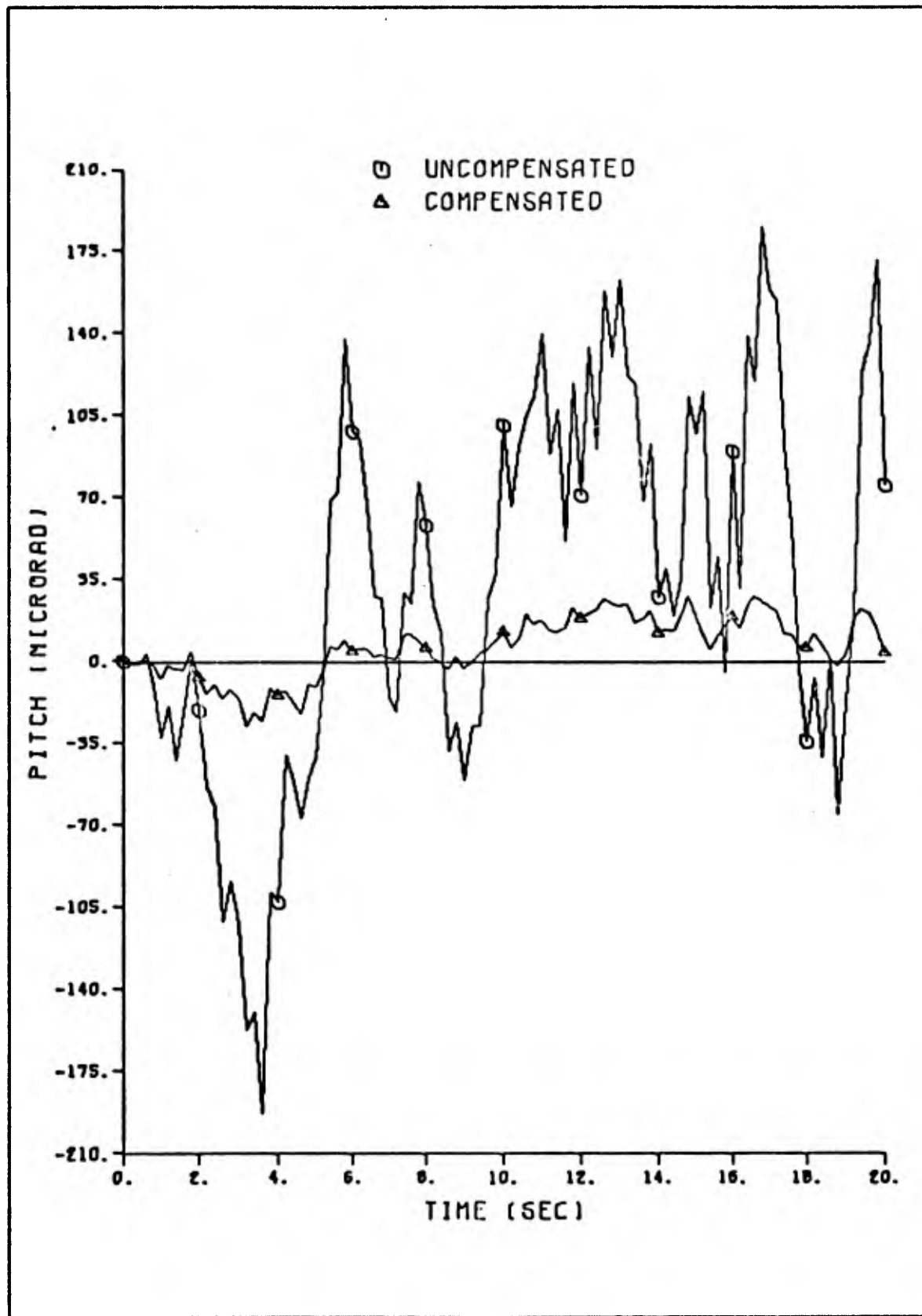
Figure 30. Comparison of Uncompensated and Compensated Pitch Response due to the Wind Gust.
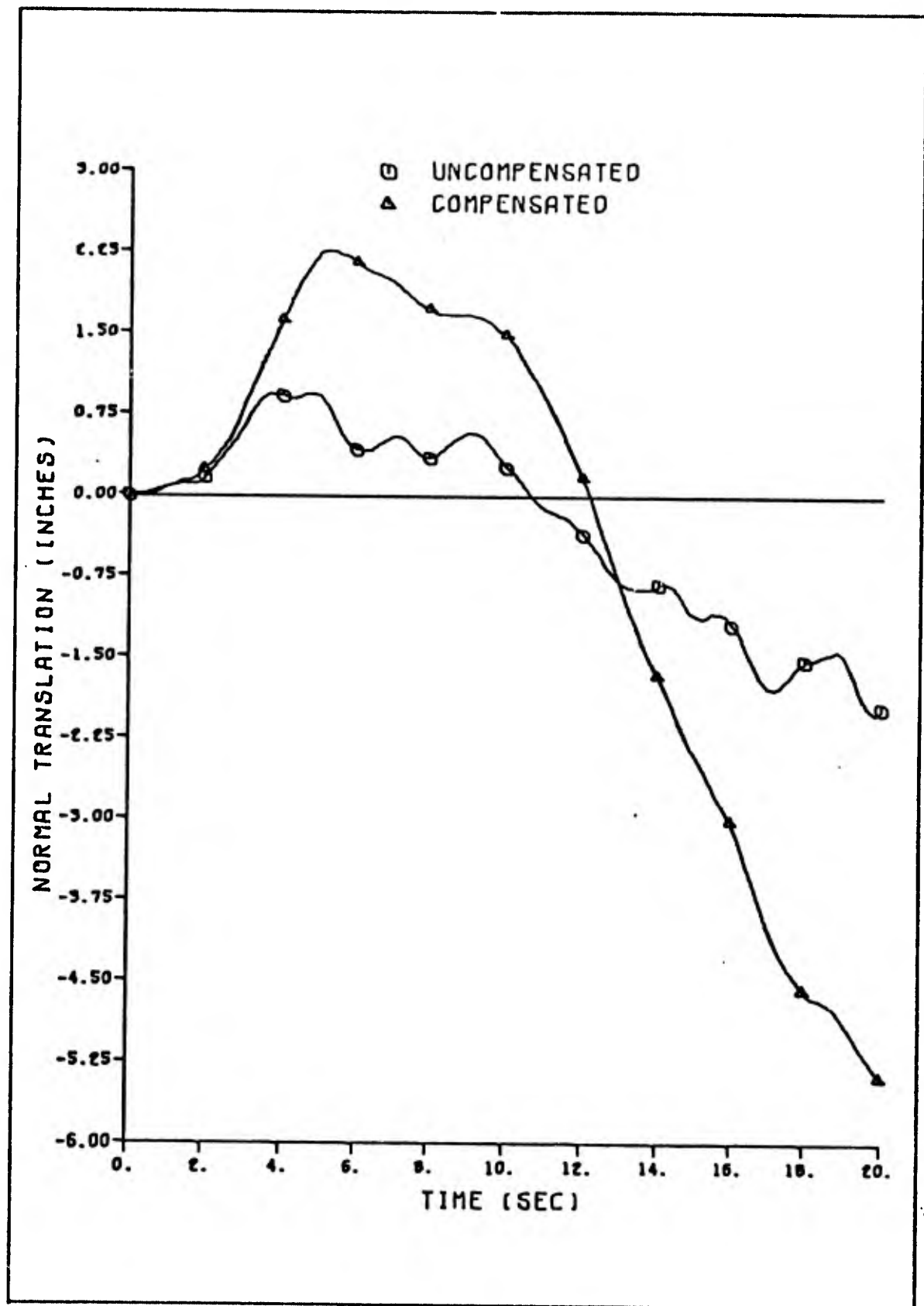
Figure 31. Comparison of Uncompensated and Compensated
Normal Translation due to the Wind Gust.
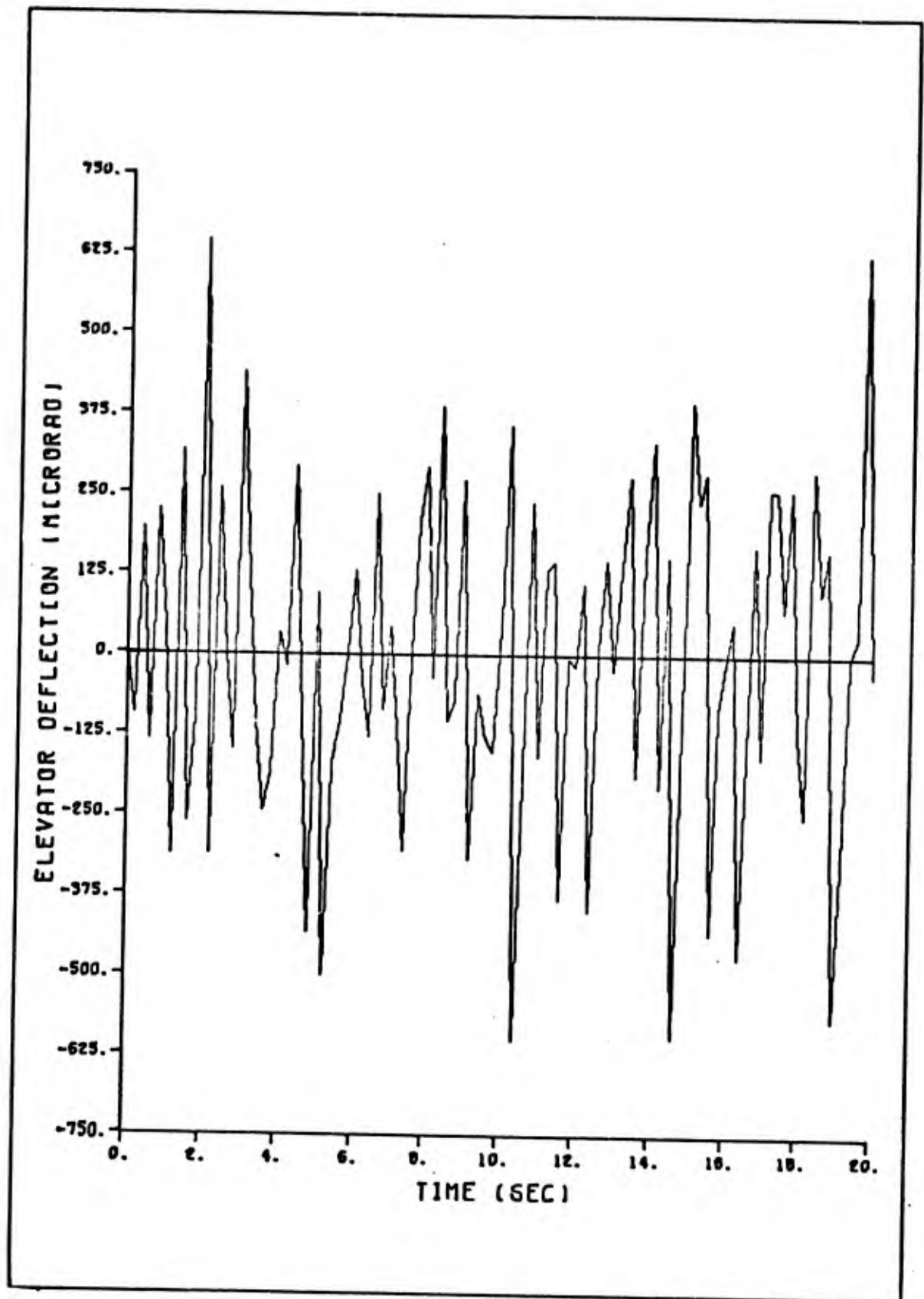
Figure 32.   Compensating Elevator Deflection
due to the Wind Gust.
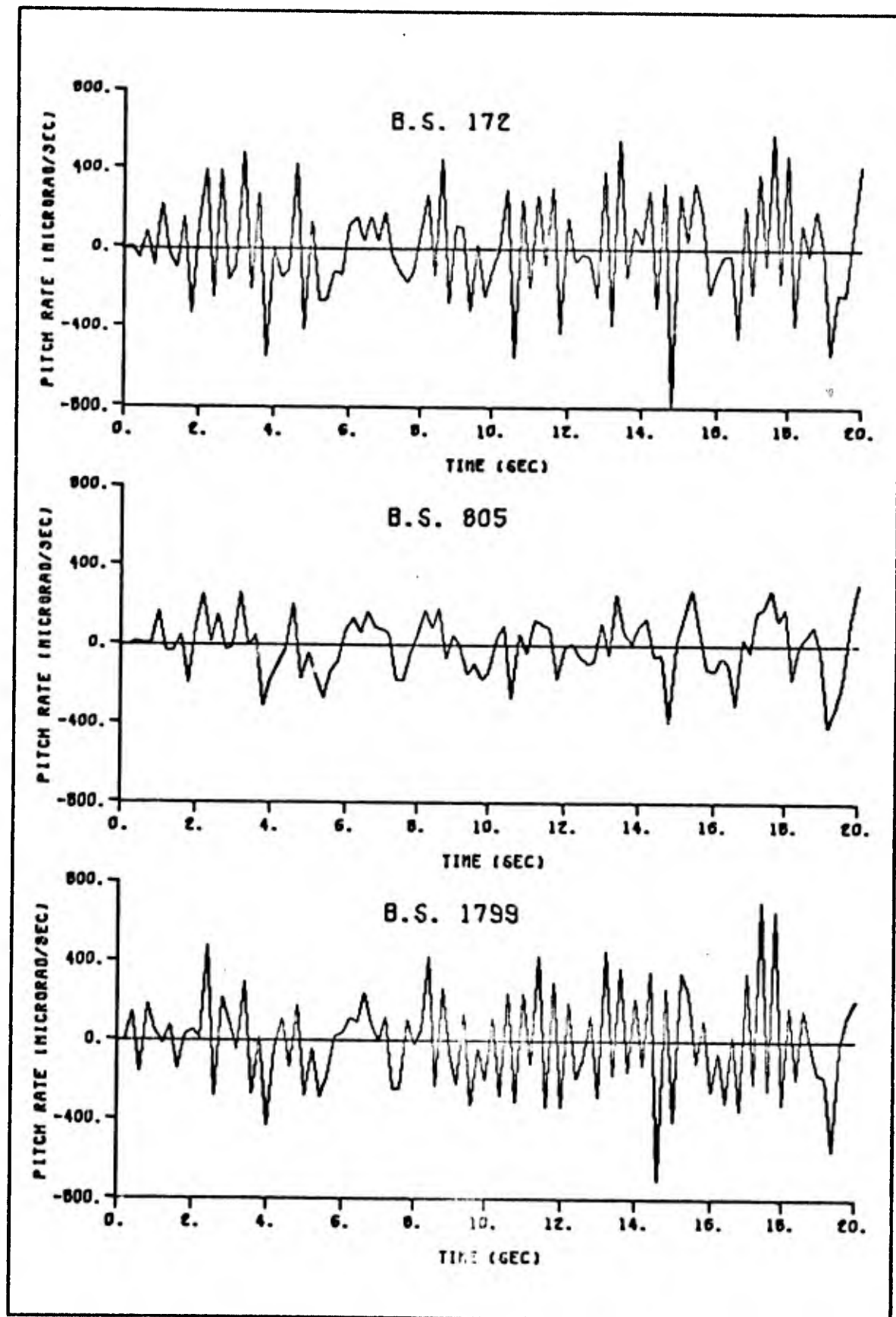
Figure 33. Contribution to ... ... Response at the three
Body Stations caused only by the Elevator.
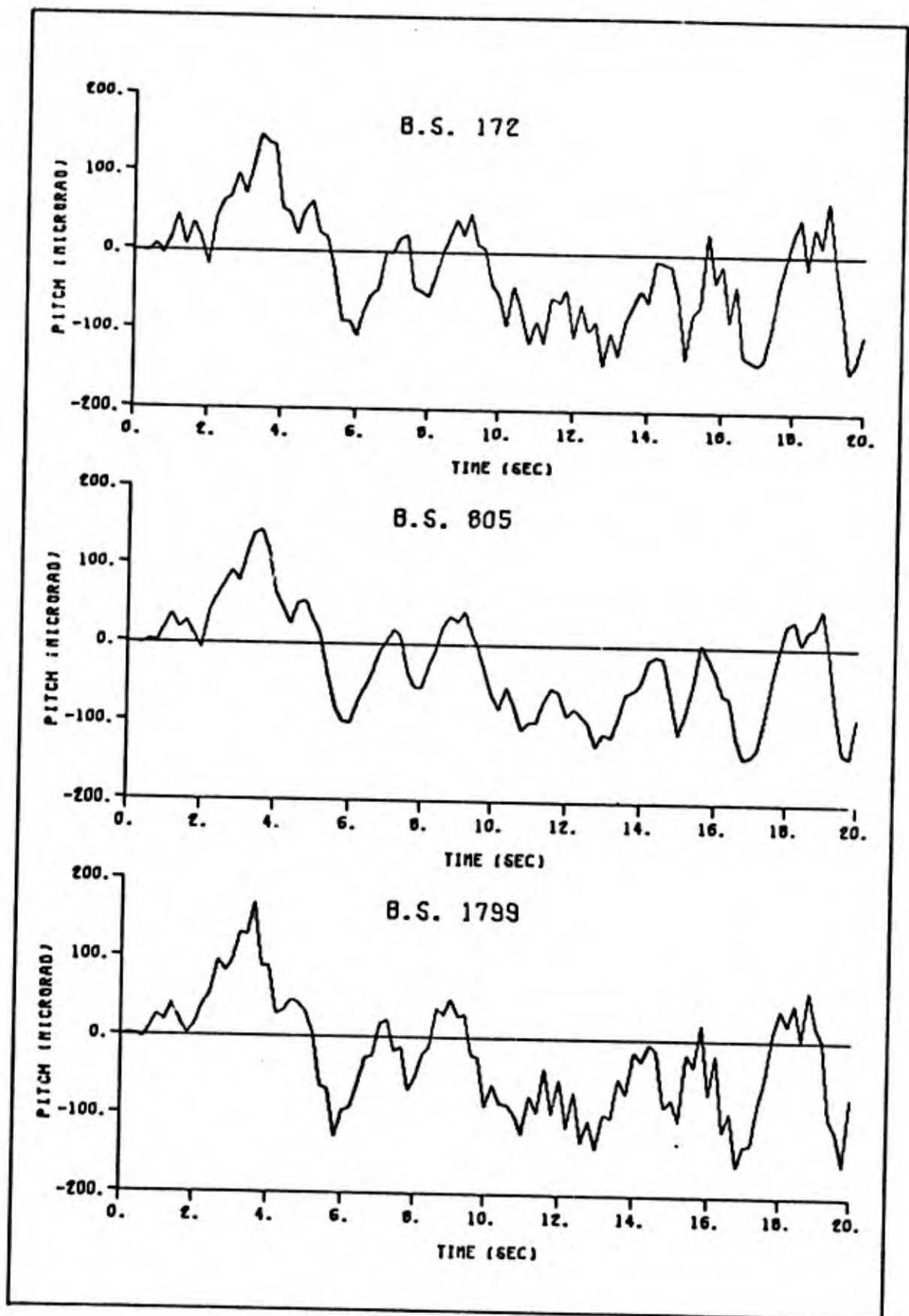
Figure 34. Contribution to Pitch Response at the three
Body Stations caused only by the Elevator.

Table XII

Comparison of rms Pitch Rate, $\dot{\theta}_{rms}$, Pitch, θ_{rms}, and Normal Translation, Z_{rms}, for the Uncompensated and Compensated Aircraft

	$\dot{\theta}_{rms}$ (10^{-6}rad/sec)	θ_{rms} (10^{-6}rad)	Z_{rms} (in.)
Uncompensated	284.2	85.50	0.927
Compensated	34.8	14.25	2.431
% Reduction	87.7	83.3	-262.

$\dot{\theta}_{172}(s)/w_g(s)$ and $\dot{\theta}_{805}(s)/w_g(s)$. These two transfer functions could have been obtained by use of the VALUE program but it was felt that the comparison of the respective responses due only to the elevator deflection would be sufficient to show that no unusual stresses or flexing occurs in the rest of the fuselage with the control system operating.

A comparison of rms pitch rate and pitch at the three body stations is made in Table XIII. The results make sense from an intuitive standpoint since the responses are greater at the two extreme body stations than they are at the more stable point near the aircraft center of gravity.

Response of Compensated System to Pilot Pitch-Rate Command as well as the Wind Gust. As discussed in the previous chapter, the effect of a pilot input to the system must be investigated. With the wind gust still present, a pitch-rate command, $\dot{\theta}_{com}$, equal to 0.05 rad/sec was introduced to the system at T = 1.0 sec and removed at T = 2.0 sec. The pitch-rate and pitch responses are shown in Figures 35 and 36 respectively for the three body stations. The elevator deflection resulting

Table XIII

Comparison of rms Pitch Rate and Pitch due only to

Elevator Deflection at B.S. 172, 805, and 1799

	Pitch Rate (10^{-6}rad/sec)	Pitch (10^{-6}rad)
B.S. 172	261.12	71.74
B.S. 805	146.77	69.67
B.S. 1799	266.64	72.91

from this pilot command is shown in Figure 37. Oscillations are present, as was expected, due to the light damping; however, the aircraft does respond relatively well. The oscillations are not too severe and die out rapidly.

Figures 35 and 36 indicate that the responses at the three body stations are similar and vary only slightly, due to the moment arms and flexing that is involved when such a command is given.
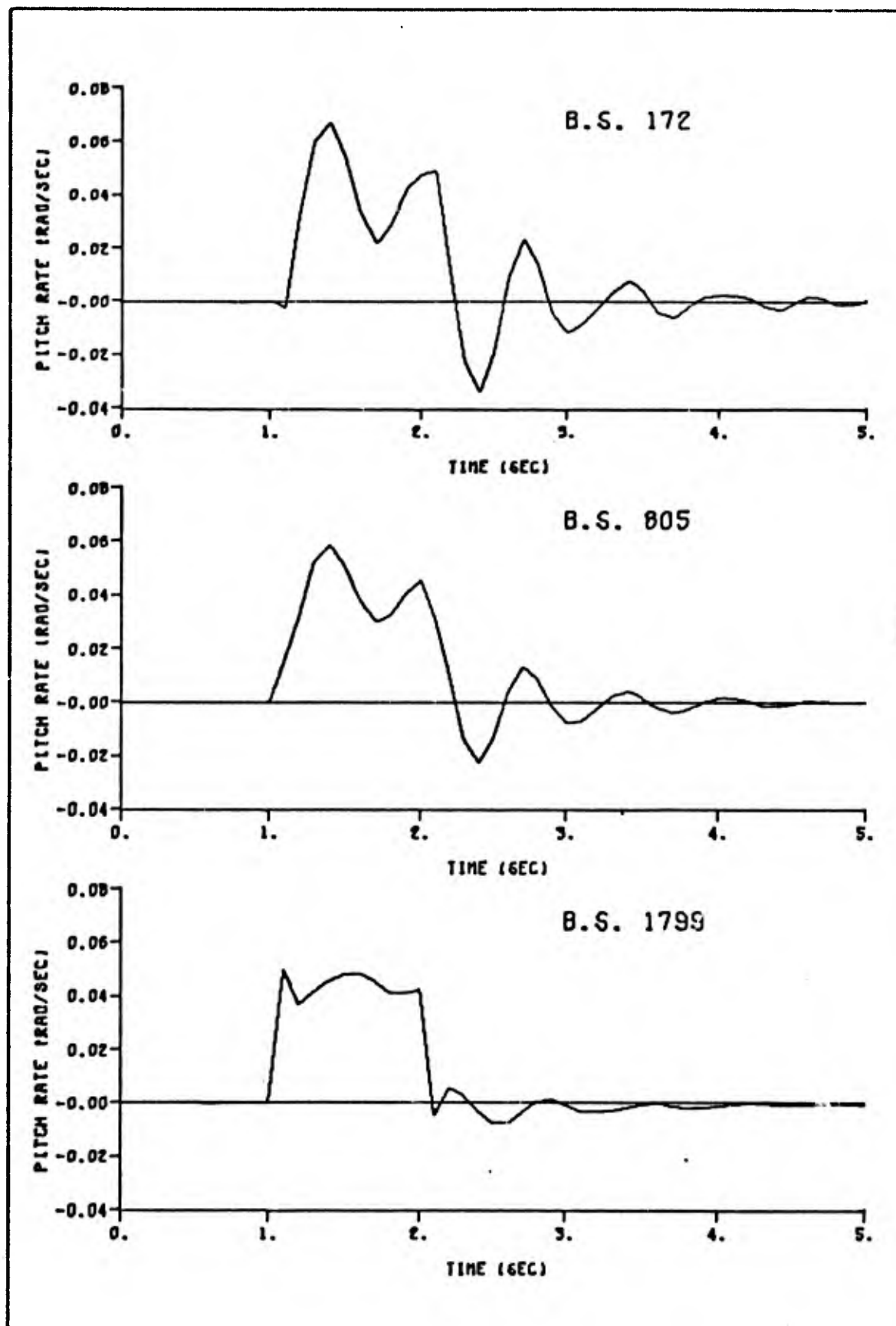
Figure 35.   Pitch-Rate Response to Pilot Pitch-Rate Command
of 0.05 rad/sec at the three Body Stations

67
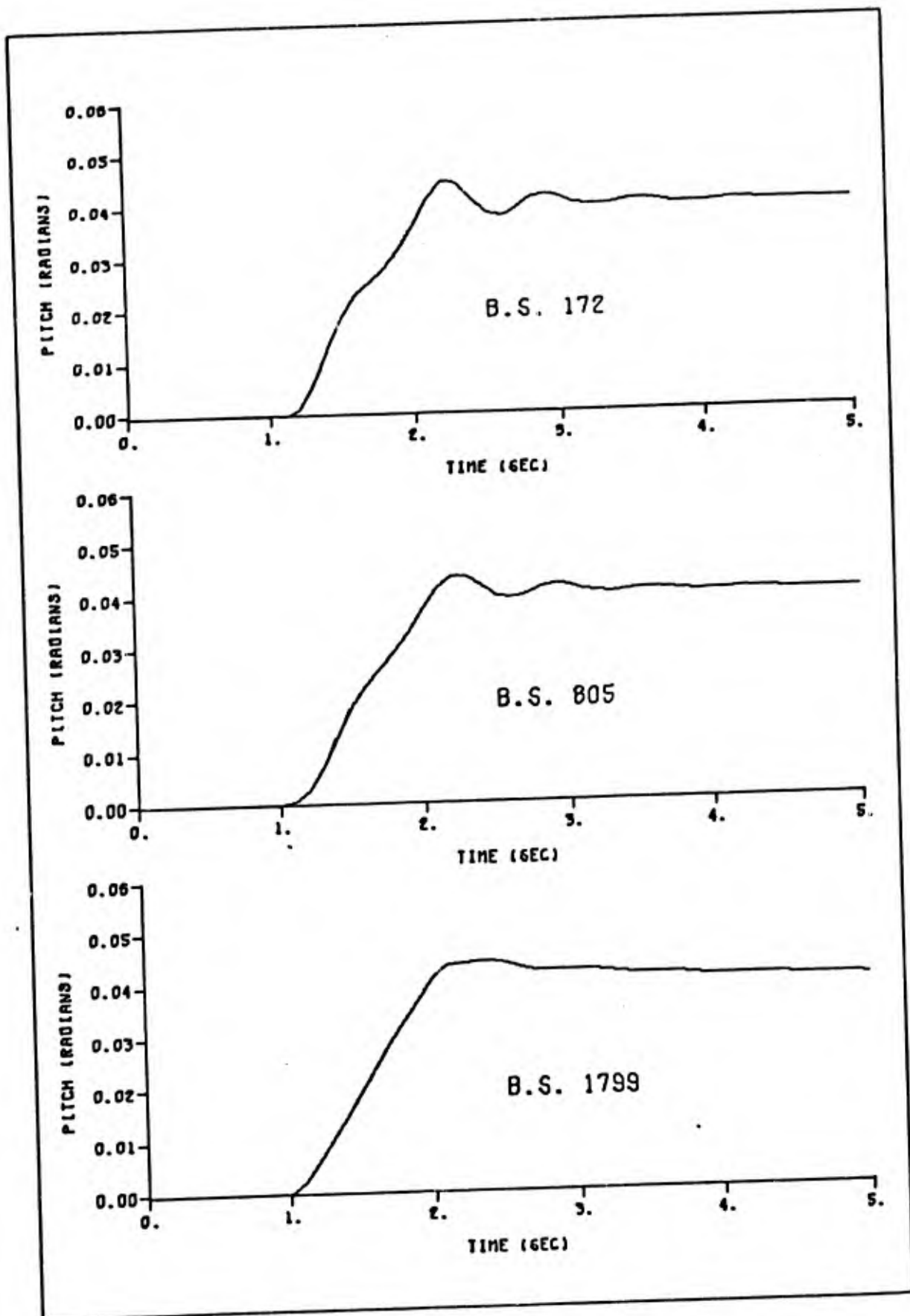
Figure 36. Pitch Response to Pilot Pitch-Rate Command of 0.05 rad/sec at the three Body Stations
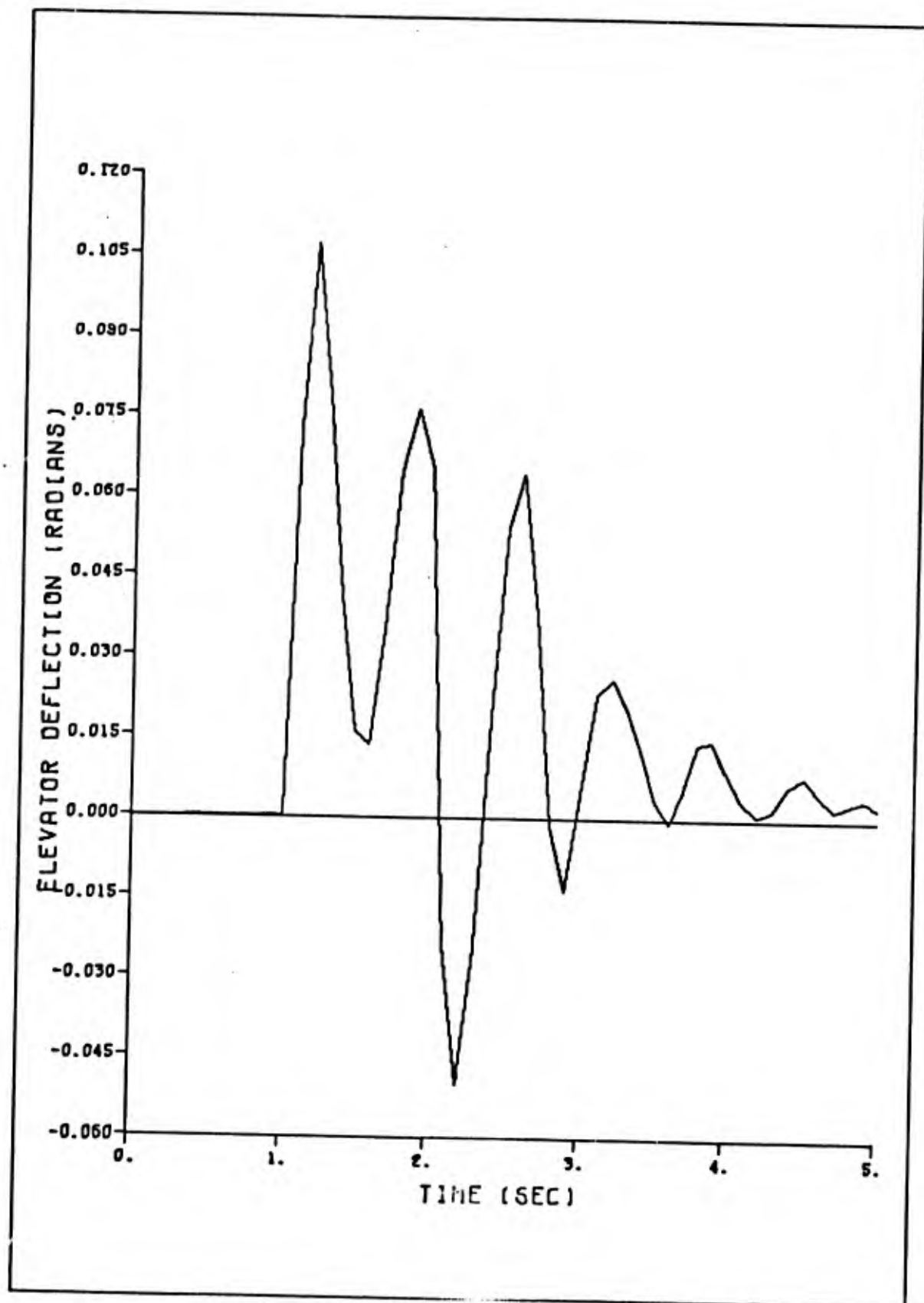
Figure 37. Elevator Deflection due to Pilot Pitch-Rate Command
of 0.05 rad/sec lasting from T = 1 sec to T = 2 sec

69

pitch is equal to the rms deviation due to normal translation gives a good indication of how well the system performs.

For the uncompensated case, where the rms normal translation is 0.927 in. and the rms variation in pitch is 85.5 microrad, simple trigonometry shows that the range where the deviations are equal is less than 1000 ft. Beyond that range the variation in pitch becomes predominant.

For the compensated case, where the rms normal translation has risen to 2.431 in. and the rms pitch has been reduced by 83.3% to a value of 14.25 microrad, the range at which the deviations are equal has risen to over 14,000 ft.

Thus, in spite of the increase in normal translation, which is still very small, the significant variations in pitch have been greatly reduced. This provides a much more stable base on which to mount the optical instruments. At the nominal design range of 40,000 ft, as was mentioned earlier in the text, the rms deviation at the target, due to pitch, for the uncompensated aircraft would be about 3 ft, whereas the compensated aircraft reduces this to about 6 in.

Although this control system provides a very good over-all stabilization of the aircraft aft-body, this study has shown that simultaneous improvements in both rms variations in pitch and rms normal translation cannot be achieved with only the elevator as the control surface.

Recommendations

Based on the experience gained during this study the following recommendations are made.

Although MIMIC served as a first aid in testing the design, a simulation technique using a hybrid computer with a digital random num-

VI. Conclusions and Recommendations

Conclusions

A control system to cancel the effects of a wind gust on pitch rate at the tail of a Boeing B-52 bomber has been designed and tested by means of a MIMIC program simulation. The first seven bending modes were included in the design and simulation to take into effect the flexible nature of the large aircraft. From the design procedure, and the MIMIC results, the following general conclusions can be drawn.

Based on the analysis of two flight conditions, it was concluded that the response of the aircraft does not vary greatly as flight conditions are changed. A representative flight condition was used for the design.

A gain of 2.0 achieved an 83.3% reduction in rms pitch variation. If increased gain could be shown to be practical, the reduction in rms pitch variation could be further improved. The limiting factors are only practical considerations, as well as safety, since the system, as modeled, is stable for all gains. However, high gain in the actual aircraft may well excite dynamic modes that have not been modeled in this thesis.

The response of the aircraft to a pitch-rate command from the pilot was shown to be good. Increasing the gain would not effect this response greatly, because the dominant roots are already very close to the zeros to which they are migrating.

As discussed in the body of the thesis, the rms deviation at the target, due to variations in pitch, is linearly increasing with range, whereas the rms deviation, due to normal translation, is constant and does not depend on range. The range at which the rms deviation due to

pitch is equal to the rms deviation due to normal translation gives a good indication of how well the system performs.

For the uncompensated case, where the rms normal translation is 0.927 in. and the rms variation in pitch is 85.5 microrad, simple trigonometry shows that the range where the deviations are equal is less than 1000 ft. Beyond that range the variation in pitch becomes predominant.

For the compensated case, where the rms normal translation has risen to 2.431 in. and the rms pitch has been reduced by 83.3% to a value of 14.25 microrad, the range at which the deviations are equal has risen to over 14,000 ft.

Thus, in spite of the increase in normal translation, which is still very small, the significant variations in pitch have been greatly reduced. This provides a much more stable base on which to mount the optical instruments. At the nominal design range of 40,000 ft, as was mentioned earlier in the text, the rms deviation at the target, due to pitch, for the uncompensated aircraft would be about 3 ft, whereas the compensated aircraft reduces this to about 6 in.

Although this control system provides a very good over-all stabilization of the aircraft aft-body, this study has shown that simultaneous improvements in both rms variations in pitch and rms normal translation cannot be achieved with only the elevator as the control surface.

Recommendations

Based on the experience gained during this study the following recommendations are made.

Although MIMIC served as a flexible aid in testing the design, a simulation technique using a hybrid computer with a digital random num-

ber generator, would allow for the system to be tested more fully. The output would be continuous and could be run for several minutes. MIMIC is restricted to plotting discrete-data output on a 100 x 100 grid. A rapidly varying output requires data output at close intervals and thus limits the total time of the plotted time response. MIMIC computation time also increases linearly for increased length of the time response. For the CYBER 75 system at the Air Force Institute of Technology the computation time necessary for a 1.0 sec real-time response was about 10.0 sec for the final system of Figure 28.

Additional transfer functions could be added to further test the effect of the system on other parts of the aircraft. At the same time a more complete evaluation of how much gain would be practical, and safe, could be made. A practical limit to the complexity of the simulation would, however, soon be met.

Bibliography

1. BII 216-?1. *Equations of Symmetric Motion for Conceptual Design of a Ride-Quality Improvement System*. Dayton, Ohio: Beta Industries, Inc., December, 1971.

2. Bisplinhoff, R. A., *et al*. *Aeroelasticity*. Reading, Mass.: Addison-Wesley Publishing Co., 1955.

3. Blakelock, J. H. *Automatic Control of Aircraft and Missiles*. New York: John Wiley and Sons, Inc., 1965.

4. Cooper, G. R. and C. D. McGillem. *Methods of Signal and System Analysis*. New York: Holt, Rinehart and Winston, Inc., 1967.

5. D'Azzo, J. J. and C. H. Houpis. *Feedback Control System Analysis and Synthesis*. New York: McGraw-Hill, Inc., 1966.

6. Greenstite, A. L. *Analysis and Design of Space Vehicle Flight Control Systems*. Vol. XV: *Elastic Body Equations*. NASA Contract Report 834. Washington: National Aeronautics and Space Administration, August, 1967.

7. Kuo, B. C. *Automatic Control Systems* (Second Edition). Englewood Cliffs, New Jersey: Prentice-Hall, Inc., 1967.

8. Peterson, H. E. and F. J. Sansom. *MIMIC Programming Manual*. Technical Document Number SEG-TDR-67-31 by the Aeronautical Systems Division, Wright-Patterson Air Force Base, Ohio, May, 1967.

9. Stockdale, C. R. *User's Reference Manual for CCV Data Reduction Computer Programs*. Report Number AFFDL-TM-72-2-FGB by the Air Force Flight Dynamics Laboratory, Wright-Patterson Air Force Base, Ohio, July, 1972.

10. Stockdale, C. R. and R. D. Poyneer. *CCV B-52 Base Data Report*. Report Number AFFDL-TM-72-1-FG-2 by the Air Force Flight Dynamics Laboratory, Wright-Patterson Air Force Base, Ohio, May, 1972.

11. Stockdale, C. R. and R. D. Poyneer. *Control Configured Vehicle Ride Control System (CCV RCS)*. Report Number AFFDL-TR-73-83 by the Air Force Flight Dynamics Laboratory, Wright-Patterson Air Force Base, Ohio, July, 1973.

12. *VALUE Program*. Unpublished manual describing the use of the VALUE program in possession of the Air Force Flight Dynamics Laboratory, Control Configured Vehicles Flight Control Division, Wright-Patterson Air Force Base, Ohio.

Appendix A

Simulation by MIMIC

Due to the complexity of the transfer functions, an analog computer simualtion, using traditional techniques, would require extensive work in diagramming and setting up the basic system. Modifications would be difficult and a large analog computer would be tied up for a considerable period of time.

An alternative method of simulating the time response of the aircraft is by use of the digital computer program MIMIC (Ref 8). It simulates the functions of an analog computer digitally. In addition, it has the capability of generating random numbers with a Gaussian distribution and a mean and standard deviation specified by the user. This proved convenient for simulating a white nose input to the wind filter to obtain the disturbance for the system.

The simulation of the 16th order transfer functions will now be discussed. Any general second-order transfer function, $P(s)$, can be written in several forms. The standard form of $P(s)$ is shown below:

$$P(s) = \frac{x(s)}{y(s)} = \frac{as^2 + bs + c}{ds^2 + es + f} \tag{A-1}$$

By cross-multiplying, shifting to the time domain, and using the dot convention to indicate differentiation with respect to time, the transfer function can be written in the following form:

$$x(t) = -\frac{1}{d}\, e\dot{x}(t) + fx(t) - a\ddot{y}(t) - b\dot{y}(t) - cy(t) \tag{A-2}$$

A solution for $x(t)$ for a given $y(t)$ would require two integrators

and two differentiators and would be block diagrammed as shown in Figure A.1 below.
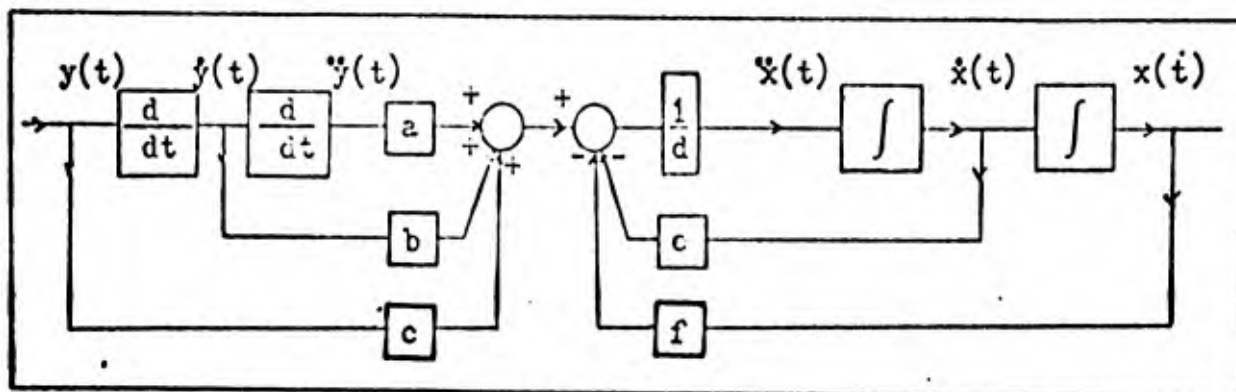
Figure A.1 Block Diagram of Equation (A-2)

MIMIC statements to simulate this transfer function can be easily written from either Eq (A-2) or the block diagram in Figure A.1. The first and second derivatives of x, for example, will be written 1DX and 2DX, respectively. The MIMIC integrator is of the form R = INT(A,B), where A is a variable to be integrated with respect to time and B is the initial condition. The MIMIC differentiator is of the form R = DER(C,D), where C is differentiated with respect to D. With this explanation, a MIMIC series of equations to simulate the transfer function shown in Figure A.1 will be given:

$$2DX = (-1./D)*(E*1DX + F*X - A*2DY - B*1DY - C*Y) \qquad (A-3)$$

$$1DX = INT(2DX,0.) \qquad (A-4)$$

$$X = INT(1DX,0.) \qquad (A-5)$$

$$1DY = DER(T,Y) \qquad (A-6)$$

$$2DY = DER(T,1DY) \qquad (A-7)$$

The input for this series of equations is y(t) and the output is x(t). However, if y(t) contains any noise it could have an adverse effect on

x(t), since the derivative of a noisy signal can become very large.

To avoid this problem a method similar to that used in making signal flow graphs will be used (Ref 7:135). The numerator and denominator of the transfer function are both divided by the highest order Laplace operator, s. For the second-order transfer function the result is:

$$P(s) = \frac{x(s)}{y(s)} = \frac{a + bs^{-1} + cs^{-2}}{d + es^{-1} + fs^{-2}} \qquad \text{(A-8)}$$

If now, Eq (A-8) is multiplied and divided by $X_{00}(s)$, for example, it remains unchanged.

$$P(s) = \frac{x(s)}{y(s)} = \frac{a + bs^{-1} + cs^{-2}}{d + es^{-1} + fs^{-2}} \frac{X_{00}(s)}{X_{00}(s)} \qquad \text{(A-9)}$$

Equating corresponding numerators and denominators

$$x(s) = aX_{00}(s) + bs^{-1}X_{00}(s) + cs^{-2}X_{00}(s) \qquad \text{(A-10)}$$

$$y(s) = dX_{00}(s) + es^{-1}X_{00}(s) + fs^{-2}X_{00}(s) \qquad \text{(A-11)}$$

where $s^{-1}X_{00}(s)$ signifies the integral with respect to time of $X_{00}(s)$ and $s^{-2}X_{00}(s)$ is one further integration of $X_{00}(s)$. Solving for $X_{00}(s)$ from Eq (A-10)

$$X_{00}(s) = \frac{1}{d} y(s) - es^{-1}X_{00}(s) - fs^{-2}X_{00}(s) \qquad \text{(A-12)}$$

Combining Eqs (A-12) and (A-11) a block diagram can be formed that only uses two integrators, as shown in Figure A.2. The necessary MIMIC statements to implement the transfer function shown in Figure A.2 are given on the next page.
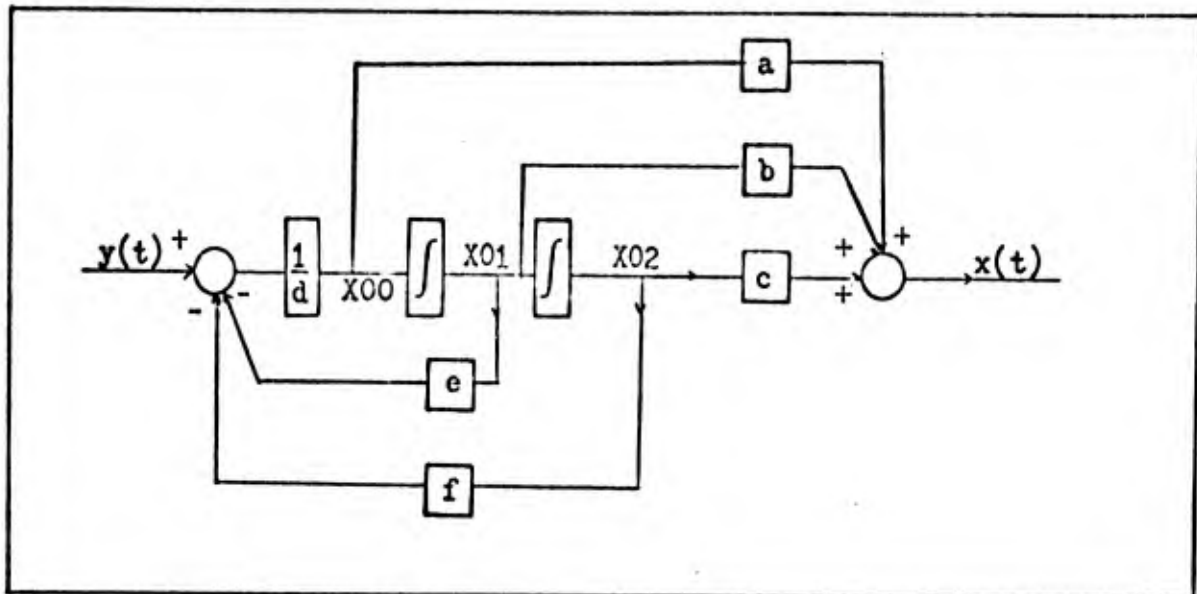
Figure A.2. Block Diagram using Equations (A-11) and (A-12)

$$X00 = (1./D)*(Y - E*X01 - F*X02) \tag{A-13}$$

$$X01 = INT(X00,0.) \tag{A-14}$$

$$X02 = INT(X01,0.) \tag{A-15}$$

$$X = A*X00 + B*X01 + C*X02 \tag{A-16}$$

where X is the output, Y is the input, X00, X01, X02 are dummy variables, and A, B, C, D, E, and F are constants.

By cascading blocks such as the one shown in Figure A.2, any transfer function can be simulated by MIMIC statements. Appendix C contains the listing of the MIMIC simulation of the final control system design and shows how the large-order transfer functions were written for use by MIMIC.

Appendix B

Root Mean Square Values Obtained using MIMIC

By definition the rms value of a particular time dependent variable, $x(t)$, is:

$$x(t)_{rms} = \sqrt{\frac{1}{T} \int_0^T x^2(t)dt} \qquad \text{(B-1)}$$

where T is the interval of time considered. This definition of rms lends itself to simulation using MIMIC. In MIMIC the variable T is always the current cumulative time which is updated at each step of the integration and a square root function is available in MIMIC. The resulting MIMIC statement for $x(t)_{rms}$ is:

$$XRMS = SQR(TINV*INT(X*X,0.)) \qquad \text{(B-2)}$$

where $\qquad TINV = 1./T$

Thus, any variable, such as pitch, pitch rate, wind gust, etc., can be substituted for X in Eq (B-2) and the resulting rms value will be found.

There are limitations to this method. Since the rms is calculated in a cumulative fashion, the value of rms output for small values of T will not be representative of the true rms value due to insufficient sampling of the variable. For random variables that are slowly time varying on the whole, after discounting the small rapid variations, the rms will not be accurate unless a representative sample is taken. For periodic variables, such as $\sin(2\pi t)$, the rms will be accurate at the end of each period.

Appendix C

Computer Listing of the Final MIMIC Program

This computer listing is the MIMIC simulation of the block diagram shown in Figure 28, with an additional gain of 5.231 added to bring the wind gust up to 1.0 ft/sec rms. The parameters listed in the first statement are: GAIN equal to 2, DTIME equal to 10, and DT1 equal to 0.2.

```
                    PAR(GAIN,CTIME,DT1)
$DELETE
C       BEGINNING OF 1DTH1/WG3 TRANSFER FUNCTION
C       V = 8223.62 IN./SEC AND ALTITUDE = 21,000. FT.
..
        X020      =WG3-2.724*X021-5.374*X022
        X021      =INT(X020,C.)
        X022      =INT(X021,C.)
        V17       =-.00105*X021
        X170      =V17-1.34*X171-37.55*X172
        X171      =INT(X170,0.)
        X172      =INT(X171,0.)
        V18       =136.66*X172+23.308*X171+X170
        X180      =V18-.318*X181-157.80*X182
        X181      =INT(X180,0.)
        X182      =INT(X181,0.)
        V19       =120.10*X182-19.184*X181+X180
        X190      =V19-.744*X191-150.55*X192
        X191      =INT(X190,C.)
        X192      =INT(X191,0.)
        V20       = 70.84*X192+.496*X191+X190
        X200      =V20-.170*X201-217.10*X202
        X201      =INT(X200,0.)
        X202      =INT(X201,C.)
        V21       =155.55*X202+0.116*X201+X200
        X210      =V21-0.694*X211-246.89*X212
        X211      =INT(X210,0.)
        X212      =INT(X211,0.)
        V22       =176.52*X212+.164*X211+X210
        X220      =V22-2.736*X221-213.72*X222
        X221      =INT(X220,0.)
        X222      =INT(X221,0.)
        V23       =238.13*X222-0.440*X221+X220
        X230      =V23-1.854*X231-370.77*X232
        X231      =INT(X230,C.)
        X232      =INT(X231,0.)
        1DTH1     =248.13*X232+1.234*X231+X230
<<
C       END OF 1DTH1/WG3 TRANSFER FUNCTION
.
```

```
<
<      BEGINNING CF NZ1/WG3 TRANSFER FUNCTION
<      V = 8223.62 IN./SEC AND ALTITUCE = 21,000. FT.
<
      X010      =WG3-2.726*X011-5.377*X012
      X011      =INT(X010,C.)
      X012      =INT(X011,0.)
      V2        =.00236*X010+.00255*X011
      X20       =V2-1.34*X21-37.550*X22
      X21       =INT(X20,0.)
      X22       =INT(X21,0.)
      V3        =58.740*X22+1.382*X21+X20
      X30       =V3-.744*X31-150.99*X32
      X31       =INT(X30,0.)
      X32       =INT(X31,0.)
      V4        =154.96*X32+.124*X31+X30
      X40       =V4-.319*X41-157.80*X42
      X41       =INT(X40,0.)
      X42       =INT(X41,0.)
      V5        =172.98*X42+.148*X41+X40
      X50       =V5-.17*X51-217.10*X52
      X51       =INT(X50,0.)
      X52       =INT(X51,0.)
      V6        =238.80*X52-.938*X51+X50
      X60       =V6-2.736*X61-213.72*X62
      X61       =INT(X60,0.)
      X62       =INT(X61,0.)
      V7        =251.37*X62+1.106*X61+X60
      X70       =V7-.694*X71-246.89*X72
      X71       =INT(X70,0.)
      X72       =INT(X71,0.)
      V8        =269.17*X72-7.034*X71+X70
      X80       =V8-1.854*X81-370.77*X82
      X81       =INT(X80,0.)
      X82       =INT(X81,0.)
      NZ1       =223.05*X82+15.114*X81+X80
<
<      END OF NZ1/WG3 TRANSFER FUNCTICN
*
```

```
c
c       BEGINNING OF 1DT172/DELE TRANSFER FUNCTION
c       V = 8223.62 IN./SEC AND ALTITUDE = 21,100. FT.
c

    Q230A      =DELE-2.724*Q231A-5.374*Q232A
    Q231A      =INT(Q230A,0.)
    Q232A      =INT(Q231A,0.)
    R24        =-1.664*Q232A -2.044*Q231A
    Q240       =R24-1.34*Q241-37.55*Q242
    Q241       =INT(Q240,0.)
    Q242       =INT(Q241,0.)
    R25        =37.620*Q242+1.330*Q241+Q240
    Q250       =R25-.318*Q251-157.80*Q252
    Q251       =INT(Q250,0.)
    Q252       =INT(Q251,0.)
    R26        =152.12*Q252+.602*Q251+Q250
    Q260       =R26-.744*Q261-150.99*Q262
    Q261       =INT(Q260,0.)
    Q262       =INT(Q261,0.)
    R27        =159.20*Q262+.406*Q261+Q260
    Q270       =R27-.170*Q271-217.10*Q272
    Q271       =INT(Q270,0.)
    Q272       =INT(Q271,0.)
    R28        =216.12*Q272+1.966*Q271+Q270
    Q280       =R28-0.694*Q281-246.89*Q282
    Q281       =INT(Q280,0.)
    Q282       =INT(Q281,0.)
    R29        =235.03*Q282+1.434*Q281+Q280
    Q290       =R29-2.736*Q291-213.72*Q292
    Q291       =INT(Q290,0.)
    Q292       =INT(Q291,0.)
    R30        =265.72*Q292+0.072*Q291+Q290
    Q300       =R30-1.854*Q301-370.77*Q302
    Q301       =INT(Q300,0.)
    Q302       =INT(Q301,0.)
    1DT172     =-472.72*Q302-0.215*Q301+Q300
c
c       END OF 1DT172 TRANSFER FUNCTION
c
```

```
c       BEGINNING OF 10T805/CELE TRANSFER FUNCTION
c       V = 8223.62 IN./SEC AND ALTITUDE = 21,000. FT.
c
        S230A    =DELE-2.724*S231A-5.374*S232A
        S231A    =INT(S230A,0.)
        S232A    =INT(S231A,C.)
        T24      = 2.110*S232A+ 2.667*S231A
        S240     =T24-1.34*S241-37.55*S242
        S241     =INT(S240,0.)
        S242     =INT(S241,0.)
        T25      =37.592*S242+1.312*S241+S240
        S250     =T25-.318*S251-157.80*S252
        S251     =INT(S250,0.)
        S252     =INT(S251,0.)
        T26      =150.94*S252+.690*S251+S250
        S260     =T26-.744*S261-150.99*S262
        S261     =INT(S260,0.)
        S262     =INT(S261,0.)
        T27      =158.33*S262+.320*S261+S260
        S270     =T27-.170*S271-217.10*S272
        S271     =INT(S270,0.)
        S272     =INT(S271,0.)
        T28      =217.43*S272+2.554*S271+S270
        S280     =T28-0.694*S281-246.69*S282
        S281     =INT(S280,C.)
        S282     =INT(S281,0.)
        T29      =228.74*S282+0.716*S281+S280
        S290     =T29-2.736*S291-213.72*S292
        S291     =INT(S290,0.)
        S292     =INT(S291,0.)
        T30      =260.69*S292 -.348*S291+S290
        S300     =T30-1.854*S301-370.77*S302
        S301     =INT(S300,0.)
        S302     =INT(S301,0.)
        10T805   =393.18*S302+2.514*S301+S300
c
c       END OF 10T805 /DELE TRANSFER FUNCTION
c
```

```
<       BEGINNING OF 1DTH11/DELE TRANSFER FUNCTION
<       V = 8223.62 IN./SEC AND ALTITUCE = 21,000. FT.
<

    X230A       =DELE-2.724*X231A-5.374*X232A
    X231A       =INT(X230A,C.)
    X232A       =INT(X231A,C.)
    V24         = 7.847*X232A+11.147*X231A
    X240        =V24-1.34*X241-37.55*X242
    X241        =INT(X240,C.)
    X242        =INT(X241,0.)
    V25         =37.500*X242+1.240*X241+X240
    X250        =V25-.318*X251-157.80*X252
    X251        =INT(X250,0.)
    X252        =INT(X251,0.)
    V26         = 92.65*X252+1.03*X251+X250
    X260        =V26-.744*X261-150.99*X252
    X261        =INT(X260,0.)
    X262        =INT(X261,0.)
    V27         =152.75*X262+.352*X261+X260
    X270        =V27-.170*X271-217.10*X272
    X271        =INT(X270,0.)
    X272        =INT(X271,0.)
    V28         =164.96*X272+.540*X271+X270
    X280        =V28-0.694*X281-246.89*X282
    X281        =INT(X280,C.)
    X282        =INT(X281,0.)
    V29         =238.37*X282+0.732*X281+X280
    X290        =V29-2.736*X291-213.72*X292
    X291        =INT(X290,0.)
    X291        =INT(X290,C.)
    X292        =INT(X291,C.)
    V30         =207.41*X292+1.974*X291+X290
    X300        =V30-1.854*X301-370.77*X302
    X301        =INT(X300,0.)
    X302        =INT(X301,0.)
    1DTH11      =284.66*X302+1.310*X301+X300 ·
<<
<       END OF 1DTH11/DELE TRANSFER FUNCTION
```

```
C
C      BEGINNING OF NZ11/DELE TRANSFER FUNCTION
C      V = 8223.62 IN./SEC AND ALTITUDE = 21,000. FT.
C

   X80A      =DELE-2.726*X81A-5.377*X82A
   X81A      =INT(X80A,0.)
   X82A      =INT(X81A,0.)
   V9        = 83.877*X82A-11.4*X81A-15.922*X80A
   X90       =V9-1.34*X91-37.55*X92
   X91       =INT(X90,0.)
   X92       =INT(X91,0.)
   V10       =37.560*X92+1.274*X91+X90
   X100      =V10-.744*X101-150.99*X102
   X101      =INT(X100,0.)
   X102      =INT(X101,0.)
   V11       =143.57*X102+.928*X101+X100
   X110      =V11-.318*X111-157.80*X112
   X111      =INT(X110,0.)
   X112      =INT(X111,0.)
   V12       =155.61*X112+.178*X111+X110
   X120      =V12-.17*X121-217.10*X122
   X121      =INT(X120,0.)
   X122      =INT(X121,0.)
   V13       =190.43*X122+.272*X121+X120
   X130      =V13-2.736*X131-213.72*X132
   X131      =INT(X130,0.)
   X132      =INT(X131,0.)
   V14       =201.54*X132+2.438*X131+X130
   X140      =V14-.694*X141-246.89*X142
   X141      =INT(X140,0.)
   X142      =INT(X141,0.)
   V15       =242.19*X142+.742*X141+X140
   X140A     =V15-1.954*X141A-370.77*X142A
   X141A     =INT(X140A,0.)
   X142A     =INT(X141A,0.)
   NZ11      =314.88*X142A+1.594*X141A+X140A
C
C
C      END OF NZ11/DELE TRANSFER FUNCTION
C
C
   GAMMA     =RNG(0.,1.)
C
C      THE RANDOM NUMBER GENERATOR GENERATES NUMBERS
C      IN   A GAUSSIAN DISTRIBUTION WITH A MEAN OF ZERO
C      AND A STANDARD DEVIATION OF 1.0.
.
```

```
C     BEGINNING CF WG/GAMMA TRANSFER FUNCTICN FOR
C     V = 8223.62 IN./SEC AND ALTITUDE = 21,000. FT.
C

      X000      =GAMMA-1.371*X001-.4700*X002
      X001      =INT(X000,0.)
      X002      =INT(X001,0.)
      WG        =2.7160*X002+6.8640*X001

C
C     END OF WG/GAMMA TRANSFER FUNCTION
C

      WG3       =5.231*WG

C
      1DTHET    =1DTH11+1DTH1
      THETA     =INT(1DTHET,0.)
      E1        =-1DTHET
      TH1       =INT(1DTH1,0.)
      TH11      =INT(1DTH11,0.)

C
C     TH1 AND TH11 ARE THE CONTRIBUTIONS TO VARIATION IN
:     PITCH DUE, RESPECTIVELY, TO THE WIND GUST AND THE
:     ELEVATOR.
:

      EX1       =E1

C
C     THE PILOT PITCH-RATE COMMAND WOULD BE ADDED AT THIS
C     POINT TO E1.  NORMALLY THE PITCH-RATE COMMAND IS
C     CONSTRAINED TO BE ZERO.
C

      EOUT      =EX1*GAIN

C
C     BEGINNING OF DELE/EOUT TRANSFER FUNCTION
C     WHICH IS THE ELEVATOR SERVOACTUATOR TRANSFER FUNCTION
C
C     A LIMITER WAS ADDED TC THE ELEVATOR TRANSFER
C     FUNCTION TO KEEP THE ELEVATOR DEFLECTION RATE
C     LESS THAN 1.4 RAD/SEC IN ABSOLUTE VALUE.
C

      1DELE     =-46.*DELE+161.7*EOUT
      1DELEL    =LIM(1DELE,-1.4,1.4)
      DELE      =INT(1DELEL,0.)

C
C     END OF DELE/EOUT TRANSFER FUNCTION
C
```

85

```
C
        NZTOT    =NZ11+NZ1

C
C       NZ1 AND NZ11 ARE THE CONTRIBUTIONS TO NORMAL
C       ACCELERATION DUE, RESPECTIVELY, TO THE WIND GUST
C       AND ELEVATOR.
C
        VZTOT    =VZ11+VZ1
        VZ1      =386.1*INT(NZ1,0.)
        VZ11     =386.1*INT(NZ11,0.)
        ZTOT     =INT(VZTOT,0.)
        Z1       =INT(VZ1,0.)
        Z11      =INT(VZ11,0.)
C
        TH805    =INT(1DT805,0.)
C
C       TH805 IS THE VARIATION IN PITCH AT B.S. 805 DUE ONLY
C       TO ELEVATOR DEFLECTION.
C
        TH172    =INT(1DT172,0.)
C
C       TH172 IS THE VARIATION IN PITCH AT B.S. 172 DUE ONLY
C       TO ELEVATOR DEFLECTION.
C
C       CALCULATION OF RMS VALUES OF THE QUANTITIES THAT
C       ARE SQUARED WITHIN THE BRACKETS.
C
        TINV     =1./T
        1DT1MS   =SQR(TINV*INT(1DTH1*1DTH1,0.))
        1D11MS   =SQR(TINV*INT(1DTH11*1DTH11,0.))
        1DTHMS   =SQR(TINV*INT(1DTHET*1DTHET,0.))
        TH1RMS   =SQR(TINV*INT(TH1*TH1,0.))
        T11RMS   =SQR(TINV*INT(TH11*TH11,0.))
        THERMS   =SQR(TINV*INT(THETA*THETA,0.))
        NZ1RMS   =SQR(TINV*INT(NZ1*NZ1,0.))
        NZ11MS   =SQR(TINV*INT(NZ11*NZ11,0.))
        NZTRMS   =SQR(TINV*INT(NZTOT*NZTOT,0.))
        Z1RMS    =SQR(TINV*INT(Z1*Z1,0.))
        Z11RMS   =SQR(TINV*INT(Z11*Z11,0.))
        ZTOTMS   =SQR(TINV*INT(ZTOT*ZTOT,0.))
        1T805S   =SQR(TINV*INT(1DT805*1DT805,0.))
        1T172S   =SQR(TINV*INT(1DT172*1DT172,0.))
        T172MS   =SQR(TINV*INT(TH172*TH172,0.))
        T805MS   =SQR(TINV*INT(TH805*TH805,0.))
        WG3RMS   =SQR(TINV*INT(WG3*WG3,0.))
        OELRMS   =SQR(TINV*INT(CELE*CELE,0.))
```

```
PERCNT    =THERMS/TH1RMS
           FIN(THERMS,.1)
           FIN(T,19.8)

OT        =OT1
OTMIN     =OT/OTIME

          OUT(T,1OTH1,1OTH11,1OTHET,THETA,TH1)
          OUT( ,THERMS,TH1PMS,WG3,1OELEL,T11RMS)
          OUT( ,OELPMS,EOUT,DELE,GAMMA,WG3RMS)
          OUT( ,PERCNT,1OT1MS,1O11MS,TH11,1T172S)
          OUT( ,NZ1,NZ11,VZ1,VZ11,1T935S)
          OUT( ,Z1,Z11,NZTOT,VZTOT,ZTOT)
          OUT( ,ZTOTMS,Z1RMS,Z11RMS,1OT805,1OT172)
          OUT( ,TH805,T605MS,TH172,T172MS,1OTHMS)
          OUT( ,NZ1RMS,NZ11PMS,NZTRMS)

          PLO(T,THETA,TH805,TH172)
          .OPT(1.,2.,1.)
          PLO(T,1OTHET,1OT805,1OT172)
          OPT(1.,2.,1.)
          PLO(T,NZTOT,NZ1)
          OPT(1.,2.,1.)
          PLO(T,1OTHET,1OTH1,1OTH11)
          OPT(1.,2.,1.)
          PLO(T,ZTOT,Z1)
          OPT(1.,2.,1.)
          PLO(T,THETA,TF1)
          OPT(1.,2.,1.)
          END
```

VITA

Charles Al'-n Harrington III was born in ████████████████████
████████████. He graduated from Johnson High School of St. Paul in
1962 and attended the University of Minnesota. His education was inter-
rupted in 1965 when he went to Finland for two and a half years, where
he served as a missionary for the Church of Jesus Christ of Latter-day
Saints. After another year at the University of Minnesota he enlisted
in the USAF in 1969. In 1972 he received his Bachelor of Science degree,
under the AECP program, from the University of Wyoming, where he was
elected to Sigma Tau. He was commissioned in 1972 and was assigned to
the Air Force Institute of Technology.

Permanent address: ███████████████
███████████████████

This thesis was typed by the author.